

**APPLICATION OF THE URBAN AIRSHED MODEL IN
THE LOWER FRASER VALLEY, BRITISH COLUMBIA**

By

Natalie M. Suzuki

B. A.Sc. (Chem. Eng.) University of British Columbia, 1983

Dipl. Meteorology University of British Columbia, 1991

A THESIS SUBMITTED IN PARTIAL FULFILLMENT OF
THE REQUIREMENTS FOR THE DEGREE OF
MASTER OF SCIENCE

in

THE FACULTY OF GRADUATE STUDIES
ATMOSPHERIC SCIENCE

We accept this thesis as conforming
to the required standard

THE UNIVERSITY OF BRITISH COLUMBIA

August 1997

© Natalie M. Suzuki, 1997

In presenting this thesis in partial fulfilment of the requirements for an advanced degree at the University of British Columbia, I agree that the Library shall make it freely available for reference and study. I further agree that permission for extensive copying of this thesis for scholarly purposes may be granted by the head of my department or by his or her representatives. It is understood that copying or publication of this thesis for financial gain shall not be allowed without my written permission.

Atmospheric Science
The University of British Columbia
2075 Wesbrook Place
Vancouver, Canada
V6T 1W5

Date:

97/08/26

Abstract

The Lower Fraser Valley (LFV) of southwestern British Columbia is periodically subject to unacceptably high concentrations of ground-level ozone (O_3). To investigate the factors which influence elevated O_3 concentrations in the LFV, a three-dimensional Eulerian model called the Urban Airshed Model was used to simulate an historical O_3 episode which occurred between July 17-19, 1985. The results showed generally satisfactory model performance for predicted O_3 levels across the region, relative to model performance parameters established elsewhere. Peak unpaired accuracies ranged from -2% to -24% and normalized gross error ranged from 35.6-36.9% over the three-day simulation. However, there was a tendency for the model to underestimate O_3 concentrations, as reflected in the normalized bias, which ranged from -29.1 to -31.3%. Spatial patterns of predicted O_3 concentrations indicated that higher O_3 concentrations were observed along the valley walls and tributary valleys than on the valley floor where most of the population resides. Overall model performance based on nitrogen dioxide levels was within established parameters, although concentrations were typically underestimated and performance at two stations was poor. As a further means of assessing model performance, three indicator species (NO_y , O_3/NO_z and H_2O_2/HNO_3) were calculated to determine the ozone sensitivity of the modelled airshed. The findings suggest that with the exception of sites located far downwind of the major source region, conditions tended to be VOC-limited.

Table of Contents

List of Tables	vi
List of Figures	viii
Acknowledgments	xiii
1 Introduction	1
1.1 Research Objectives	11
1.2 Methodology	11
1.3 Thesis Outline	11
2 Technical Description of Models	13
2.1 Urban Airshed Model	13
2.1.1 Governing Equations	13
2.1.2 Modelled Processes	16
2.1.3 Advection	16
2.1.4 Turbulent Diffusion	17
2.1.5 Surface Removal Processes	19
2.1.6 Chemical Processes	19
2.1.7 Emissions	23
2.2 CSU-RAMS	24
3 Episode and Domain Selection	26
3.1 Episode Selection	26

3.1.1	Data Availability	27
3.1.2	Characterization of a Typical Episode	29
3.1.3	Characterization of the Selected Episode	30
3.2	Domain Selection	39
4	Model Inputs	41
4.1	Boundary and Initial Conditions	41
4.1.1	BOUNDARY	41
4.1.2	REGIONTOP	43
4.1.3	AIRQUALITY	44
4.1.4	TOPCONC	44
4.2	Meteorological Data	45
4.2.1	WIND	45
4.2.2	DIFFBREAK	47
4.2.3	TEMPERATUR	52
4.2.4	METSCALARS	52
4.3	Emissions Data	53
4.3.1	Mobile Sources	55
4.3.2	Point Sources	56
4.3.3	Gasoline Marketing Sources	58
4.3.4	Area Sources	61
4.3.5	US Sources	63
4.4	Terrain Data	63
4.5	Chemical Parameters	64
4.6	Simulation Control Parameters	64

5	Model Results and Discussion	66
5.1	Model Performance Criteria	66
5.2	Ozone	67
5.3	Nitrogen Dioxide	84
5.4	Discussion	99
6	Summary	107
	List of References	109

List of Tables

1.1	UAM Applications	10
2.1	State species in CBM-IV	22
3.1	Location of air quality monitoring sites in the LFV, 1985.	27
3.2	Exceedances of ambient O ₃ objectives in the LFV, 17-21 July 1985.	38
4.1	UAM input files	42
4.2	Clean boundary conditions, South Coast Air Quality Management District (SCAQMD, 1990).	43
4.3	Maximum predicted and observed values of z _i at sites in Delta, Surrey and QEP, Vancouver between 17-19 July 1985.	52
4.4	Annual emissions estimates for the BC (1985) and Washington (1990) LFV	54
4.5	Episodic adjustments of motor vehicle emissions	56
4.6	Default landuse types and terrain factors (Sheih et al., 1986).	64
5.1	Observed and predicted maximum one-hour O ₃ concentrations in ppb and corresponding hour (PST) at monitoring stations in the LFV, 17-19 July 1985.	79
5.2	Model performance based on predicted and observed maximum one-hour O ₃ concentrations at stations in the LFV, 17-19 July 1985.	82
5.3	Model O ₃ performance statistics for the LFV, 17-19 July 1985.	83

5.4	Observed (Obs.)and predicted (Pred.) maximum one-hour NO ₂ concentrations in ppb at monitoring stations in the LFV, 17-19 July 1985, along with the respective time of day (Hr).	96
5.5	Model performance based on observed and predicted maximum one-hour NO ₂ concentrations at stations in the LFV, 17-19 July 1985.	97
5.6	Model NO ₂ performance statistics for the LFV, 17-19 July 1985.	98

List of Figures

1.1	Map of the Lower Fraser Valley showing topography, coastline, major population centres and geographical features.	3
3.1	Map of LFV, showing location of air quality and meteorological monitoring sites present in July 1985. Coastline and 100 m contours are shown by solid and dashed lines, respectively. Units are in UTM coordinates ($\times 10^3$ m)	28
3.2	(a) Sea level pressure (hPa); (b) 850 hPa temperature ($^{\circ}\text{C}$); (c) 850 hPa geopotential height (m); and (d) 500 hPa geopotential height (m), all for 17 July 1985 at 1200Z (0400 PST). Small rectangle in southeast quarter of each plot identifies modelling domain.	31
3.3	(a) Sea level pressure (hPa); (b) 850 hPa temperature ($^{\circ}\text{C}$); (c) 850 hPa geopotential height (m); and (d) 500 hPa geopotential height (m), all for 18 July 1985 at 1200Z (0400 PST). Small rectangle in southeast quarter of each plot identifies modelling domain.	32
3.4	(a) Sea level pressure (hPa); (b) 850 hPa temperature ($^{\circ}\text{C}$); (c) 850 hPa geopotential height (m); and (d) 500 hPa geopotential height (m), all for 19 July 1985 at 1200Z (0400 PST). Small rectangle in southeast quarter of each plot identifies modelling domain.	33

3.5	(a) Sea level pressure (hPa); (b) 850 hPa temperature (°C); (c) 850 hPa geopotential height (m); and (d) 500 hPa geopotential height (m), all for 20 July 1985 at 0000Z (19 July at 1700 PST). Small rectangle in southeast quarter of each plot identifies modelling domain.	34
3.6	(a) Sea level pressure (hPa); (b) 850 hPa temperature (°C); and (c) 500 hPa geopotential height (m), all for 21 July 1985 at 1200Z (0400 PST). Small rectangle in southeast quarter of each plot identifies modelling domain.	36
3.7	Hourly temperature (solid lines) and wind vectors (arrows) at (a) YVR and (b) YXX, 16-21 July 1985.	37
3.8	Modelling domain, as delineated by thick, solid lines. Coastline and 100 m contours depicted by thin, solid lines and dotted lines, respectively.	40
4.1	Surface (level 1) wind fields prepared for UAM at (a) 0900 PST and (b) 1500 PST, 17 July 1985. Vector length is proportional to wind speed. Observations shown by thick arrows. Wind speeds in m/s.	48
4.2	Surface (level 1) wind fields prepared for UAM at (a) 0900 PST and (b) 1500 PST, 18 July 1985. Vector length is proportional to wind speed. Observations shown by thick arrows. Wind speeds in m/s.	49
4.3	Surface (level 1) wind fields prepared for UAM at (a) 0900 PST and (b) 1500 PST, 19 July 1985. Vector length is proportional to wind speed. Observations shown by thick arrows. Wind speeds in m/s.	50
4.4	Mixed layer depth at sites in Delta (top panel), Surrey (middle panel) and Queen Elizabeth Park (QEP) (lower panel), Vancouver. Lines depict predicted values; circles show observed data.	51

4.5	(a) VOC and (b) NO _x emissions (in t/d) from mobile sources in the LFV. Washington sources were not included.	57
4.6	Annual (a) VOC and (b) NO _x emissions (in t/y) from point sources in the LFV. Circles denote point source emissions. Circle diameter is proportional to emissions.	59
4.7	VOC emissions (in t/d) from gasoline marketing sources in the LFV. Sources from Washington were not included.	60
4.8	(a) VOC and (b) NO _x emissions (in t/d) from area sources in the LFV. Washington sources were not included.	62
5.1	Predicted and observed O ₃ concentrations at stations T02, T03, T04 and T05 in the LFV, 17-19 July 1985. Solid lines represent predicted concentrations and hatched lines show the range in neighbouring grid cells. Open circles indicate observations.	68
5.2	Predicted and observed O ₃ concentrations at stations T07, T09 and T14 in the LFV, 17-19 July 1985. Solid lines represent predicted concentrations and hatched lines show the range in neighbouring grid cells. Open circles indicate observations.	69
5.3	Predicted and observed O ₃ concentrations at stations T15, T16, T11 and T12 in the LFV, 17-19 July 1985. Solid lines represent predicted concentrations and hatched lines show the range in neighbouring grid cells. Open circles indicate observations.	70
5.4	Contours of predicted O ₃ at 20 ppb intervals on 17 July 1985 at (a) 0900 PST, (b) 1200 PST, (c) 1500 PST and (d) 1800 PST. Large numbers indicate observed concentrations. Missing values are indicated by "-99".	72

5.5	Contours of predicted O ₃ at 20 ppb intervals on 18 July 1985 at (a) 0900 PST, (b) 1200 PST, (c) 1500 PST and (d) 1800 PST. Large numbers indicate observed concentrations. Missing values are indicated by "-99".	74
5.6	Contours of predicted O ₃ at 20 ppb intervals on 19 July 1985 at (a) 0900 PST, (b) 1200 PST, (c) 1500 PST and (d) 1800 PST. Large numbers indicate observed concentrations. Missing values are indicated by "-99".	76
5.7	Comparison of predicted vs. observed O ₃ concentrations (above) and comparison of residual (predicted-observed) vs. observed O ₃ concentrations (below), all sites 17-19 July 1985.	81
5.8	Predicted and observed NO ₂ concentrations at stations T02, T03, T04 and T05 in the LFV, 17-19 July 1985. Solid lines show predicted values. Open circles indicate observed data.	85
5.9	Predicted and observed NO ₂ concentrations at stations T07, T09 and T14 in the LFV, 17-19 July 1985. Solid lines show predicted values. Open circles indicate observed data.	86
5.10	Predicted and observed NO ₂ concentrations at stations T15, T16, T11 and T12 in the LFV, 17-19 July 1985. Solid lines show predicted values. Open circles indicate observed data.	87
5.11	Contours of predicted NO ₂ at 20 ppb intervals on 17 July 1985 at (a) 0900 PST, (b) 1200 PST, (c) 1500 PST and (d) 1800 PST. Large numbers indicate observed concentrations.	88
5.12	Contours of predicted NO ₂ at 20 ppb intervals on 18 July 1985 at (a) 0900 PST, (b) 1200 PST, (c) 1500 PST and (d) 1800 PST. Large numbers indicate observed concentrations.	90

5.13	Contours of predicted NO ₂ at 20 ppb intervals on 19 July 1985 at (a) 0900 PST, (b) 1200 PST. (c) 1500 PST and (d) 1800 PST. Large numbers indicate observed concentrations.	92
5.14	(a) Comparison of predicted vs. observed O ₃ concentrations, and (b) comparison of residual (predicted-observed) vs. observed O ₃ concentrations, all sites 17-19 July 1985.	95
5.15	Sensitivity indicators based on predictions at stations T02, T03 and T05. Triangles show values for 18 July, diamonds for 19 July.	104
5.16	Sensitivity indicators based on predictions at stations T07, T09 and T14. Triangles show values for 18 July, diamonds for 19 July.	105
5.17	Sensitivity indicators based on predictions at stations T15, T11 and T12. Triangles show values for 18 July, diamonds for 19 July.	106

Acknowledgments

Throughout this project, I have benefited from the help of many people to whom I am deeply grateful. First and foremost, I would like to thank Dr. Douw Steyn, my supervisor, for being a constant source of ideas and encouragement, and for refusing to give up on me. I would also like to thank my other committee members, Dr. Tim Oke and Dr. Ian McKendry, who provided useful comments on my draft thesis.

Special thanks go to Dr. Xiaoming Cai who was responsible for the meteorological fields used in my simulations; Bruce Thomson of Environment Canada who provided support in carrying out this work and who continues to carry the torch in terms of airshed modelling in the Lower Fraser Valley; Dr. Don Singleton (NRC), Dr. Rob McLaren (York University) and Sue Boehme (NRC) for providing assistance in the development of the emissions input files; and Al Percival of the Greater Vancouver Regional District for providing the air quality data.

Vincent Kujala and Jim Mintha provided valuable assistance in sorting out my computer woes. Paul Jance was responsible for the one great map in this document. Additional thanks go to the staff of the Air Resources Branch, Ministry of Environment, Lands and Parks, and particularly to Dr. Richard Bennett and Hu Wallis, for their encouragement and understanding.

Finally, I would like to thank my family, and in particular, my husband Roy Hourston, for being a constant source of encouragement and the calm in the eye of the storm - I couldn't have done it without you!

Chapter 1

Introduction

Ozone (O_3) is a colourless and reactive gas that is found in trace amounts in the atmosphere. In the troposphere, it is formed during the reaction of nitrogen oxides (NO_x) and volatile organic compounds (VOCs) in the presence of sunlight (Haagen-Smit, 1952). It is known to affect enzyme systems in the lungs and to cause a decrease in pulmonary function (Rowe *et al.*, 1983; Bates and Vedal, 1994; Brauer and Brook, 1997), to cause foliar injury to vegetation (*e.g.* Runeckles and Chevone, 1992; Lefohn *et al.*, 1997; Treshow and Anderson, 1989; Wright, 1988)), and to cause the rapid degradation of materials such as rubber.

The current Maximum Acceptable National Air Quality Objective (NAAQO) for O_3 is 82 ppb. Between 1984-1992, exceedances of this objective in the Lower Fraser Valley (LFV) of British Columbia (BC) occurred on 8.5% of all days during the months of July-September. Due to the periodically unacceptable levels of O_3 in the LFV, the region was designated as one of three O_3 non-attainment areas under the national NO_x /VOC Management Plan (CCME, 1990) and required to submit interim targets for emission caps to reduce O_3 concentrations. The South Atlantic Region and the Windsor-Quebec City Corridor were the other two designated non-attainment areas.

Relative to the eastern non-attainment zones, the LFV is isolated from other source regions by virtue of local topography. As shown in Figure 1.1, the LFV is a funnel-shaped valley, beginning near the town of Hope and spreading westward to the Strait of Georgia, approximately 120 km away. The LFV is enclosed to the north by the Coast

Mountains, and to the southeast by the Cascade Mountains. The northern valley walls are punctuated by a series of north-south tributary valleys.

The LFV has a current population of roughly 2 million persons which is growing rapidly at a rate of approximately 0.04 million per year (GVRD, 1994). The major population centre is the City of Vancouver, which lies on the western edge of the LFV. However, much of the current growth is occurring in areas to the east of Vancouver. Associated with the growth in population is an increase in the number of motor vehicles. Recent estimates indicate that motor vehicles in the LFV contribute roughly 80% of pollutants associated with O₃ formation (GVRD, 1994).

While the population and its associated activities influence pollutant emissions, the physical environment in which the LFV is situated has a profound influence on local circulation patterns, and, hence, on the transport of pollutants within the valley. Under certain synoptic conditions, temperature differences between the Strait of Georgia and the adjacent land surface give rise to daytime sea breezes and nighttime land breezes in the LFV (Emslie, 1968; Hay and Oke, 1985; CSC, 1982; Steyn and Faulkner, 1986; Steyn et al., 1990; Miao, 1993, Cai and Steyn, 1995). The differential heating and cooling between valley walls and valley floor may also give rise to slope and drainage winds (Hay and Oke, 1985; Mass, 1982). The so-called "chimney effect", in which pollutants are vented along heated valley walls, has been shown to contribute to the development of polluted layers aloft (McKendry et al., 1997). The role of tributary valleys in providing a cleansing mechanism has also been observed, in which daytime up-valley flows carrying O₃-rich air are followed by nocturnal downslope flows characterized by low O₃ concentrations (Banta et al., 1997).

Under stagnant conditions, these thermally induced winds may result in the recirculation and buildup of O₃ and its precursors to unsatisfactory levels. Steyn et al. (1990) characterized such an episode which took place between 1-3 September 1988. On 3

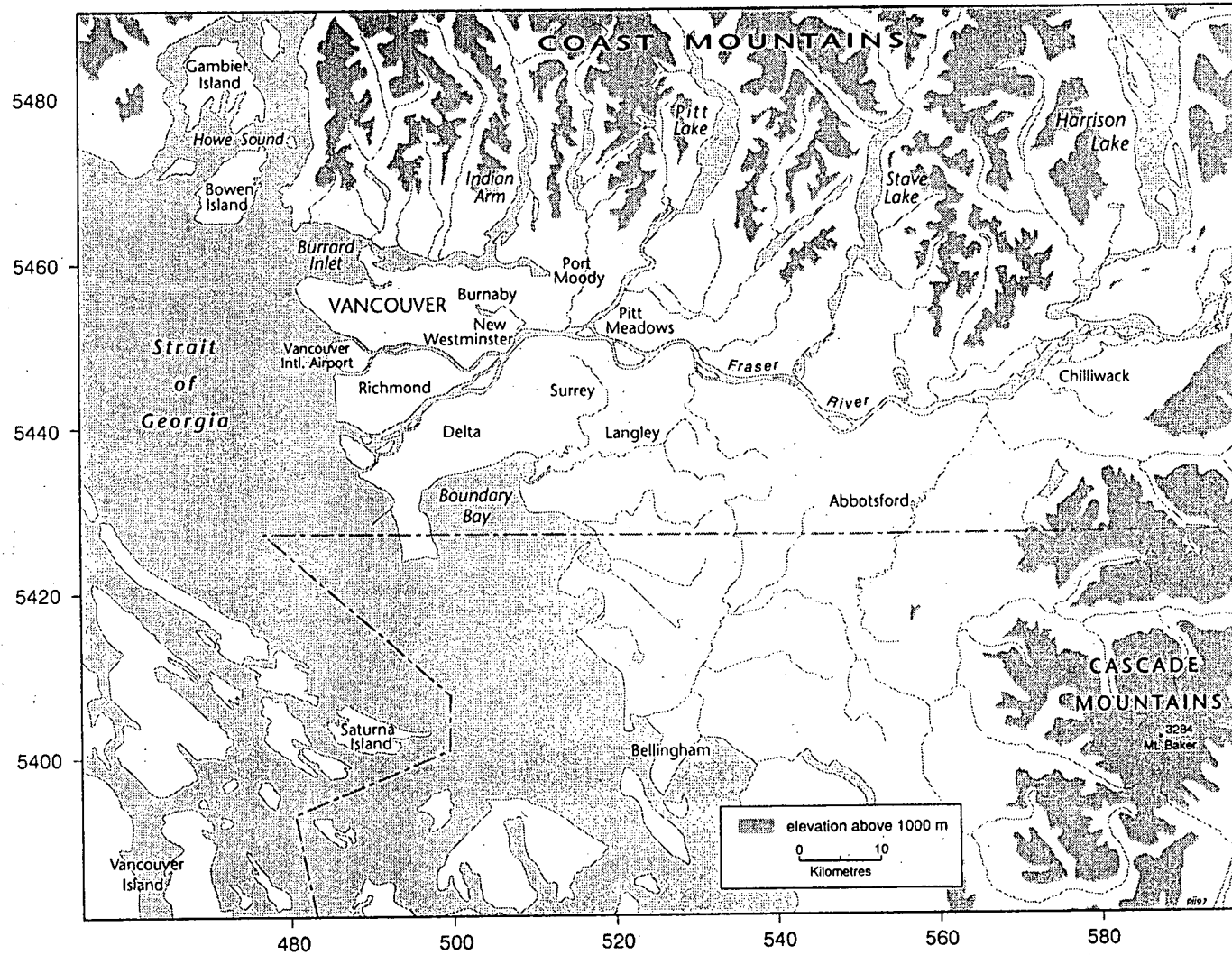
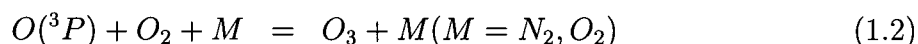
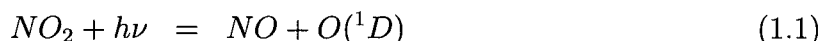


Figure 1.1: Map of the Lower Fraser Valley showing topography, coastline, major population centres and geographical features.

September, a maximum one-hour O_3 concentration of 213 ppb was recorded. This was one of the highest O_3 concentrations ever recorded in Canada. Pacific'93 (Steyn et al., 1997) represented an intensive field study conducted during the summer of 1993 to better understand the chemical and physical factors, at the surface and aloft, which contribute to O_3 episodes in the LFV.

Because O_3 is predominantly a secondary product in the troposphere, its control is achieved through the control of its precursors, NO_x and VOCs. However, a very non-linear relationship exists between O_3 and its precursors. The fundamental reactions involved in the photochemical formation of O_3 are as follows (from NRC, 1991):



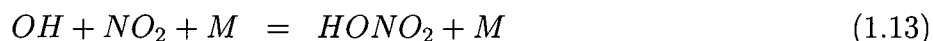
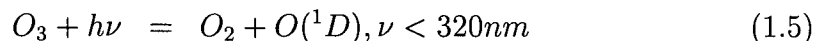
Here, the production of NO_2 requires the consumption of O_3 . Hence, in the absence of other species to enhance the NO -to- NO_2 conversion, a photostationary state is assumed, in which the concentration of O_3 can be estimated as

$$[O_3] = j_1[NO]/k_2[NO] \quad (1.4)$$

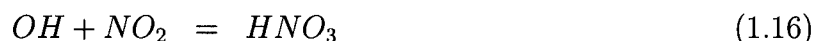
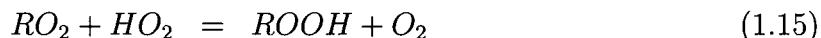
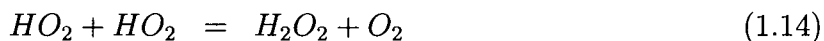
where j_1 is the photodissociation constant for reaction 1.1 and k_2 is the rate constant for reaction 1.3.

In the polluted troposphere, odd-hydrogen species play a key role in enhancing the conversion of NO to NO_2 . These species include: the hydroxyl radical (OH), the hydrogen peroxy radical (HO_2) and the organic peroxy radical (RO_2). The hydroxyl radical is formed through the photolysis of O_3 and the subsequent reaction of $O(^1D)$ with water vapour. The peroxy radicals are predominantly formed through the photolysis of

aldehydes and other intermediate VOCs. The reactions are summarized as follows:



Major sinks of the odd-hydrogen species include the following:



The formation of peroxyacetyl nitrate (PAN) is another potential sink, particularly in urban environments.

The numerous competing reactions reflect the fact that the relationship between O_3 and its precursors is highly nonlinear. Isoleths of constant O_3 concentrations plotted for various mixtures of VOCs and NO_x (e.g. NRC, 1991) show that reductions in NO_x levels at constant VOC concentrations may result in higher or lower O_3 levels, depending on whether the environment is VOC- or NO_x -limited. To add to the complexity, these conditions will vary both temporally and spatially within a single airshed.

Two fundamentally different approaches can be taken to determine whether NO_x or VOC reductions are the most effective means of controlling O₃ levels: (i) an observation-based approach and (ii) an emission-based approach, utilizing photochemical air models.

The observation-based approach utilizes atmospheric observations at a given site to determine the sensitivity of real air masses to changes in O₃ precursors. Applications range in complexity from comparing these observations to expected values, to using the observations as inputs to a photochemical model.

The simplest techniques utilize ambient concentrations of individual species, or the ratio of different species which consistently assume different values depending on whether the conditions are NO_x- or VOC-sensitive. These species or ratios of species are referred to as sensitivity indicators. Examples are the VOC-to-NO_x ratio, total nitrogen (NO_y) concentration, formaldehyde (HCHO) to NO_y ratio, O₃-to-NO_z ratio (where NO_z=NO_y-NO_x) and hydrogen peroxide (H₂O₂) to nitric acid (HNO₃) ratio. Each is described in the following.

The VOC-to-NO_x ratio is an obvious indicator to describe how reductions in VOC and NO_x emissions affect O₃ concentrations. The transition between VOC-sensitive and NO_x-sensitive conditions typically occurs near a VOC-to-NO_x ratio of about 8:1 (NRC, 1991). NO_x-limited conditions occur at lower values while VOC-limited conditions occur at higher values. In practice, ratios obtained from measurements taken in the early morning (*e.g.* 0600-0900 LAT) at the urban centre are typically used. Milford et al. (1990) expressed the following concerns with this approach:

- The air mass sampled in the urban centre during the morning may not be the one that produces peak O₃ concentrations later in the day and further downwind.
- Contributions from precursor sources after the sampling period are ignored.
- The reactivity of the VOC mixture is not considered.

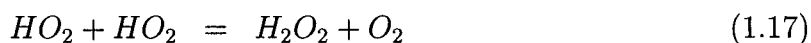
- Urban plumes tend to shift from VOC-sensitive to NO_x-sensitive as they move downwind because NO_x becomes depleted more quickly than VOCs.

NO_y includes all nitrogen species which can be converted into NO_x during photochemical activity: NO_x, PAN, HNO₃, nitrous acid (HONO), all organic nitrates and nitrate radicals. It can therefore be viewed as a NO_x reservoir. Unlike NO_x, which is relatively short-lived, NO_y has a similar lifetime as O₃. Studies have shown that where afternoon NO_y is greater than 20 ppb, conditions are VOC-sensitive (Milford et al., 1989; Rao et al., 1993; Sillman et al., 1993; Milford et al., 1994). A limitation with respect to this indicator is the difficulty in measuring NO_y.

A reactivity-weighted alternative to the VOC-to-NO_x ratio is the ratio of HCHO to NO_y. Formaldehyde is readily photolysed, yielding by-products which react to form odd-hydrogen species. As such, the HCHO-to-NO_y ratio is a much better indicator of O₃ sensitivity than the VOC-to-NO_x ratio. Studies indicate that a transition from VOC- to NO_x-sensitive conditions occurs near ratios of 0.28 (Sillman, 1995).

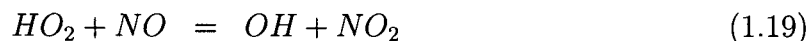
The photolysis of O₃ is another major source of odd-hydrogen species. As the concentration of aldehydes generally increases with O₃ concentration, it may be assumed that the source of odd-hydrogen species is proportional to O₃. NO_z represents the reaction products of NO_x. Hence, the ratio of O₃-to-NO_z may be used to describe the transition from NO_x- to VOC-sensitive chemistry. Sillman (1995) reported this transition near a ratio of 7, where values less than 7 represent VOC-sensitive conditions.

The ratio of H₂O₂-to-HNO₃ represents the competition between reactions 1.17 and 1.18 for odd hydrogen.

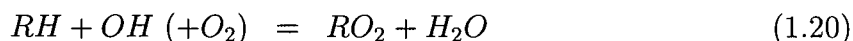


Both H₂O₂ and HNO₃ are major sinks of odd hydrogen. Where H₂O₂ dominates, OH

(and therefore O_3) increases with increasing NO_x :



and decreases with increasing VOCs:



Where HNO_3 dominates, OH (and therefore O_3) decreases with increasing NO_x . The transition from NO_x to VOC-sensitive chemistry occurs near ratios of 0.3-0.5 (Sillman, 1995).

While sensitivity indicators can provide guidance on which precursor should be reduced to attain the most efficient reduction in O_3 levels, they cannot provide a quantitative estimate of what that change will be, nor can they predict how the changes will vary spatially over an entire airshed. For that, it is necessary to employ a photochemical model which can represent the pertinent physical and chemical processes in the atmosphere which affect ozone concentrations.

Photochemical models were first developed in the early 1970's, in response to the passage of the Clear Air Act Amendments in the United States. These amendments established provisions for uniform national air quality standards and ordered states to develop abatement programs to meet these standards. Modelling became a necessary tool to demonstrate attainment.

There are three basic types of photochemical model: (i) box models, (ii) trajectory (Lagrangian) models, and (iii) grid-based (Eulerian) models. Seinfeld (1988) provides an overview of each model type.

Box models are the most simplistic, as they treat the domain as a single cell. The ground and the inversion height represent the lower and upper boundaries. Emissions are assumed to mix uniformly and instantaneously throughout the domain. A characteristic

wind is specified, and the inversion height is allowed to vary with time, thereby providing a ventilation mechanism for the domain.

Lagrangian models follow a single column of air that is advected by the mean horizontal wind. The column is defined by the ground and the inversion height, and may be divided into vertical layers. Emissions are injected into the column as it passes over emission sources. Chemical transformations, removal processes and vertical diffusion can be simulated.

In Eulerian models, the domain is divided into a number of grid cells. The governing equations representing atmospheric processes are then solved for each grid cell. Eulerian models typically require more detailed input data and greater computer resources than the other two model types. However, they are the only models that can predict the temporal and spatial variations in pollutant patterns in a three-dimensional domain. Hence, Eulerian models are best-suited for urban air quality studies such as in the LFV where a prognostic capability is required. Major Eulerian photochemical models in use in North America include the following: Urban Airshed Model Version IV (UAM-IV) (Morris and Myers, 1990); UAM-V (Haney et al., 1990); CIT (McRae et al., 1982; McRae and Seinfeld, 1983); California Air Resources Board airshed model (CALGRID) (Yamartino et al., 1992); the Regional Acid Deposition Model (RADM) (Chang et al., 1987); and the Regional Oxidant Model (ROM) (Lamb, 1983).

Within the LFV, the use of two different photochemical models has been recently reported. The CALGRID model was used in conjunction with the Mesoscale Compressible Community Model (MC2) to evaluate model performance for an O₃ episode occurring between 17-21 July 1985 (Hedley and Singleton, 1997; Hedley et al., 1997) and to evaluate the effectiveness of various alternative fuel scenarios (Hedley et al., 1996). Systems Applications International applied the UAM-V to evaluate model performance for the same July 1985 episode (Lolk et al., 1995) and to evaluate emission control scenarios

Table 1.1: UAM Applications

Location	References
Atlanta Baton Rouge Denver Los Angeles Basin Netherlands New York Santa Barbara/Ventura Co. St. Louis/ Philadelphia Tokyo, Japan	Morris et al. (1990a) Haney et al. (1990) Dennis and Downton (1984) SCAQMD (1990) Bultjes and Reynolds (1982) Rao et al. (1987) Tesche and McNally (1991) Morris et al. (1990b) Wakamatsu et al., (1990)

for BC Hydro (Haney, 1997).

In this research, the UAM-IV will be used. It is the preferred model for O₃ regulatory analysis in the United States, as specified by the U.S. Environmental Protection Agency (U.S. EPA). It has been used extensively throughout the United States and in other countries, as shown in Table 1.1.

This research was begun in parallel with the CALGRID application in the LFV. While it represents a less advanced treatment than the UAM-V or CALGRID models, the UAM-IV is an established model which has been well-documented. Although not the purpose of this research, this study provides further reinforcement of the findings obtained in the other modelling applications in the LFV.

1.1 Research Objectives

The goal of this research is to apply the UAM-IV to the LFV. Model performance will be evaluated in terms of the ability of the model to recreate an historical O₃ episode. Established statistical parameters will be applied to assess the results. Sensitivity indicators will also be calculated from model output as a further means of assessing model performance.

1.2 Methodology

The first step will be the selection of an historical multi-day ozone episode to be modelled. This will be followed by model domain selection, which is dependent on the circulation patterns observed or expected during the episode as well as the important sources that are to be included in the study. Episode and domain selection will then define the meteorological, emissions and air quality data required by the model, including the spatial and temporal scales to be used. The model will be run to simulate the historical episode, and predicted O₃ and NO₂ concentrations compared against observed values. Model performance will be characterized in terms of the acceptable range of statistical performance indicators established from a review of other modelling studies. Finally, the model results will be compared with established indicators to assess the sensitivity of the modelled airshed to VOC and NO_x.

1.3 Thesis Outline

In Chapter 2, the theory behind the UAM-IV is presented. Individual modules comprising the model are described.

In Chapter 3, the characteristics of the selected O₃ episode and a description of the modelling domain are presented. The preparation of model input files to describe the

meteorology, emissions and air quality during the episode is described in Chapter 4.

Model results are compared against observational data in Chapter 5. Model performance is characterized based on the ability of the model to predict spatial and temporal variations in O₃ and NO₂ concentrations. Sensitivity indicators calculated based on model results are also presented. Major findings are summarized in Chapter 6.

Chapter 2

Technical Description of Models

Although the focus of this study is the application of UAM-IV, additional models have been used by others to produce meteorological fields and emission estimates. In the following, a detailed description of the UAM and its modelled processes will be followed by brief descriptions of the mesoscale model, CSU-RAMS, and the models used to estimate source emissions.

2.1 Urban Airshed Model

The development of the UAM dates back to 1969 when the National Air Pollution Control Administration (NAPCA), a predecessor of the U.S. EPA, contracted with Systems Applications Inc. (SAI) to develop an air quality model which could be used to assess urban O_3 and to evaluate control strategies for abatement programs. An overview of model development is provided by Scheffe and Morris (1993).

2.1.1 Governing Equations

The UAM simulates the physical and chemical fate of inert or chemically reactive species in the atmosphere through solution of the species continuity equation:

$$\begin{aligned} \frac{\delta c_i}{\delta t} = & \\ & - \frac{\delta(u \cdot c_i)}{\delta x} - \frac{\delta(v \cdot c_i)}{\delta y} - \frac{\delta(w \cdot c_i)}{\delta z} \\ & + \frac{\delta}{\delta x} \left(K_H \frac{\delta c_i}{\delta x} \right) + \frac{\delta}{\delta y} \left(K_H \frac{\delta c_i}{\delta y} \right) + \frac{\delta}{\delta z} \left(K_V \frac{\delta c_i}{\delta z} \right) \end{aligned}$$

$$+ R_i + S_i + L_i \quad (2.21)$$

where

c_i is the concentration of species i which has been averaged spatially (x, y, z) over the volume of a grid cell and temporally (t) over the interval of an integration time step;

u , v and w are wind velocities in the x , y and z directions, respectively;

K_H and K_V are horizontal and vertical eddy diffusivities;

R_i is net rate of production of species i by chemical reactions;

S_i is emission rate of species i ; and

L_i is net rate of removal of species i by dry deposition.

By assuming that the chemical species do not alter the meteorology to any significant degree, Equation 2.21 can be solved independently of the coupled Navier-Stokes and energy equations (Reynolds et al., 1974). Due to the presence of nonlinear terms in the equation, a numerical solution is required. To facilitate the use of finite difference methods, the vertical dimension is normalized to an independent variable ρ :

$$\rho = \frac{z - H_b(x, y, t)}{H_t(x, y, t) - H_b(x, y, t)} \quad (2.22)$$

where H_b and H_t are the elevations of the surface and top of the domain, respectively.

Upon transformation of vertical coordinate z to ρ , and after neglecting cross-derivative diffusion terms which are assumed to be negligibly small, Equation 2.21 becomes

$$\begin{aligned} \frac{\delta}{\delta t}(\Delta H \cdot c_i) + \frac{\delta}{\delta x}(u \cdot \Delta H \cdot c_i) + \frac{\delta}{\delta y}(v \cdot \Delta H \cdot c_i) + \frac{\delta}{\delta \rho}(W \cdot c_i) = \\ \frac{\delta}{\delta x}(K_H \Delta H \frac{\delta c_i}{\delta x}) + \frac{\delta}{\delta y}(K_H \Delta H \frac{\delta c_i}{\delta y}) + \frac{\delta}{\delta \rho}(K_V \frac{\delta c_i}{\Delta H \delta \rho}) + \\ + R_i \Delta H + S_i \Delta H \end{aligned} \quad (2.23)$$

where

$$W = w - u\left(\frac{\delta H_b}{\delta x} + \rho\frac{\delta\Delta H}{\delta x}\right) - v\left(\frac{\delta H_b}{\delta y} + \rho\frac{\delta\Delta H}{\delta y}\right) - \rho\frac{\Delta H}{\delta t} \quad (2.24)$$

and

$$\Delta H = H_t(x, y, t) - H_b(x, y, t) \quad (2.25)$$

As noted by Reynolds et al. (1974), Equation 2.23 is an approximate equation as opposed to the fundamental equation governing the dynamic behaviour of pollutants in the atmosphere. Its application is subject to the following limitations:

- the time resolution Δt is large compared with the Lagrangian time scale of turbulence;
 - gradients in the mean velocity field;
 - gradients in the mean turbulence velocity correlations;
 - gradients in the source emission rates;
 - changes in the rate of production or depletion of a species by chemical reactions.
- the average distance that a fluid particle travels in Δt is small compared with the characteristic spatial scales for
 - gradients in the mean velocity field;
 - gradients in the mean turbulence velocity correlations;
 - gradients in the source emission rates.

Based on data obtained in the Los Angeles Basin, Reynolds *et al.* (1974) found that Equation 2.23 was applicable for perturbations in the concentration field with horizontal scales greater than 2 km, vertical scales greater than 20 m, and temporal scales greater than 10^3 s.

Equation 2.23 is solved using the method of time-splitting, or fractional steps, as proposed by Yanenko (1971). During each time step, the equation is solved for

1. advection/diffusion in the x -direction;
2. advection/diffusion in the y -direction;
3. injection of pollutant emissions and advection/diffusion in the z -direction;
4. chemical transformations.

The master or advection time step is determined based on grid size and maximum wind speed. To maintain numerical stability, the chemistry and vertical diffusion time steps must be an integral portion of the advection time step.

2.1.2 Modelled Processes

The mechanisms used to describe the transport, removal and chemical transformation of pollutants in the atmosphere are presented in the following.

2.1.3 Advection

The horizontal dispersion of pollutants is primarily through advection. The advective part of Equation 2.23:

$$\frac{\delta}{\delta t}(\Delta H \cdot c_i) + \frac{\delta}{\delta x}(u \cdot \Delta H \cdot c_i) = 0 \quad (2.26)$$

and

$$\frac{\delta}{\delta t}(\Delta H \cdot c_i) + \frac{\delta}{\delta y}(v \cdot \Delta H \cdot c_i) = 0 \quad (2.27)$$

is solved using the Smolarkiewicz scheme (1983), which is a positive definite upstream scheme reported to be less diffusive and more computationally efficient than the SHASTA scheme (Boris and Book, 1973) applied in previous versions of the UAM. A detailed description of this scheme is provided in Morris and Myers (1990).

2.1.4 Turbulent Diffusion

The diffusive part of Equation 2.23:

$$\frac{\delta}{\delta t}(\Delta H \cdot c_i) = \frac{\delta}{\delta x}(K_H \Delta H \frac{\delta c_i}{\delta x}) \quad (2.28)$$

is solved using an explicit finite difference method. Turbulent fluxes are parameterized using a closure approximation frequently referred to as either gradient transport theory or K-theory, where it is assumed that turbulent fluxes are proportional to local gradients. The proportionality constant (K_H in the horizontal; K_V in the vertical) is known by a variety of names, including eddy viscosity and eddy diffusivity.

K_H and K_V are difficult to measure. Given that in the horizontal, advection generally dominates over diffusion, a nominal constant value of $50 \text{ m}^2 \cdot \text{s}^{-1}$ is given to K_H . Greater care is given to the treatment of K_V , as diffusion often dominates over advection in the vertical. K_V is calculated as a function of stability class, ground-level wind speed, reference height, surface roughness and height of the grid cell. For stable conditions,

$$K_V = \frac{(ku_* z) \exp(-\frac{|v_g| fz}{|u_*| u_*})}{1 + 4.7 \frac{z}{L}} \quad (2.29)$$

for neutral conditions where $0 < z \leq 0.45 \frac{u_*}{f}$,

$$K_V = \frac{u_*^2}{f} (\alpha_0 + \alpha_1 \lambda^2 + \alpha_3 \lambda^3 + \alpha_4 \lambda^4) \quad (2.30)$$

for neutral conditions where $z > 0.45 \frac{u_*}{f}$,

$$K_V = 0.01 m^2/s \quad (2.31)$$

and for unstable conditions:

$$K_V = w_* z_i \beta_0 + \beta_1 \zeta + \beta_2 (2\zeta^2 - 1) + \beta_3 (4\zeta^3 - 3\zeta) + \beta_4 (8\zeta^4 - 8\zeta^2 + 1) \quad (2.32)$$

where

$$\lambda = \frac{zf}{u_*},$$

$$\zeta = 2 \frac{z}{z_i} - 1,$$

$$w_* = u_* - \left(\frac{1}{k} \frac{z_i}{L}\right)^{1/3},$$

f =Coriolis parameter,

k =von Karman constant,

u_* =friction velocity,

z_i =inversion height,

v_g =geostrophic wind component,

L =Monin-Obukhov length,

and the coefficients α_i and β_i are

$$\alpha_0 = 7.396 \times 10^{-4} \quad \beta_0 = 0.152$$

$$\alpha_1 = 6.082 \times 10^{-2} \quad \beta_1 = 0.080$$

$$\alpha_2 = 2.532 \quad \beta_2 = -0.039$$

$$\alpha_3 = -1.272 \times 10 \quad \beta_3 = 0.032$$

$$\alpha_4 = 1.517 \times 10 \quad \beta_4 = 0.020$$

For lapse rates less than $-0.011^\circ\text{C}/\text{m}$ above the mixing layer, Equation 2.30 or Equation 2.31 for neutral conditions is used. Otherwise, if neutral or unstable conditions are present in the lower levels, then K_V aloft is set to 0.01 m^2 . If stable conditions are present in the lower levels, then K_V aloft is calculated using Equation 2.29.

2.1.5 Surface Removal Processes

Dry deposition is the only surface removal process treated in the UAM. It is treated as a three-stage process:

1. transport of pollutants through the atmosphere to just above the surface;
2. transport of pollutants to the actual surface;
3. uptake of the pollutants by vegetation or surface material through absorption, adsorption or chemical reaction.

The UAM utilizes a deposition velocity concept, in which the deposition velocity V_{di} is inversely proportional to the sum of the resistance to transport R_t and the resistance to surface removal R_{si} :

$$V_{di} = \frac{1}{R_t + R_{si}} \quad (2.33)$$

R_t is a function of wind velocity at 10m elevation and friction wind velocity, while R_{si} is a function of pollutant and surface types. The deposition velocity is then related to the uptake flux F_{di} by the following equation:

$$F_{di} = V_{di} \cdot C_{gi} \quad (2.34)$$

where C_{gi} is the ground level concentration of species i . A more detailed description of the parameterization of surface removal processes is given in Killus (1984).

2.1.6 Chemical Processes

Chemical transformations taking place in the atmosphere are described by a chemical kinetic mechanism. This mechanism is comprised of a set of reactions and associated rate constants in the form of coupled ordinary differential equations.

To explicitly model all the pertinent species and reactions taking place in the atmosphere would require a prohibitive number of computations and CPU time. In fact, Peters et al. (1995) report that the integration of chemical rate equations can consume as much as 98% of the total CPU time in Eulerian modelling simulations. Two major approaches have been developed to reduce the number of hydrocarbon species which are included in the chemical mechanism: the lumped molecule approach and the lumped structure approach. The former method organizes hydrocarbons using molecular surrogates. Examples are the SAPRC mechanism (Carter, 1990) which is used in the CALGRID photochemical model, and the Stockwell mechanism (Stockwell, 1990) which is used in the Regional Acid Deposition Model (Chang et al., 1987). The latter method disaggregates hydrocarbons on the basis of bond type. As this approach requires fewer chemical reactions, it is computationally more efficient. The Carbon Bond IV Mechanism (CBM-IV), which is used in the UAM, represents a lumped structure approach (Whitten et al., 1980; Gery et al., 1988, 1989).

Four types of species are considered in the CBM-IV:

- inorganic species which are treated explicitly: ozone, NO_x and HO_x chemistry;
- organic species which are treated explicitly:
 - formaldehyde, because it is formed in all oxidation reactions involving hydrocarbons and is very reactive;
 - ethene, because it constitutes a large fraction of hydrocarbon emissions, is unusually unreactive for an alkene, and yields a high percentage of formaldehyde under most conditions;
 - isoprene, because it constitutes a large fraction of biogenic hydrocarbon emissions and is very reactive.

- organic species which are represented by carbon (C) bond surrogates:
 - paraffins: single C bonds;
 - olefins: C-C double bonds;
 - aldehydes: C-CHO bond and also 2-alkenes which tend to react very quickly to produce aldehyde products.
- organic species which are represented by molecular surrogates:
 - toluene: seven-C species used as surrogates for monoalkylbenzene structures;
 - xylene: eight-C species used as surrogates for dialkyl- and trialkylbenzenes.

The CBM-IV represents a condensed version of the CBM-EX which is described in Gery et al. (1988). CBM-EX is a more detailed mechanism that contains over 120 reactions.

A number of steps were carried out to condense this mechanism:

- eliminate unimportant reactions and products,
- create a universal peroxy radical, thereby eliminating many organic peroxy radicals,
- apply mathematical and algebraic manipulations to limit the number of reactions, and
- lump secondary reaction products, especially relating to isoprene chemistry.

The condensed version contains 33 state species, as shown in Table 2.1.

More than 80 reactions are included in the mechanism. Due to the wide range of rate constants involved, the differential equations describing the mechanism are referred to as a “stiff” system. To facilitate computations, quasi-steady state assumptions are used for the low-mass, fast-reacting (*i.e.* stiff) species. The Crank-Nicholson algorithm is applied to solution of the other state species.

Table 2.1: State species in CBM-IV

Species Name	Representation
nitric oxide	NO
nitrogen dioxide	NO2
nitrogen trioxide	NO3
dinitrogen pentoxide	N2O5
nitrous acid	HONO
nitric acid	HNO3
peroxynitric acid	PNA
oxygen atom (singlet)	O1D
oxygen atom (triplet)	O
hydroxyl radical	OH
water	H2O
ozone	O3
hydroperoxy radical	HO2
hydrogen peroxide	H2O2
carbon monoxide	CO
formaldehyde	FORM
high-molecular-weight aldehydes	ALD2
peroxyacyl radical	C2O3
peroxyacyl nitrate	PAN
paraffin carbon bond	PAR
secondary organic oxy radical	ROR
olefinic carbon bond	OLE
ethene	ETH
toluene	TOL
cresol and higher-molecular-weight phenols	CRES
toluene-hydroxyl radical adduct	TO2
methylphenoxy radical	CRO
high-molecular-weight aromatic oxidation ring fragment	OPEN
xylene	XYL
methylglyoxal	MGLY
isoprene	ISOP
NO-to-NO ₂ operator	XO2
NO-to-nitrate operator	XO2N

Dodge (1989, 1990) reviewed three chemical mechanisms used in photochemical models: CBM-IV, the Carter-Atkinson-Lurmann-Lloyd (CAL) mechanism (Carter et al., 1986; Lurmann et al., 1987) which is part of the SAPRC family of models, and a mechanism developed by Stockwell (1988) for use in RADM (Chang et al., 1987). Both the SAPRC and Stockwell mechanisms use a lumped molecule approach, although the latter utilizes a generalized organic species to represent similar organics. In general, Dodge found good agreement between the three mechanisms, and points out that this should be expected, since the developers relied on the same kinetic data evaluation sources during mechanism development. The major differences involve predictions under high levels of NO_x and aromatics, and at low temperatures. Of particular note, the CBM-IV consistently predicted lower concentrations of ozone at low temperatures.

Jefferies and Tonnesen (1994) compared results obtained using the SAPRC90 (Carter, 1990) and CBM-IV chemical mechanisms in a Lagrangian box model. Both mechanisms gave similar predictions of total reactivity and O_3 maxima. However, at low NO_x levels, the SAPRC90 mechanism was more reactive and produced higher O_3 maxima, while the CBM-IV mechanism produced more nitrate and became NO_x -limited earlier in the day.

2.1.7 Emissions

Emissions within an airshed originate from a wide range of sources, including point, area, mobile and biogenic sources. Methodologies used by others to develop emission estimates in the LFV are discussed in Chapter 4.

For the purposes of simulating these emissions within an Eulerian model such as the UAM, emissions data must be processed so that (i) spatial and temporal distributions reflect the simulation period, (ii) emissions are injected into the appropriate vertical grid cell, and (iii) organic species are attributed to the appropriate surrogate group.

The Emissions Preprocessor System Version 1.0 (EPS1.0) was developed to prepare

emission inventories that are compatible with the format required by the UAM (Causley, 1990). The spatial and temporal allocation of emissions and the chemical speciation are achieved by associating spatial, temporal and source codes with the appropriate distribution factors.

Emissions injected into a grid cell are mixed instantaneously throughout the cell. Ground-level emissions are input to the lowest level of grid cells. Elevated emissions are injected to the appropriate vertical cell corresponding to the total effective plume rise Δh_p , which is calculated by an emissions preprocessor using the algorithms recommended by Briggs (1971) and summarized in Morris and Myers (1990).

2.2 CSU-RAMS

The lack of an extensive wind monitoring network, the complexity of the terrain in the LFV, and the importance of mesoscale flows such as land/sea breezes and mountain/valley winds necessitated the use of a prognostic non-hydrostatic model. For these reasons, the Colorado State University Regional Atmospheric Modelling System (CSU-RAMS), hereafter referred to as RAMS, was chosen to generate the three-dimensional wind fields which are required by the UAM.

RAMS is a second-generation model to the CSU Mesoscale Model (CSUMM) developed by Pielke (1974). It is very flexible, representing a merging of three different atmospheric models: a non-hydrostatic cloud model and two hydrostatic mesoscale models (McNider and Pielke, 1981; Tremback et al., 1986; Tripoli and Cotton, 1982). It is based upon the full set of primitive dynamical equations, and includes optional parameterizations for such processes as turbulent diffusion, terrestrial radiation, and moist processes (Walko and Tremback, 1991). Solution of these equations is through finite difference methods. To improve the efficiency of numerical solutions, the Arakawa-C grid

stagger is employed.

RAMS has been applied in a number of studies in the LFV. Steyn and McKendry (1988) used a primitive version of RAMS to simulate meteorological fields in the LFV for 23 August 1985. Miao and Steyn (1994) simulated conditions on the same day using RAMS2a. Steyn and Cai (1994) applied RAMS2a to an O₃ occurring between 17-20 July 1985. Cai and Steyn (1995) repeated this simulation using the next-generation mode, RAMS3a.

Chapter 3

Episode and Domain Selection

Model performance is evaluated on the basis of its ability to replicate observed O₃ concentrations during a particular historical episode. Domain selection is dependent on defining the area of interest and then adjusting for the meteorological conditions during the episode which may affect airflow into and out of the region. Hence, both episode and domain selection must precede the preparation of model inputs, as they help define the air quality, emissions and meteorological databases to be used. In the following, the criteria and rationale for episode and domain selection are presented.

3.1 Episode Selection

An O₃ episode which occurred between 17-20 July 1985 was selected for further study. Episode selection was based on the following criteria (after Seinfeld, 1988):

- The episode exhibited elevated O₃ concentrations.
- The episode was a multi-day event.
- The episode was characteristic of typical O₃ episodes in the region.
- Satisfactory databases of aerometric, emissions and meteorological data were available to characterize the modelling domain during the episode.

A more detailed description of the episode and of the available data is provided in the following.

Table 3.1: Location of air quality monitoring sites in the LFV, 1985.

Station ID	Location	UTME (x 10 ³ m)	UTMN (x 10 ³ m)
T01	Downtown Vancouver	491.3	5458.7
T02	Kitsilano, Vancouver	488.2	5456.6
T03	Marpole	492.1	5450.4
T04	Kensington Park, Burnaby	502.1	5458.4
T05	Confederation Park, Burnaby	499.9	5459.0
T06	Second Narrows	598.5	5460.8
T07	Anmore	510.2	5461.9
T08	Lions Gate STP	490.3	5462.9
T09	Rocky Point Park, Pt. Moody	511.1	5458.4
T10	Eagle Ridge	512.9	5459.0
T11	Abbotsford Airport	545.5	5430.4
T12	Chilliwack Airport	576.8	5444.6
T13	North Delta	507.3	5445.0
T14	Burnaby Mountain	506.8	5458.3
T15	Surrey East	522.4	5442.2
T16	Pitt Meadows	521.7	5450.9

3.1.1 Data Availability

The GVRD and the B.C. Ministry of Environment, Lands and Parks (MELP) operate a relatively dense network of air quality monitors in the LFV. In July 1985, O₃ data were monitored at 16 sites as shown in Figure 3.1 and Table 3.1. The highest density of stations was found along Burrard Inlet, in the vicinity of major oil refineries. The spatial resolution of O₃ data in the central valley was and still is comparatively poor, although sites in Abbotsford, Chilliwack and, more recently, Hope provide valuable information on the eastern extent of O₃ episodes.

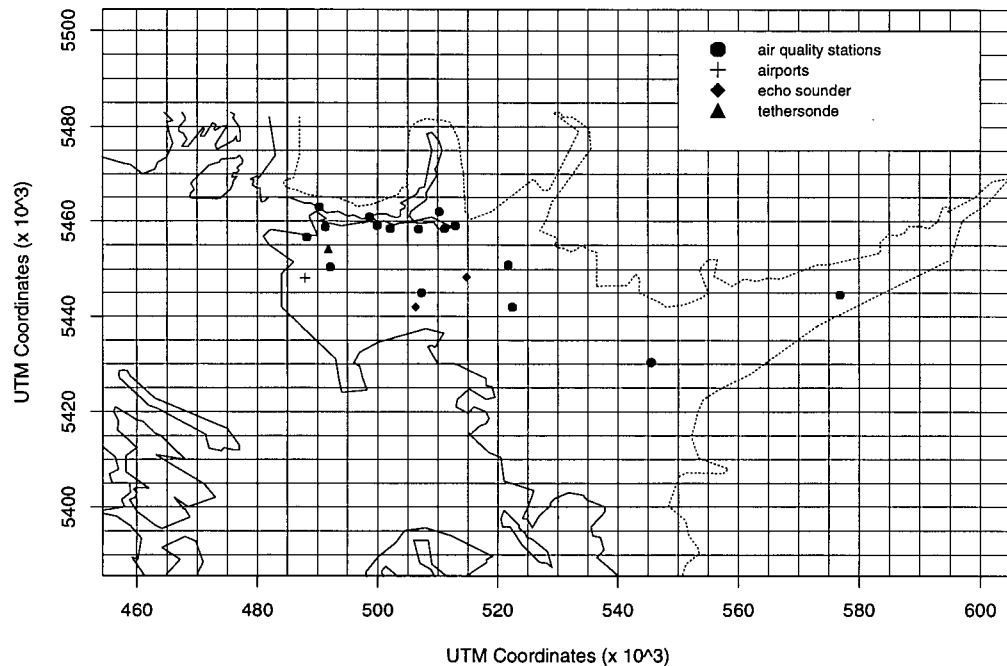


Figure 3.1: Map of LFV, showing location of air quality and meteorological monitoring sites present in July 1985. Coastline and 100 m contours are shown by solid and dashed lines, respectively. Units are in UTM coordinates ($\times 10^3$ m)

Temperature, humidity, cloud cover and wind data are regularly collected at the Vancouver International Airport (YVR), which is located along the coast, and Abbotsford International Airport (YXX), which is located in the central valley. Additional wind and temperature data are collected at some of the GVRD and MELP monitoring stations, as listed in Cai and Steyn (1995).

Augmenting the regularly available air quality and meteorological data are the following datasets obtained during or for 1985:

- an emissions inventory prepared for base year 1985 (GVRD, 1988);
- tethersonde data from Queen Elizabeth Park (QEP) in Vancouver for 17 and 19 July 1985, obtained as part of a study into the development of the mixed layer in

the Lower Mainland (Steyn and Wallis, 1986);

- back-trajectory analyses from three sites in the region for 17, 19 and 20 July 1985 (Coligado, 1988).

Such information is important for both model input preparation and model performance evaluation.

3.1.2 Characterization of a Typical Episode

Between May and September, the most prevalent synoptic regimes for surface O₃ events in southwestern British Columbia are persistent or slow-moving anticyclones which are eastward extensions of the North Pacific High (CSC, 1985). Anticyclones are generally associated with light winds and large-scale subsidence resulting in the adiabatic warming of the subsiding air, clear skies, and the formation of temperature inversions aloft. The lack of synoptic forcing allows for the development of local thermally induced flow patterns such as sea breeze/land breeze circulations and mountain/valley circulations, which may result in the recirculation and accumulation of pollutants in the airshed (Steyn and Faulkner, 1986).

In a study of the climatology of O₃ episodes in the LFV, McKendry (1994) characterized the various synoptic patterns related to ozone episodes at station T09 in Port Moody. He found that of the days in which O₃ concentration exceeded 82 ppb at T09, 47% were associated with the presence of a low-level thermal trough and a 500 hPa upper level-ridge of high pressure, in agreement with the general findings of Taylor (1991). The remaining episode days were characterized by either an upper-level low off the British Columbia coast combined with a weak surface pressure gradient (44% of episode days) or a persistent southerly flow at 500 hPa and weak flow at the surface (6% of episode days). McKendry also found that episode days are associated with a reduction in the

strength of the sea breeze, suggesting that the thermal trough acts to suppress sea breeze development.

3.1.3 Characterization of the Selected Episode

Synoptic Meteorological Profile

Daily surface pressure fields, temperature fields at 850 hPa, and geopotential height fields at 850 hPa and 500 hPa between 17-21 July 1985 are shown in Figures 3.2-3.6. A persistent feature throughout the episode was the broad surface high extending northward over the Pacific Ocean, off the west coasts of British Columbia and Washington. Superimposed on this were two additional features which McKendry (1994) identified as characteristic of ozone episodes in the region: a low-level thermal trough and an upper-level ridge.

The thermal trough was aligned over the coast of southwestern BC on 18 and 19 July. Associated with this trough was warm air advection from the southeast, as evident in the 850 hPa temperature plots which showed temperatures over the region increase from about 16°C on 18 July to 20°C the next day. During this period, the upper-level ridge at 500 hPa migrated slowly eastward. Geopotential heights over southwestern BC increased from 5800 m to greater than 5820 m. Surface O₃ concentrations measured in the LFV indicated elevated O₃ levels (*i.e.* >82 ppb) at several sites between 18-20 July. By 21 July, the O₃ episode was over. The surface trough had migrated inland and 850 hPa temperatures had dropped to approximately 18°C. Upper-level geopotential heights remained above 5820 m, but flow patterns changed from meridional to nearly zonal.

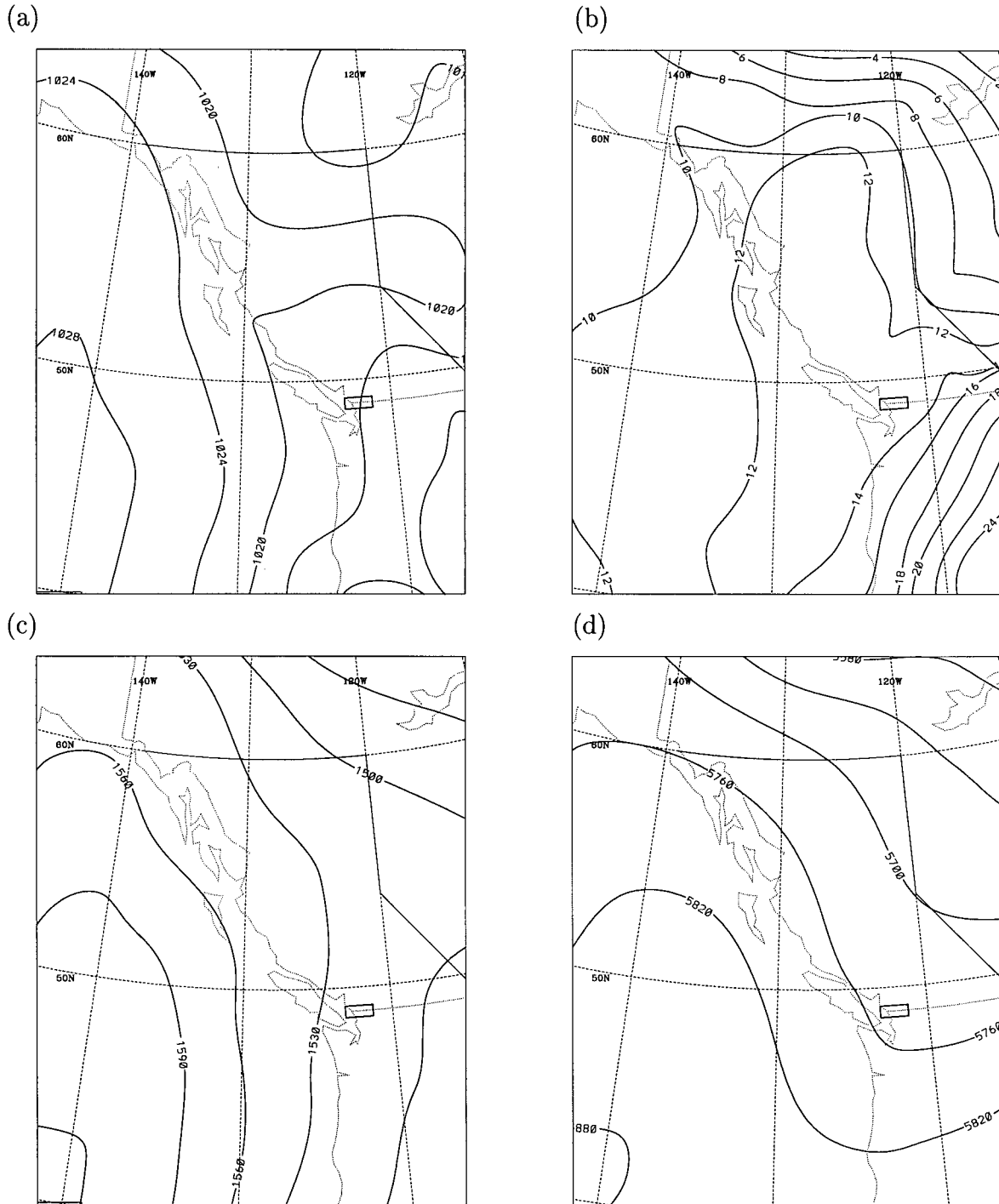


Figure 3.2: (a) Sea level pressure (hPa); (b) 850 hPa temperature (°C); (c) 850 hPa geopotential height (m); and (d) 500 hPa geopotential height (m), all for 17 July 1985 at 1200Z (0400 PST). Small rectangle in southeast quarter of each plot identifies modelling domain.

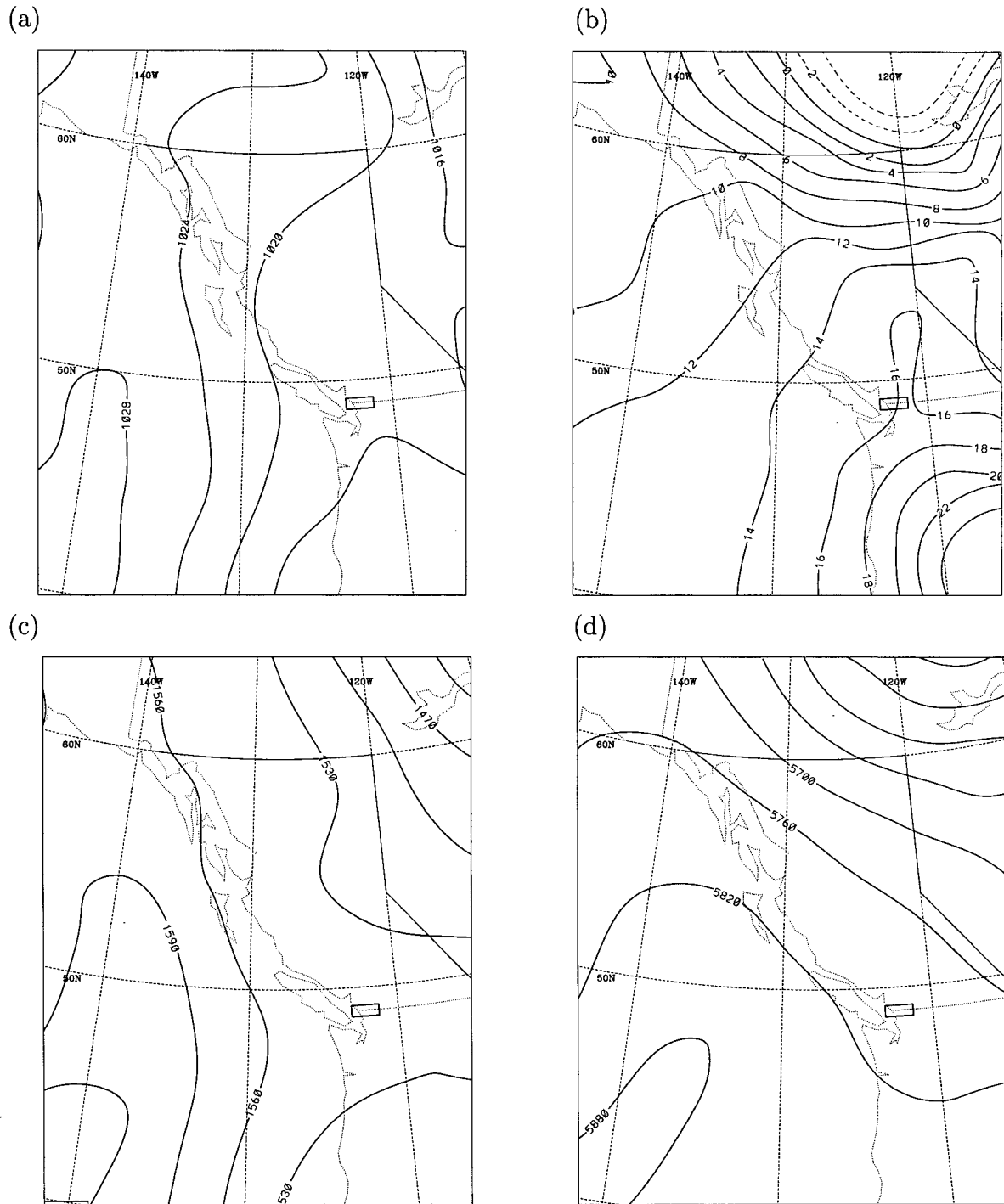


Figure 3.3: (a) Sea level pressure (hPa); (b) 850 hPa temperature ($^{\circ}\text{C}$); (c) 850 hPa geopotential height (m); and (d) 500 hPa geopotential height (m), all for 18 July 1985 at 1200Z (0400 PST). Small rectangle in southeast quarter of each plot identifies modelling domain.

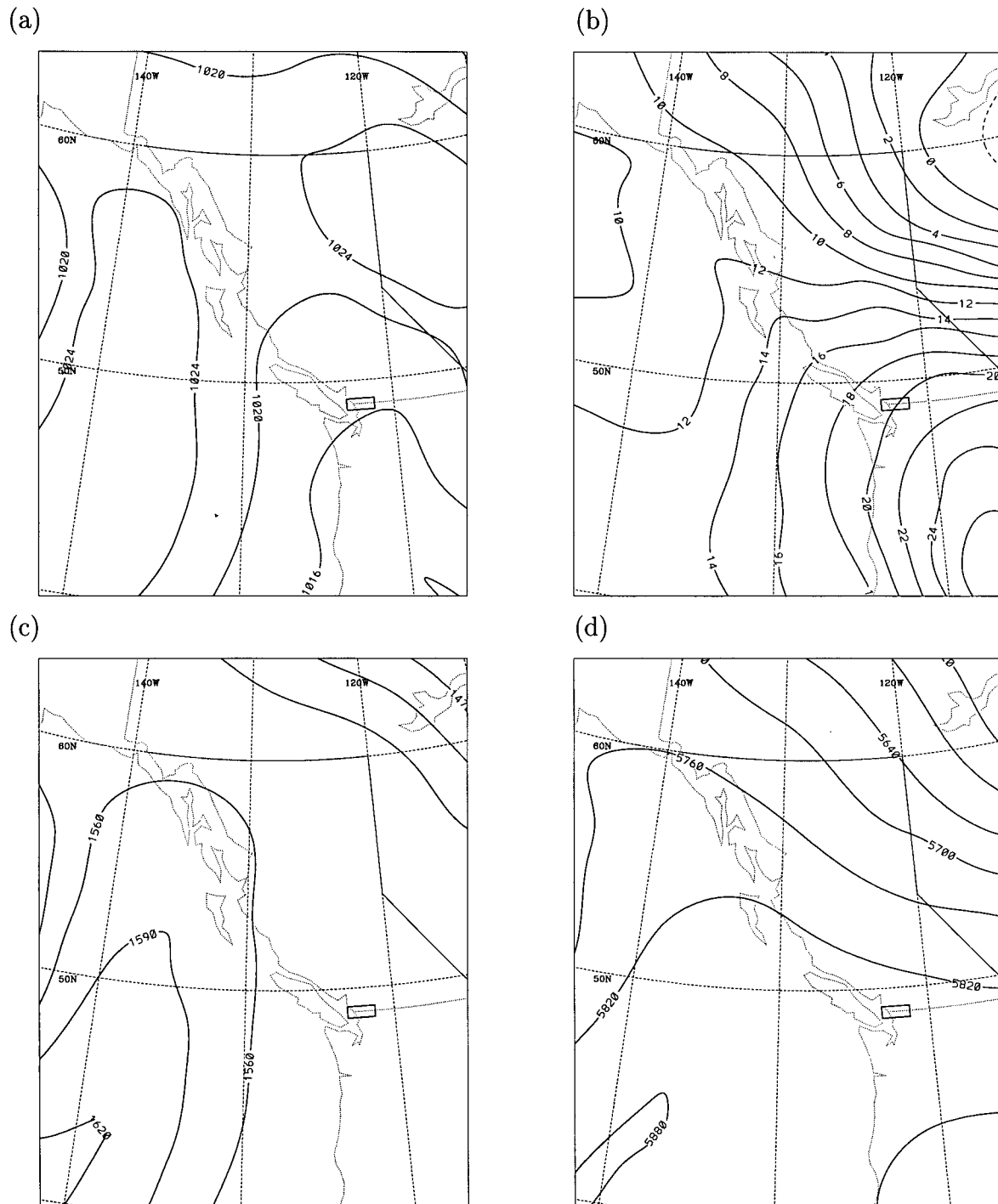


Figure 3.4: (a) Sea level pressure (hPa); (b) 850 hPa temperature (°C); (c) 850 hPa geopotential height (m); and (d) 500 hPa geopotential height (m), all for 19 July 1985 at 1200Z (0400 PST). Small rectangle in southeast quarter of each plot identifies modelling domain.

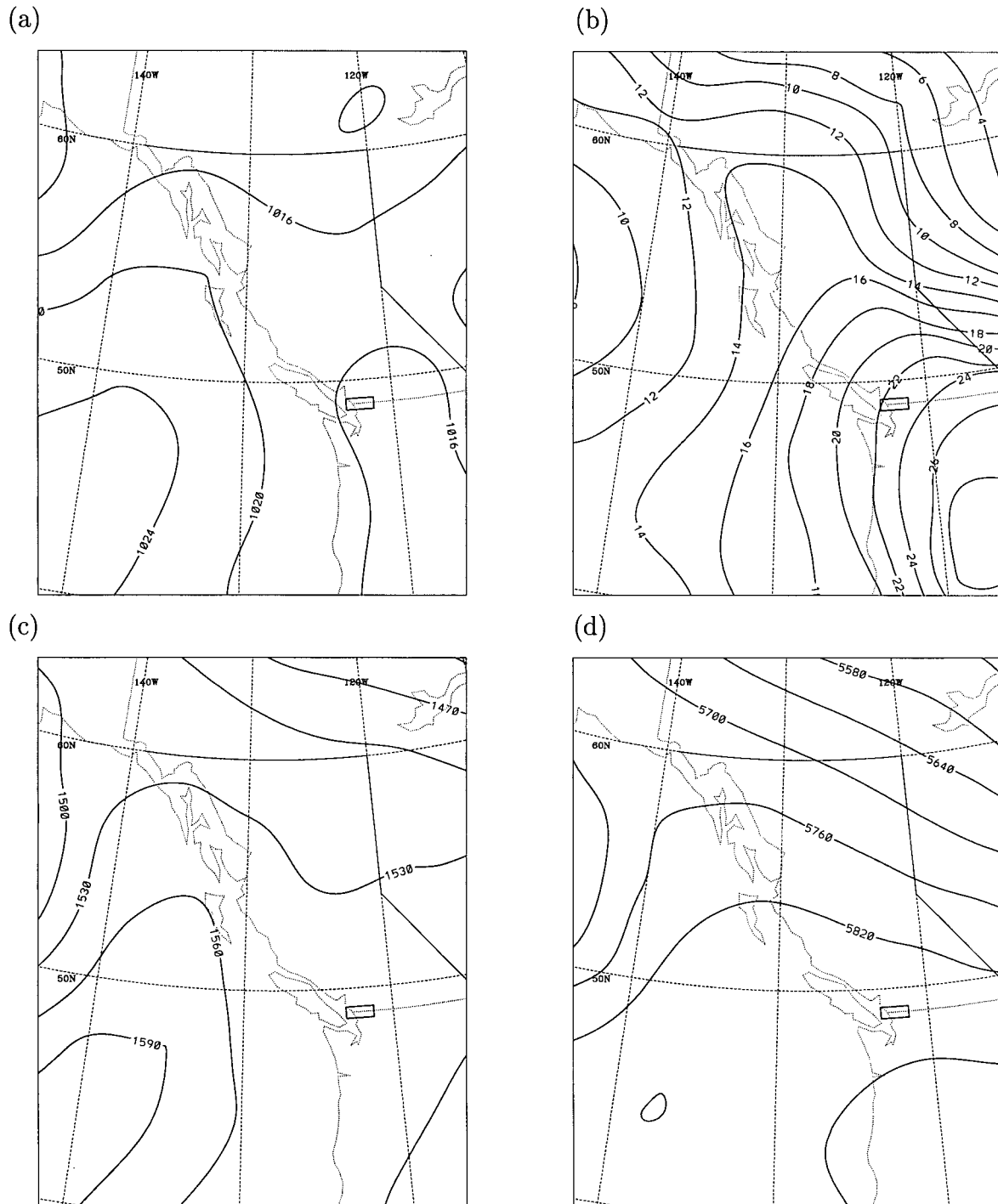


Figure 3.5: (a) Sea level pressure (hPa); (b) 850 hPa temperature ($^{\circ}\text{C}$); (c) 850 hPa geopotential height (m); and (d) 500 hPa geopotential height (m), all for 20 July 1985 at 0000Z (19 July at 1700 PST). Small rectangle in southeast quarter of each plot identifies modelling domain.

Mesoscale Meteorological Profile

The episode was characterized by high temperatures, clear skies, light onshore breezes during the daytime and extended periods of calm or offshore winds at night, as indicated by measurements at YVR and YXX which are shown in Figures 3.7(a) and (b), respectively. Maximum surface temperatures during the episode peaked at 27.4°C at YVR and 33.2°C on 19 July, and remained high on the 20th. Daytime winds at YVR and YXX on 18 and 19 July were predominantly westerly. On 20 July, the day in which the highest O₃ concentrations were observed, a southerly component was evident at both sites. Of note, these patterns were also observed during an extreme O₃ episode occurring in September 1988 (Steyn et al., 1990). While several hours of calm were observed at YXX on the morning of 21 July, strong easterlies were observed at YVR. While still warm, daytime temperatures on 21 July were significantly lower than observed on the preceding days.

Acoustic sounder measurements at sites in Delta and Surrey indicated that with the exception of 17 July, elevated daytime thermal structures were strong and consistent throughout the episode (Steyn and Wallis, 1986). Maximum mixed layer depths (MLDs) at the Delta site decreased from about 620 m on 17 July to 590 m on 19 July. At the Surrey site, maximum MLDs decreased from approximately 840 m on 17 July to 650 m on 18 and 19 July. For comparison purposes, the maximum MLD observed at the Surrey site during the September 1988 episode was 470 m (Steyn et al., 1990). Tethersonde measurements from Queen Elizabeth Park, Vancouver indicated that maximum MLDs decreased from approximately 530 m on 17 July to 320 m on 19 July.

Air Quality Profile

A number of stations in the LFV reported exceedances of the one-hour Maximum Acceptable Level for O₃ (82 ppb) between 18-20 July 1985, and four of the stations

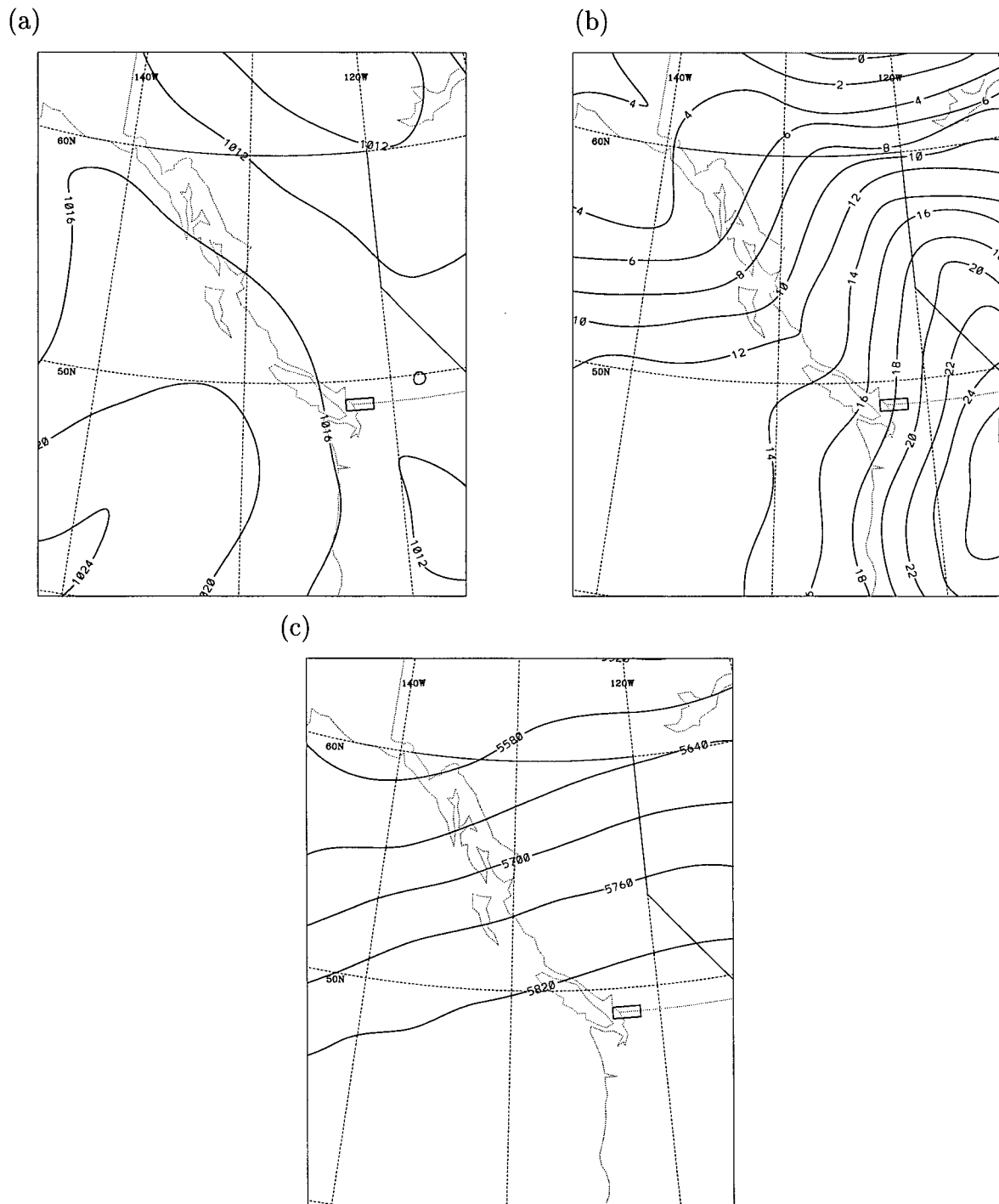


Figure 3.6: (a) Sea level pressure (hPa); (b) 850 hPa temperature (°C); and (c) 500 hPa geopotential height (m), all for 21 July 1985 at 1200Z (0400 PST). Small rectangle in southeast quarter of each plot identifies modelling domain.

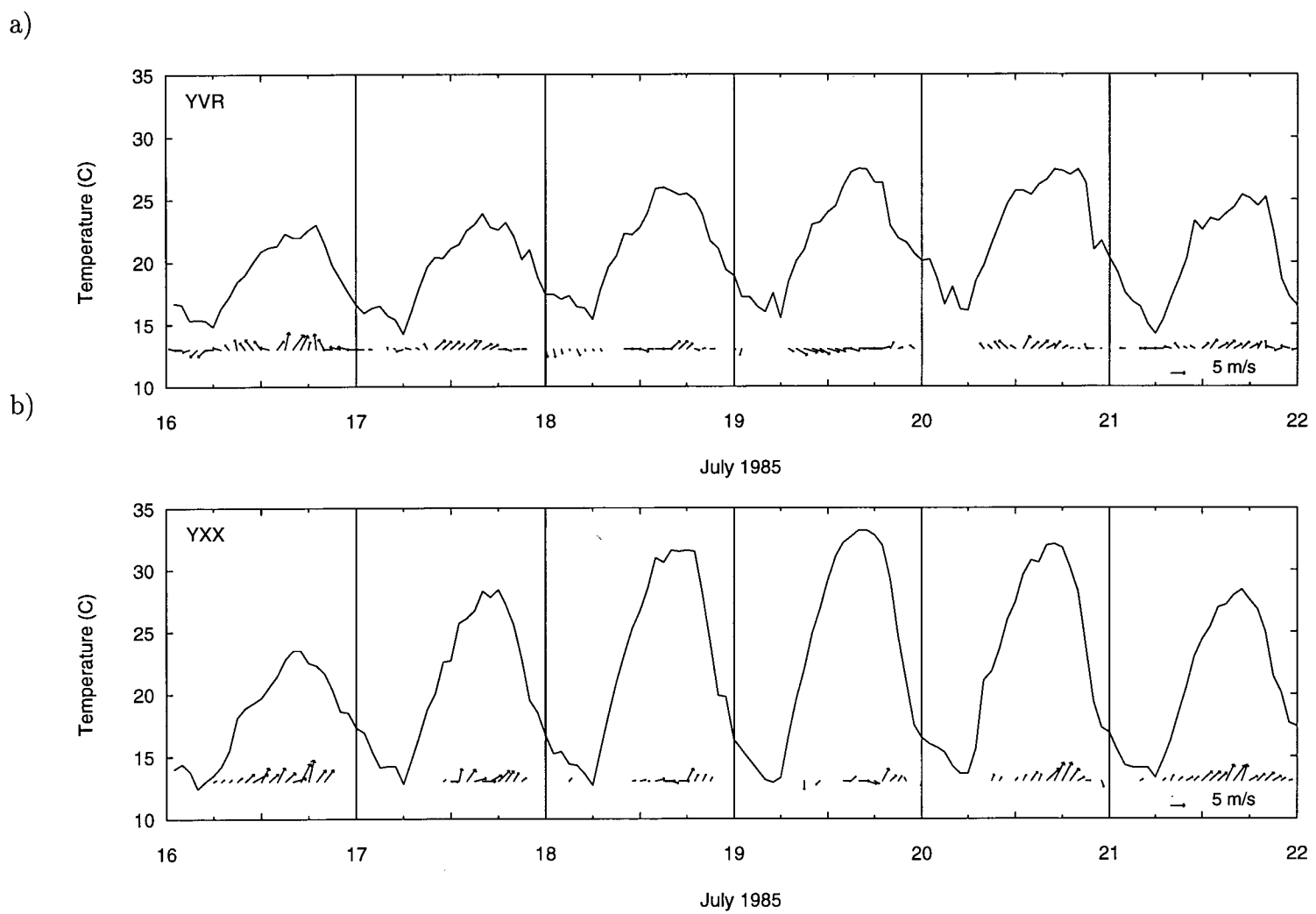


Figure 3.7: Hourly temperature (solid lines) and wind vectors (arrows) at (a) YVR and (b) YXX, 16-21 July 1985.

Table 3.2: Exceedances of ambient O₃ objectives in the LFV, 17-21 July 1985.

Date	Number of Stations Exceeding:			Ozone Maxima (ppb)
	Maximum Desirable (51 ppb)	Maximum Acceptable (82 ppb)	Maximum Tolerable (153 ppb)	
July 17	6/11	0/11	0/11	69
July 18	9/12	3/12	0/12	104
July 19	7/12	4/12	0/12	107
July 20	12/12	6/12	0/12	110
July 21	7/12	0/12	0/12	80

reported exceedances on consecutive days. A summary of the number of exceedances is presented in Table 3.2. The highest recorded concentrations during the episode were 107 ppb at station T12 in Chilliwack on July 19 and 110 ppb at station T15 in Surrey on July 20. The lowest O₃ concentrations and the highest NO₂ concentrations were observed at sites located slightly upwind or within the urban core (stations T02, T03, T04 and T05). Conversely, the highest O₃ concentrations and the lowest NO₂ concentrations were found at sites downwind of the urban plume (T15, T16, T11 and T12). Elevated O₃ levels were also found at T07 and T09, which are located at the eastern end of Burrard Inlet and in close proximity to oil refineries which were operating at the time. High nighttime O₃ concentrations at T14, located on Burnaby Mountain, reflect the buildup of O₃ aloft and the lack of available NO_x sources near this elevated site.

No exceedances of the one-hour Maximum Acceptable Level for NO₂ (210 ppb) were observed during the episode. However, elevated concentrations were observed at stations

T04 and T05 in Burnaby. The highest concentrations recorded during the episode were 100 ppb at T05 on 18 July and 86 ppb at T05 on 19 July.

3.2 Domain Selection

The selected modelling domain is as shown in Figure 3.8. The dimensions of the domain were 140 km by 110 km, with the origin located at UTM coordinates 460000 E and 5390000 N. For a grid cell size of 5 km by 5 km, this translated to a domain of 28 by 22 cells. Domain selection was based on the following criteria (after Seinfeld, 1988):

1. domain boundaries should contain all important current and future emission sources;
2. necessary air quality, emissions and meteorological data should be available for the domain; and
3. local circulation cells should be well-contained within the domain boundaries.

As described in the previous section, air quality, emissions and meteorological data were available for the British Columbia side of the LFV. However, similarly detailed data were not available for the Washington State side. Clearly, both the British Columbia and Washington sides of the LFV had to be included in the modelling simulation in order to capture the major sources and recirculating wind patterns transporting pollutants in the valley. A back-trajectory study by Coligado (1988) for 17, 19 and 20 July 1985 indicated that air parcels originating from the Washington State side of the LFV produced maximum one-hour O_3 concentrations that were as high or higher than air parcels originating in the GVRD. Preliminary trajectory studies performed by Miao (1993) for a sea breeze day (23 August 1985) indicated that sea breeze circulation and upslope/downslope winds were important pollutant transport mechanisms in the LFV. A larger domain is also preferable from the point of view of minimizing boundary effects on the main area

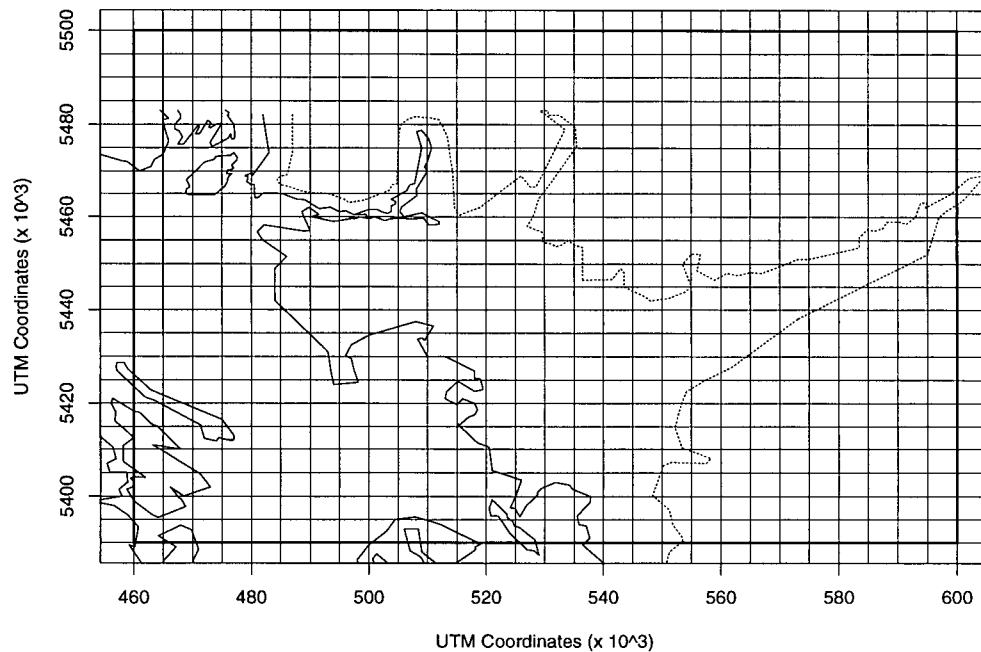


Figure 3.8: Modelling domain, as delineated by thick, solid lines. Coastline and 100 m contours depicted by thin, solid lines and dotted lines, respectively.

of interest. However, this is tempered by the added computational requirements and the availability of observational data to help characterize the expanded domain.

The selected domain size encompasses most of the LFV, with the exception of the town of Hope, BC to the east, and areas to the south of Bellingham, Washington. It is very similar to the typical domain size of 140 km x 120 km (4 km by 4 km grid cells) that was found by Tesche (1991) in reviewing 67 papers and reports on UAM studies.

Chapter 4

Model Inputs

UAM simulations require a total of 13 input files, as listed in Table 4.1. These files are used to define boundary and initial conditions, meteorological fields, emissions, terrain, chemical parameters and simulation control parameters. Further details regarding the preparation of these files are provided in the following.

4.1 Boundary and Initial Conditions

The preparation of files describing model boundaries, associated boundary conditions and initial conditions are described in this section.

4.1.1 BOUNDARY

The BOUNDARY files specifies (i) time-invariant lateral boundaries, and (ii) average hourly pollutant concentrations in each boundary cell. Dimensions of the modelling domain were 140 by 110 km, beginning at 460000 UTM E and 5390000 UTM N, as discussed in Section 3.2. Due to a lack of monitoring data near the domain boundaries, clean boundary conditions were based on those used by the South Coast Air Management District for the Los Angeles Basin (SCAQMD, 1990). These values are listed in Table 4.2. Reactive organic gas (ROG) and carbon monoxide (CO) concentrations of 10.3 ppbv and 200 ppbv, respectively, compare well with total non-methane hydrocarbon and CO concentrations of 9.4 ppbv and 161 ppbv measured during low-level (0.1 km) flights off the west coast of Vancouver Island in April 1985 (Greenberg et al., 1990). This suggests

Table 4.1: UAM input files

Input File	Description
BOUNDARY	specifies the lateral domain boundaries and the concentrations of each species along each boundary.
REGIONTOP	specifies the height of the top of the domain; this height may vary in time and space.
AIRQUALITY	specifies the concentrations of each species in each grid at the start of the simulation.
TOPCONC	specifies the hourly concentrations of each species for each grid cell along the top of the domain.
TERRAIN	specifies the roughness and deposition factors for each grid cell along the bottom of the domain.
DIFFBREAK	specifies the hourly mixed layer depth (or diffusion break) during the daytime and the hourly inversion height at night.
WIND	specifies the hourly u and v wind components for each grid cell, the hourly maximum wind speed, and the hourly average wind speed along each boundary.
TEMPERATUR	specifies the hourly gridded temperature field.
METSCALARS	specifies the hourly values of meteorological parameters that do not vary spatially. This includes the NO_2 photolysis rate constant, the concentration of H_2O vapour, the temperature gradients above and below the diffusion break, atmospheric pressure and exposure class.
EMISSIONS	specifies hourly gridded emissions from low-level species.
PTSOURCE	specifies hourly emissions from elevated sources which are injected into the appropriate grid cells. This file includes stack parameters.
CHEMPARAM	specifies the species to be simulated, reaction rate constants, upper and lower bounds, activation energies, reference temperature, and resistances to surface sinks.
SIMCONTROL	specifies the period of simulation, model options, and information on the integration time steps.

Table 4.2: Clean boundary conditions, South Coast Air Quality Management District (SCAQMD, 1990).

Species	Concentrations (ppm)
NO	0.00025
NO2	0.0005
O3	0.04
OLE	0.00055
PAR	0.00622
TOL	0.0000914
XYL	0.00004
FORM	0.0005
ALD2	0.0005
ETH	0.00011
MEOH	0.0001
ETOH	0.0001
ISOP	0.0001
total ROG	0.0103
CO	0.2

that the SCAQMD boundary conditions at least provide the correct order of magnitude for the LFV application.

4.1.2 REGIONTOP

The REGIONTOP file specifies the top of the modelling domain. General practice is to set it to a constant level approximately 50 to 200 m above the maximum mixed layer depth (Morris and Myers, 1990). In the present application, it was set to coincide with a height of 1372 m in the RAMS sigma coordinate system. The following conversion was

used to obtain terrain-parallel coordinates:

$$z_{top} = \frac{(H - z_s)}{H} \cdot 1372m \quad (4.35)$$

where z_{top} is the height of the top of the modelling domain, H is the top of the RAMS domain (19 km) and z_s is the surface elevation. The height of 1372 m was obtained through consideration of the number and heights of the vertical layers used in RAMS which would provide adequate resolution of the mesoscale flows important in pollutant transport in the LFV.

4.1.3 AIRQUALITY

Initial conditions are provided in the AIRQUALITY file. The initial concentrations are based on observations made at the simulation start time. To obtain a three-dimensional concentration field, station values were first interpolated horizontally using an inverse distance weighting factor. Chemical species were assumed to be well-mixed below the inversion height, and were scaled back to the concentrations at the top of the modelling domain which were specified by the REGIONTOP file. Where initial concentrations were not available for certain species, clean air conditions as used in the BOUNDARY file (Table 4.2) were applied.

4.1.4 TOPCONC

Boundary conditions aloft are defined in the TOPCONC file. In the absence of monitoring data at this elevation, clean boundary conditions as shown in Table 4.2 were used.

4.2 Meteorological Data

Meteorological output to describe wind fields, mixing heights and surface temperatures were generated in a mesoscale modelling study using the RAMS2a model (Steyn and Cai, 1994). Treatment of the data within the current research was limited to conversion of the data to a format compatible with the UAM.

4.2.1 WIND

The WIND file contains gridded, hourly-averaged values of horizontal wind components u and v , hourly maximum wind speeds, and hourly averaged wind speeds for each boundary. The values of u and v were obtained by adjusting RAMS output to the format and grid coordinates required for the wind preprocessor UAMWIND.

A feature of UAM-IV is that cell heights vary with the height of the mixed layer depth. In contrast, the vertical structure of RAMS is fixed. Vertical interpolation of RAMS output to a structure compatible with UAM input requirements can mask such important local-scale features as sea breezes and land breezes. For the purpose of this application, cell heights in the WIND preprocessor were fixed to levels coinciding with cell heights in the lower eight layers of the RAMS model. Cell interfaces were set at the following heights above ground level: 100 m, 215 m, 347 m, 499 m, 674 m, 875 m, 1106 m and 1372 m. Cell heights were adjusted from sigma coordinates to terrain-following coordinates as described in Section 4.1.2.

Horizontal wind fields also required adjustments. The wind vectors u and v are calculated at the centre of each grid cell in the UAM, while they are calculated along perpendicular grid faces in RAMS, as summarized in Steyn and Cai (1994). The RAMS wind fields were for a grid size of 2.5 km by 2.5 km and a domain origin of 453750

UTM E and 5385750 UTM N. To convert to the UAM domain, a six-point inverse-distance-weighted interpolation scheme was applied to RAMS-generated values of u and v . Interpolations near domain boundaries were based on four- or three-point schemes, depending on the availability of neighbouring grid cells.

The wind fields were subject to further adjustments in UAMWND. Vertical velocity w is calculated based on three-dimensional divergence minimization. A stability adjustment is then applied to ensure zero vertical velocities at the top of the domain. Horizontal velocities u and v are then adjusted until the calculated divergence is within acceptable parameters. UAMWND produces hourly, gridded horizontal wind speeds (in km/h) for each layer, in addition to hourly maximum wind speeds and average wind speeds along the boundaries.

Wind fields produced by UAMWND at 0900-1000 PST and 1500-1600 PST for each day of the episode are shown in Figure 4.1-4.3. Vector length is proportional to wind speed. Observed winds at Vancouver International Airport (YVR), the University of British Columbia (UBC - located on the northwest tip of the City of Vancouver) and Abbotsford International Airport (YXX) are indicated by thicker arrows. Aside from the morning of 17 July, when initialization effects are still evident, morning wind patterns were characterized by strong northwesterly winds channelling down the Strait of Georgia. The simulated wind fields captured the start of the onshore sea breeze, which typically began about 1000 PST. However, it is evident that the modelled wind fields had a much stronger southerly component than the winds observed at YVR and UBC. By late afternoon, the onshore wind pattern had been firmly established, while wind speeds over the Strait of Georgia had slackened considerably.

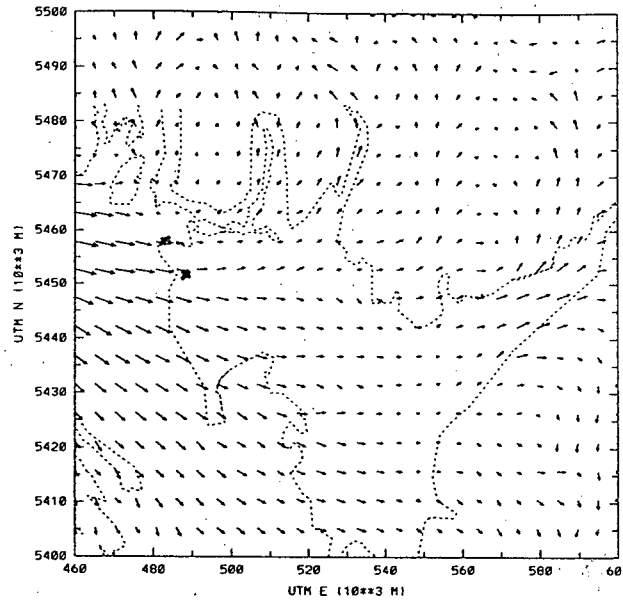
Another characteristic of the afternoon wind fields is the strong southerly winds over such north-south channels as Indian Arm, Pitt River/Pitt Lake, Stave River/Stave Lake and Harrison River/Harrison Lake. These channels lie to the north of the major emissions

area, and as such these flow patterns have large implications on pollutant transport to these wilderness/recreational areas.

4.2.2 DIFFBREAK

The DIFFBREAK file specifies hourly, gridded heights of the daytime mixed layer and the nocturnal inversion base (hereafter referred to as z_i). The DIFFBREAK preprocessor calculates z_i using an algorithm developed by Kelly (1981) in which z_i is defined as the level at which the potential temperature exceeds that based on screen-level temperature measurements. To maintain dynamical consistency with other meteorological parameters, potential temperature estimates from the RAMS model were used. Modelled results and observed data for sites in Delta, Surrey, and Queen Elizabeth Park (QEP), Vancouver are shown in Figure 4.4. Predicted and observed daily maxima are presented in Table 4.3. Predicted values represent hourly averages. Data obtained from QEP are based on an evaluation of tethered sonde soundings. Data from the Delta and Surrey sites are from acoustic sounder measurements. No observations from QEP and Delta were available for 18 July. Figure 4.4 indicates that aside from the first day of the simulation, when model start-up effects may have dominated, predicted values generally agreed with observed data in terms of the magnitude and timing of the daily maxima. However, there was a tendency to underestimate z_i . At the Surrey site, the simulated development of the mixed layer was somewhat delayed compared to observed data, although the magnitude of the daily maximum z_i agreed well. At QEP on 19 July, the morning development of z_i was well-characterized, but the second maxima during the mid-afternoon was not captured.

(a)



(b)

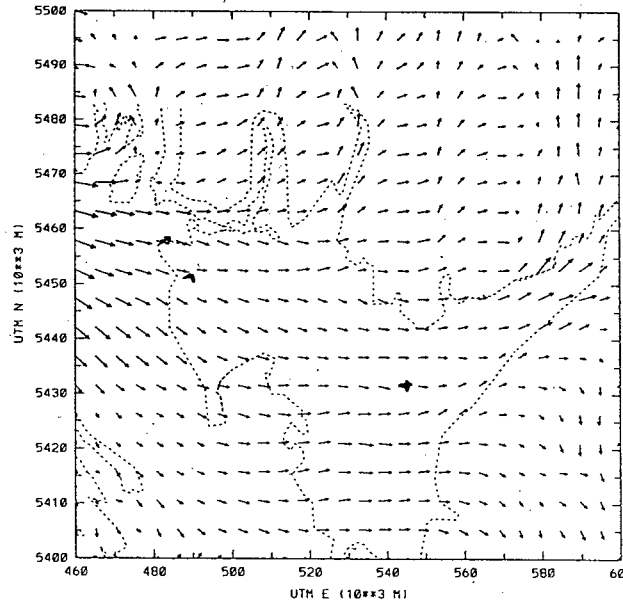
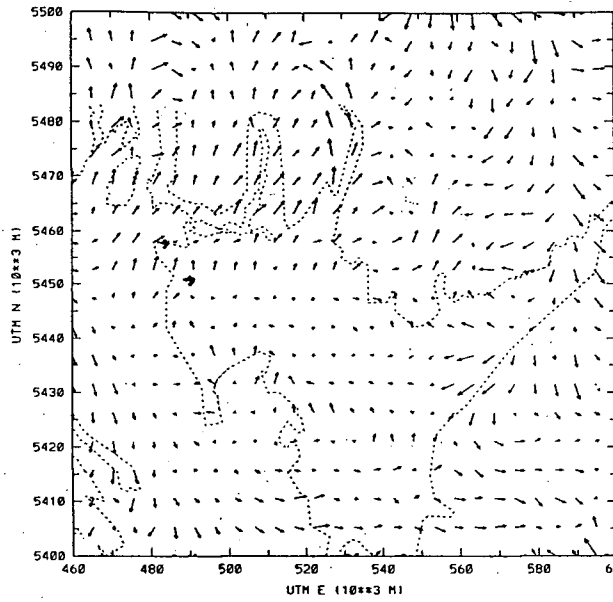


Figure 4.1: Surface (level 1) wind fields prepared for UAM at (a) 0900 PST and (b) 1500 PST; 17 July 1985. Vector length is proportional to wind speed. Observations shown by thick arrows. Wind speeds in m/s.

(a)



(b)

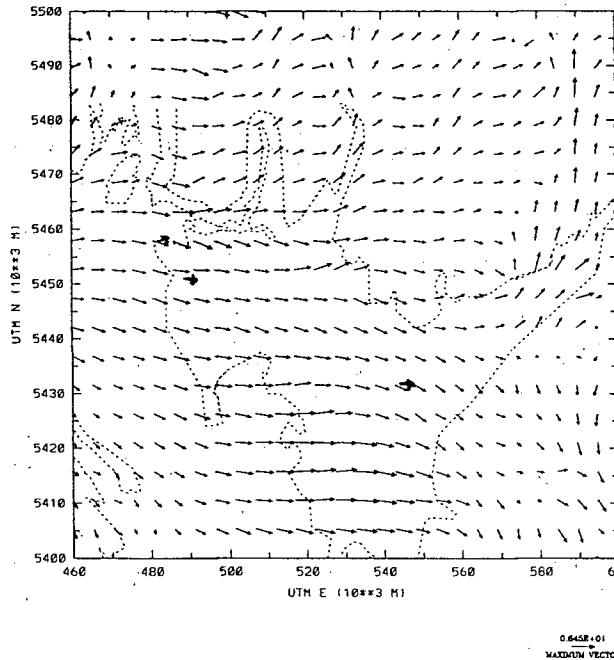
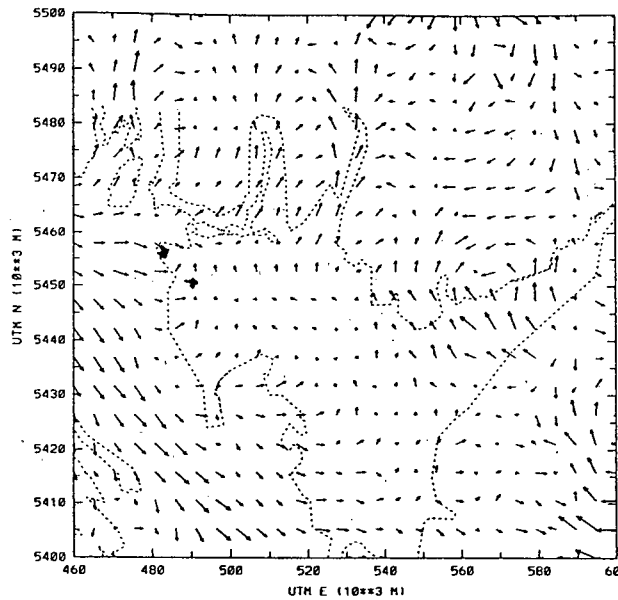


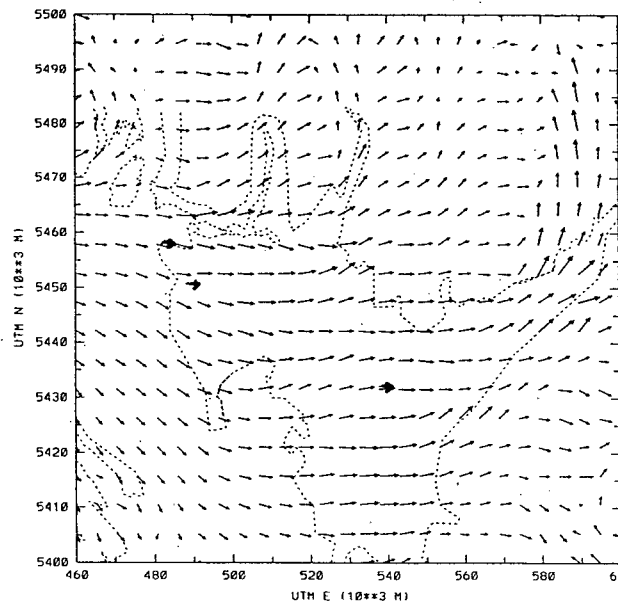
Figure 4.2: Surface (level 1) wind fields prepared for UAM at (a) 0900 PST and (b) 1500 PST, 18 July 1985. Vector length is proportional to wind speed. Observations shown by thick arrows. Wind speeds in m/s.

(a)



0.007E+01
MAXIMUM VECTOR

(b)



0.700E+01
MAXIMUM VECTOR

Figure 4.3: Surface (level 1) wind fields prepared for UAM at (a) 0900 PST and (b) 1500 PST, 19 July 1985. Vector length is proportional to wind speed. Observations shown by thick arrows. Wind speeds in m/s.

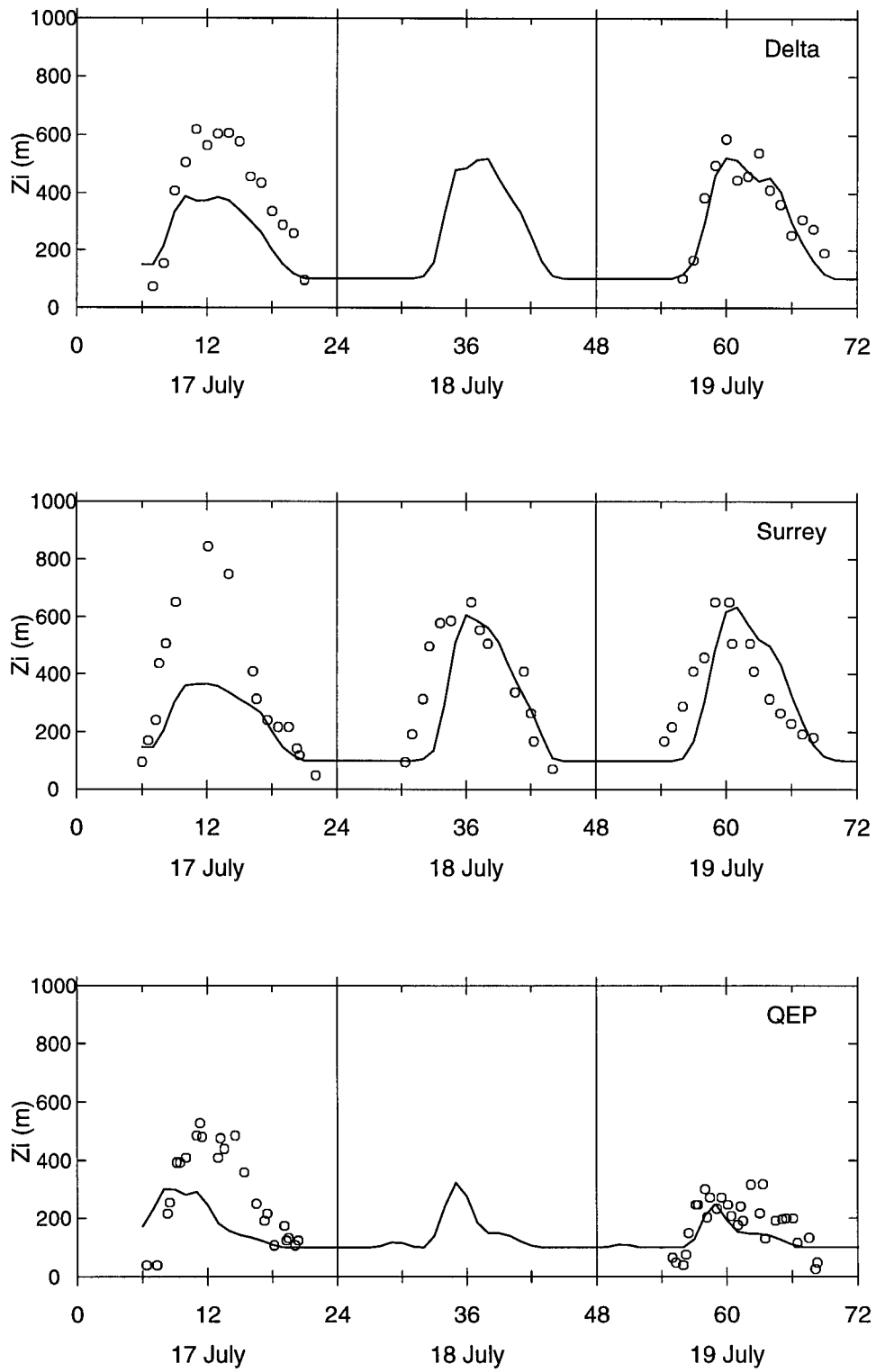


Figure 4.4: Mixed layer depth at sites in Delta (top panel), Surrey (middle panel) and Queen Elizabeth Park (QEP) (lower panel), Vancouver. Lines depict predicted values; circles show observed data.

Table 4.3: Maximum predicted and observed values of z_i at sites in Delta, Surrey and QEP, Vancouver between 17-19 July 1985.

Location	17 July		18 July		19 July	
	Obs.	Pred.	Obs.	Pred.	Obs.	Pred.
Delta	619	389	-	518	522	587
Surrey	844	365	651	605	651	634
QEP	527	301	-	322	317	274

4.2.3 TEMPERATUR

Hourly gridded surface temperatures are required to simulate temperature-dependent chemistry. Together with mixing heights (Section 4.2.2) and atmospheric lapse rates (Section 4.2.4), the temperature data are used to generate a three-dimensional temperature field. For this application, temperature data were obtained from RAMS output rather than an interpolation of surface-based measurements due to the limited number of observations available. Temperature data were horizontally adjusted using a six-point smoothing scheme to convert to the UAM coordinate system.

4.2.4 METSCALARS

The METSCALARS file contains data for six meteorological parameters which are assumed to be spatially invariant:

- NO₂ photolysis rate: This parameter was calculated as a function of the day of the year and location using the preprocessor program SUNFUNC.
- exposure class: This parameter represents a measure of the near-surface stability due to heating or cooling. It was treated as a function of solar zenith angle, which

was obtained from the SUNFUNC output, and total observed cloud cover. Cloud cover estimates were based on airport observations at YVR and YXX. Averaged over the two sites, hourly cloud cover was less than 5/10th on 17 July. Clear skies were reported 18-19 July.

- surface pressure: Atmospheric pressure is used in the conversion of emissions from molar units to concentration units by volume. The default value of 1 atm (101.3 kPa) was used.
- atmospheric lapse rates below and above the diffusion break: Hourly lapse rates below the diffusion break were based on hourly averaged lapse rates calculated from RAMS output. Similar treatment for the lapse rate above the diffusion break resulted in unrealistic estimates. Instead, lapse rates derived from tethered sonde measurements at a site in Langley during Pacific'93 for similar meteorological conditions were used (Pryor, personal communication).
- water vapour concentration: Concentrations are required for chemical reactions which contain water as a reactant. Values were calculated from relative humidity and surface temperature measurements obtained at YVR and YXX.

4.3 Emissions Data

The EMISSIONS and PTSOURCE files contain hourly speciated emissions from merged low-level and elevated sources, respectively. These files were prepared by passing emissions data through the emissions preprocessing system EPS1.0 (Causley, 1990).

BC emissions data were based on the GVRD emissions inventory for base year 1985 (GVRD, 1988). Included in the inventory were emission estimates for the following criteria pollutants: VOCs, NO_x, CO, sulphur oxides (SO_x) and total particulate (TSP).

Table 4.4: Annual emissions estimates for the BC (1985) and Washington (1990) LFV

Sector	SOx tonnes/year	NOx tonnes/year	TSP tonnes/year	CO tonnes/year	VOC tonnes/year
B.C.:					
mobile	3217	46632	116335	394525	55619
area	1026	3058	3831	5212	33796
point	8842	8722	21844	12908	7729
gas	0	0	0	0	7194
total	13085	58412	142010	412645	104338
Wash.:					
mobile	303	4742	3600	35048	4795
area	388	1189	3232	16915	22113
point	9244	4592	1906	45163	7246
total	9935	10523	8738	97126	34154
TOTAL	23020	68935	150748	509771	138492
% B.C.	56.8	84.7	94.2	80.9	75.4
% Wash.	43.2	15.3	5.8	19.1	24.6

A similar inventory of emissions from U.S. sources in the LFV was not available for base year 1985. For comparison purposes, 1985 estimates from BC sources and 1990 emission estimates from U.S. sources (B.H. Levelton, 1993) are provided in Table 4.4.

Using improved methodologies, refinements were subsequently made to the 1985 inventory which resulted in changes to emission estimates (GVRD, 1994). Total NOx emissions from all sources decreased by 1.7%. Total VOC and CO emissions increased by 5.9% and 16.4%, respectively. Masked within these overall changes were substantial changes within certain sectors. Most notably, NOx emissions from point sources

decreased by 23.5% and VOC emissions from area sources increased by 34.1%. As the final emission estimates were not available at the time that the input files were being prepared for the simulation, the revised estimates were not used in this study. However, as noted in the following, some refinements were incorporated in an effort to provide better temporal and spatial characterization.

4.3.1 Mobile Sources

The mobile emissions inventory was comprised of emissions from vehicular, aircraft and airport, rail and marine sources. Motor vehicles were the dominant source, contributing 92.2% of total mobile emissions (GVRD, 1988). Hence, particular attention was paid to the preparation of motor vehicle emissions for application in the UAM.

Motor vehicle emissions were based on speed classes and vehicle kilometres travelled (VkmT) estimates from the GVRD's regional transportation model Emme/2, and emission factors calculated using MOBILE3, a computerized system developed by the U.S. EPA. MOBILE3 calculations were performed using a base temperature of 10°C. Temperature is known to have a strong effect on evaporative emissions from mobile sources. Based on MOBILE4 emission factors, Cardelino and Chameides (1990) estimated that for an increase in ambient temperatures from 22°C to 29°C, mobile emissions in the Atlanta study area would increase 47%. MOBILE3 did not contain an algorithm responsive to changes in ambient temperature, nor did it consider area-specific gas volatilities or evaporative running losses, the latter of which may contribute an additional 20% to VOC emissions (Pierson et al., 1990). To adjust the emission factors to represent episodic temperatures, correction factors were obtained using output from Mobile 4.1c (McLaren, personal communication), the Canadian version of MOBILE4.1 which represented the most recent advancements in the MOBILE series of emission models at the time. A summary of the resultant emissions is given in Table 4.5 and Figure 4.5. Deviations

Table 4.5: Episodic adjustments of motor vehicle emissions

Scenario	Ambient Temperature (°C)	NOx Emissions (tonnes/day)	VOC Emissions (tonnes/day)
Base	10.0	158.2	189.9
17 July 1985	23.1	161.5	181.2
18 July 1985	22.5	161.9	179.9
19 July 1985	27.6	155.5	191.3

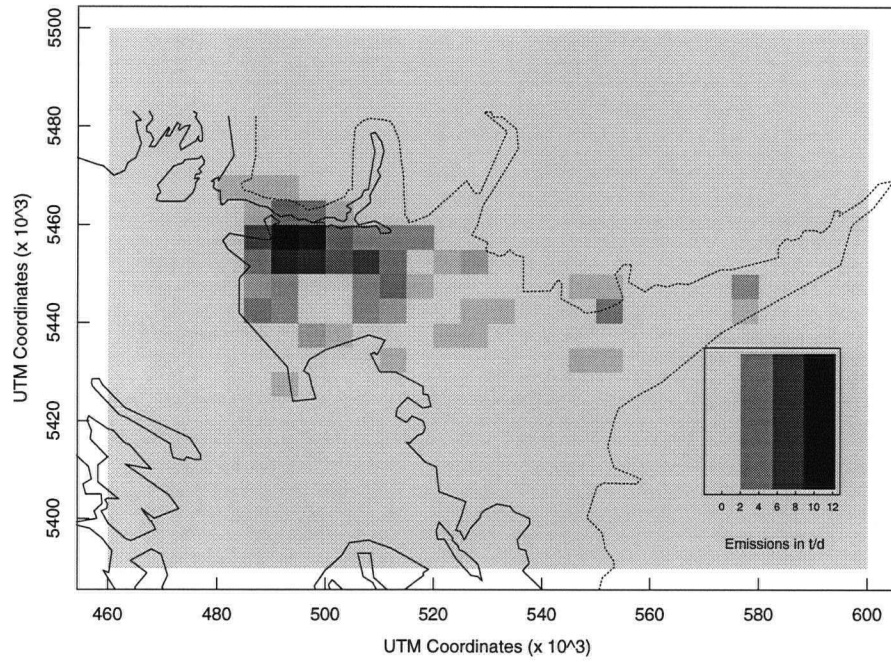
from the base case emissions were surprisingly small. The NRC attribute this finding to the loose preparation techniques employed for the MOBILE3 simulations, and also to the fact that episodic temperatures were not exceptionally high (*i.e.* not above 30°C) (McLaren, personal communication).

4.3.2 Point Sources

Point sources refer to facilities under management permit and generally include all major industrial operations. For the current modelling application, emissions from a total of 341 BC point sources (GVRD, 1988) and four of the largest U.S. point sources in the LFV (Franzmann, personal communication) were included. A more detailed treatment of U.S. emissions was not available at the time model inputs were being prepared.

Annual VOC and NOx emissions are shown in Figure 4.6(a) and (b), respectively. Clearly, the largest VOC sources were located along the eastern end of Burrard Inlet and to the north of Bellingham. Petroleum refineries were associated with the majority of these emissions. In contrast, the largest NOx sources were located along the Fraser River in Delta and Richmond (cement plants). The BC Hydro Burrard Thermal Generating

(a)



(b)

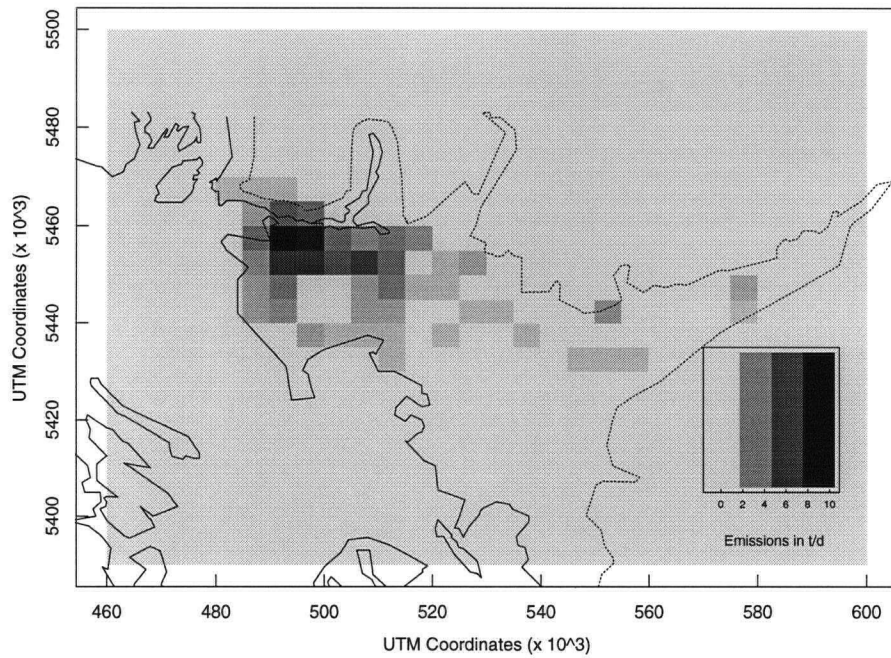


Figure 4.5: (a) VOC and (b) NO_x emissions (in t/d) from mobile sources in the LFV. Washington sources were not included.

Plant, which is one of the largest stationary NO_x sources in the LFV when operating at full capacity, was not operating in 1985.

Stack parameters were required to classify each source as low-level or elevated. Stack parameters were available for twenty of the largest facilities in the Lower Mainland and for the U.S. sources. The following default values were used for the remaining sources: stack height 3.0 m, stack diameter 0.2 m, stack velocity 4.0 m/s and stack temperature 294.0 K (Causley, 1990). Elevated sources were defined as those sources where emissions occurred above the elevated plume height cutoff of 50 m. The remaining sources were treated as low-level sources. Emissions data from the elevated sources were passed through the PTSOURCE preprocessor, where plume rise calculations were made to determine the vertical cell into which emissions would be injected. Emissions from low-level sources were passed through the EMISSIONS preprocessor.

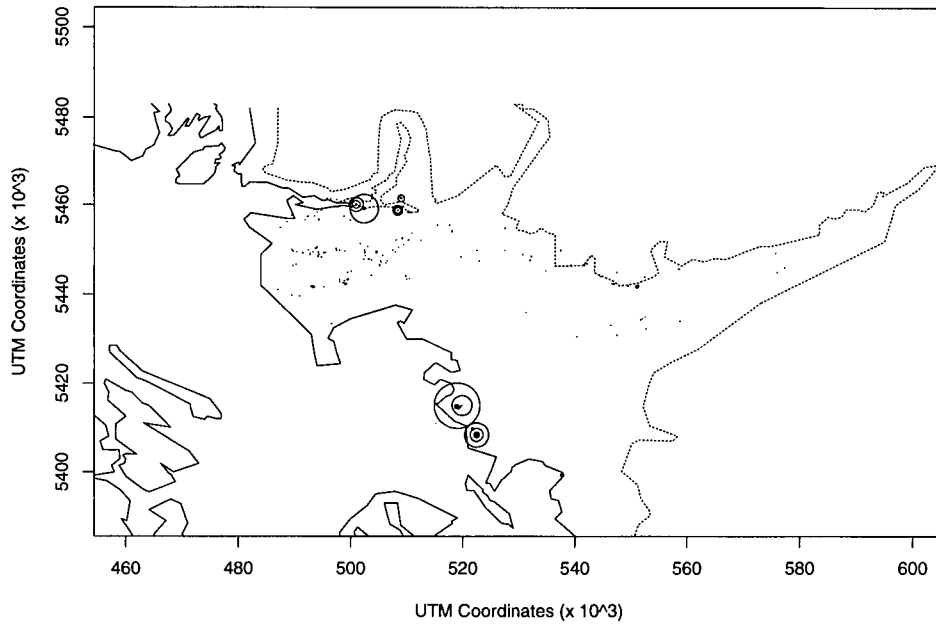
Temporal adjustments to the emissions were limited to seasonal and day-of-the-week adjustments. Episodic adjustments were not attempted due to the large effort required to check operating records of the individual facilities and the amount of time elapsed since the 1985 episode.

4.3.3 Gasoline Marketing Sources

Gasoline marketing sources were primarily comprised of bulk storage facilities, loading facilities, and service stations. Those refinery sources already covered under the point source category were not included. Contributions from this sector were small, accounting for only 7% of total VOC emissions. Service stations were responsible for almost 47% of this amount, while truck loading and bulk users accounted for approximately 19% and 15%, respectively (B.H. Levelton, 1989). The spatial variations in annual VOC emissions are represented in Figure 4.7.

Emissions from gasoline marketing sources are affected by ambient temperature, and

(a)



(b)

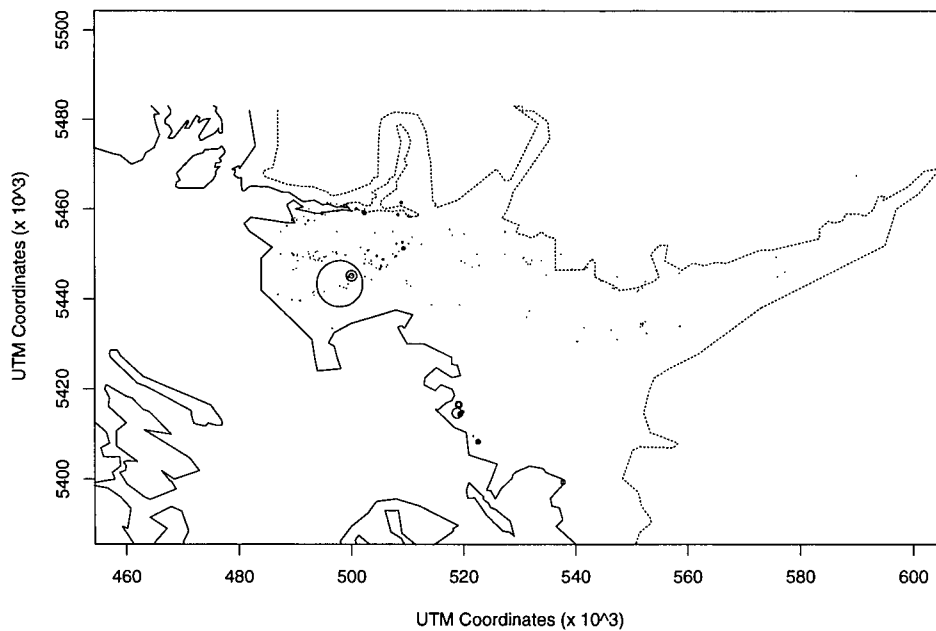


Figure 4.6: Annual (a) VOC and (b) NO_x emissions (in t/y) from point sources in the LFV. Circles denote point source emissions. Circle diameter is proportional to emissions.

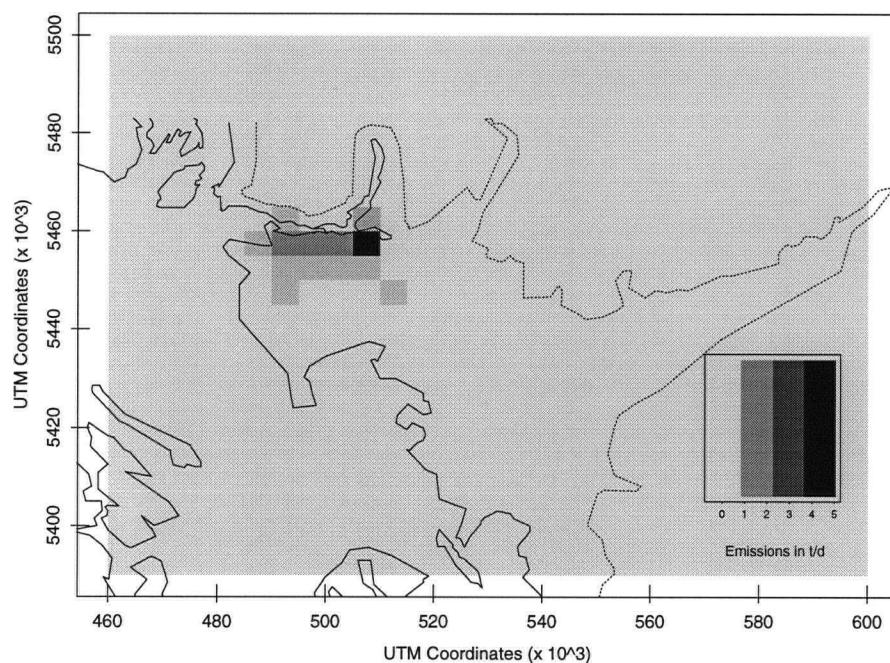


Figure 4.7: VOC emissions (in t/d) from gasoline marketing sources in the LFV. Sources from Washington were not included.

in the case of external floating tanks, by wind speed. Equations based on those used in the original calculations (B.H. Levelton, 1989) were applied to estimate month-specific and day-specific correction factors for emissions from truck loading facilities, bulk storage tanks and service station vehicle refueling. Losses from underground storage tanks at service stations were not considered. These emissions are dependent on initial fuel temperature, which in turn is strongly dependent on earth temperature as well as time between fuel drops, tank thermal time constant and initial and added fuel volume (Nichols and Hardcastle, 1983). Given the complexity of these calculations and the fact that soil temperatures are not expected to greatly vary below depths of 0.75 m (Oke, 1978), particularly over a three-day period, episodic corrections were not attempted.

Hourly emissions from truck loading facilities were estimated, and found to vary by as

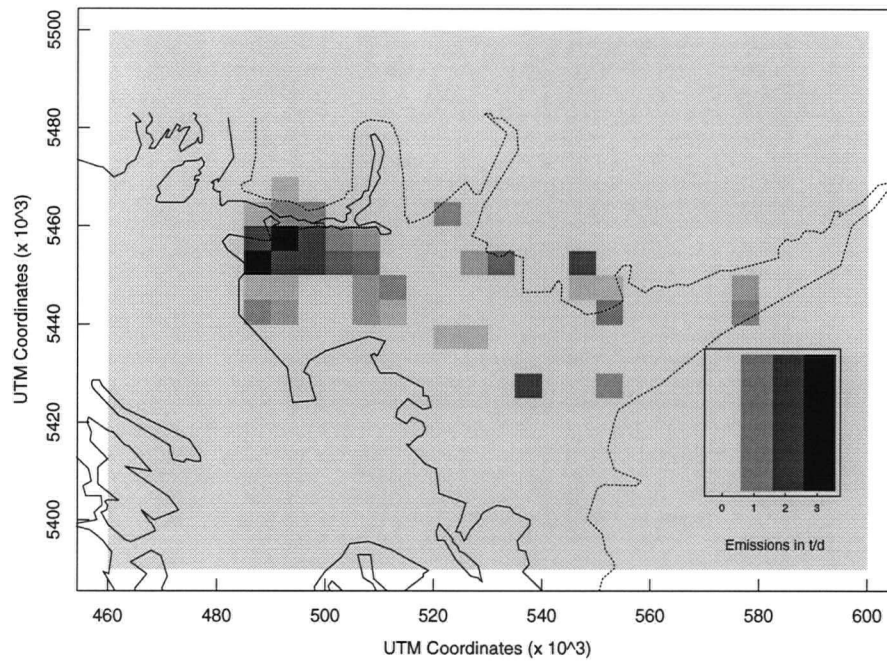
much as 30% over the course of a day. However, given the fact that VOC emissions from gas marketing sources are dominated by emissions from mobile, area and point sources, and that no episodic corrections were made for point sources, further adjustments to the emissions were not merited.

4.3.4 Area Sources

Area sources comprised all sources not covered in the above-mentioned categories. This inventory included emissions from natural sources, combustion operations, solid waste incineration and general evaporative losses. The general methodology used to estimate the base case emissions consisted of using surrogate quantities with emission factors which were independent of temperature or season. Space heating emissions were adjusted to reflect variations with heat load, and particulate emissions were adjusted to reflect variations with wind speed. However, for biogenic emissions and evaporative solvent losses, which respectively comprised 60% and 30% of area source VOC emissions, no such adjustments were provided. In addition, reference temperatures were not reported for the given emission factors. Hence, episodic adjustments of the biogenic and evaporative emissions were not possible based on the available data.

To address the seasonality and diurnal nature of biogenic emissions, emission factors generated using PC-BEIS and recommended by Lamb were applied to existing land use factors. These factors were used in the final biogenic emission estimates for the 1990 emissions inventory (B.H. Levelton and Western Research, 1993), which was not available in its final form at the time at which these inputs were being prepared for the simulation. Total area emissions in the LFV are summarized in Figure 4.8.

(a)



(b)

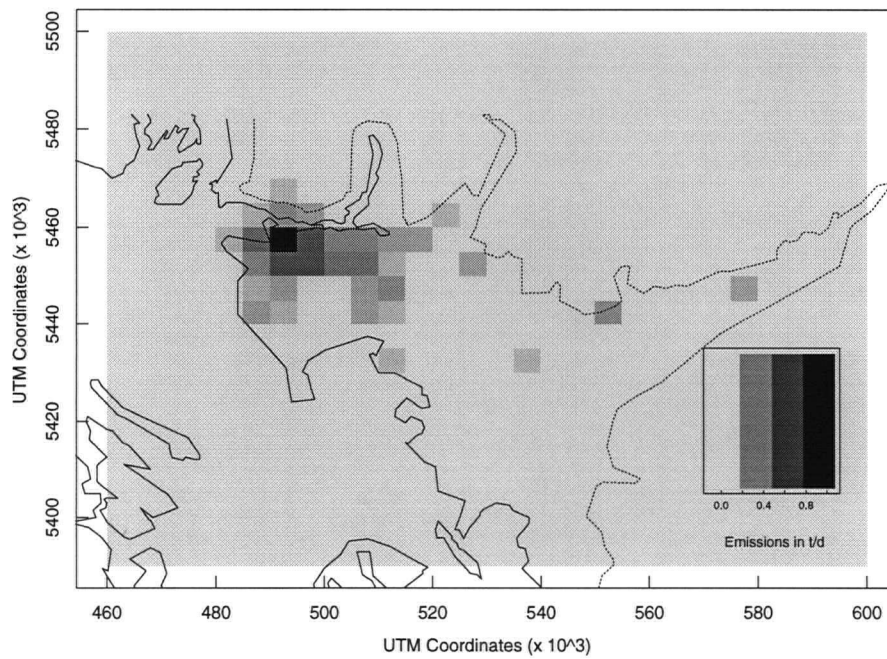


Figure 4.8: (a) VOC and (b) NO_x emissions (in t/d) from area sources in the LFV. Washington sources were not included.

4.3.5 US Sources

As seen in Table 4.4, emissions in the LFV are dominated by emissions from BC sources. U.S. sources account for approximately 15% of total NO_x emissions and 25% of total VOC emissions in the LFV. As noted previously, detailed emissions from the Washington inventory were not available at the time model inputs were being prepared. However, emissions from the following point sources were included: the Intalco aluminum smelter, Georgia Pacific, and the BP Oil and ARCO oil refineries. In 1987, these four industrial complexes contributed approximately 7900 tonnes of VOCs and 4500 tonnes of NO_x. Compared to total point source estimates in the 1990 inventory, this would account for more than 100% of VOC and NO_x emissions.

A rough estimate of biogenic emissions from U.S. sources was also included in the simulation. This was done by applying emission factors developed by Lamb (B.H. Levelton and Western Research, 1993) to land use types derived by Miao (1993) for the U.S. domain.

4.4 Terrain Data

The TERRAIN file describes the characteristics of the underlying surface. It specifies (i) gridded roughness lengths, and (ii) gridded deposition factors for the domain. Both roughness lengths and deposition factors are based on studies by the Argonne National Laboratory (Sheih et al., 1986) for specific landuse types. Landuse types found in the LFV were based on those used by Miao (1993), who relied on local landuse maps and observations. Landuse types found in the LFV are listed in Table 4.6 along with the corresponding terrain factors.

Table 4.6: Default landuse types and terrain factors (Sheih et al., 1986).

Landuse Type	Surface Roughness (m)	Deposition Factor
Urban	3.00	0.2
Agricultural	0.25	0.5
Coniferous forest including wetlands	1.00	0.3
Mixed forest	1.00	0.3
Water	0.0001	0.03
Non-forest wetlands	0.15	0.3
Mixed agricultural and range	0.10	0.5

4.5 Chemical Parameters

The CHEMPARAMS file contains a list of the chemical species, reaction properties, and stoichiometric coefficients for the reactions found in CBM-IV. Although not reproduced here, a detailed description may be found in Morris and Myers (1990).

4.6 Simulation Control Parameters

The SIMCONTROL file contains simulation control data which specifies

- simulation start and end times and dates;
- simulation options such as flags for restart, surface removal, and availability of point source, temperature and terrain data;
- maximum time step and maximum number of time steps;

- minimum chemistry time step, maximum number of iterations, relative error tolerance, and a darkness criterion to determine if night chemistry is necessary;
- output and print options.

The 66-hour simulation was carried out for the period between 0600 LST on 17 July 1985 and 2400 PST on 19 July 1985. The surface removal option was used. A maximum time slice and the maximum number of time slices in a time step were set at 0.1 hour and 1, respectively, as recommended by Morris and Myers (1990). Recommended criteria for chemistry time step (.00001 hour), maximum number of iterations (20) and relative error tolerance required for convergence of the chemistry step (.02) were also used.

Chapter 5

Model Results and Discussion

The criteria used to assess model results are presented, followed by an evaluation of model performance based on concentrations predicted for O₃ and its precursor NO₂. Factors which may have influenced model performance are discussed. Sensitivity indicators are determined for various sites as a further means of assessing model performance.

5.1 Model Performance Criteria

Model performance is evaluated in terms of the model's ability to reproduce diurnal and spatial patterns of pollutant concentrations during a 66-hour simulation extending from 0600 PST on 17 July 1985 to 2400 PST on 19 July 1985. This will be done by

- comparing time series of predicted and observed concentrations,
- comparing contours based on predicted concentrations with observed values,
- comparing predicted and observed maximum concentrations for each station for each day of the simulation,
- comparing the values of statistical parameters (peak accuracy, bias and gross error) to accepted criteria.

Based on a review of photochemical modelling studies, Tesche et al. (1990) reported that on average, photochemical simulations produce peak (unpaired) accuracies, overall bias and gross error statistics of $\pm 15-20\%$, $\pm 5-15\%$ and $30-35\%$, respectively. The California

Air Resources Board (CARB) recommends similar statistics as typical UAM performance goals for O₃ (CARB, 1990). Corresponding performance goals for NO₂ are $\pm 50\%$, $\pm 30\%$ and 50% , respectively. These criteria will be applied to model output as a means of assessing the acceptability of model performance.

5.2 Ozone

Time series comparing observed and predicted O₃ concentrations are shown in Figures 5.1-5.3 for the 11 monitoring stations reporting O₃ concentrations during this episode. Symbols represent hourly observed concentrations while the solid, thick lines represent predicted concentrations that have been hourly averaged and distance-weighted from the grid averages of the four nearest grid cells. Hatched lines indicate the range of minimum and maximum predicted concentrations over the nine nearest grid cells. Stations have been grouped together as follows:

- Stations T02, T03, T04 and T05 are within or near the urban core;
- Stations T07 and T09 are suburban sites that are located at the eastern end of Burrard Inlet, and T14 is an elevated site located on Burnaby Mountain, and
- Stations T15, T16, T11 and T12 are suburban or rural sites located downwind of the main source area.

A number of observations can be made from the time series shown in Figures 5.1-5.3:

- The model can reproduce the typical diurnal O₃ patterns in which peak concentrations are observed during mid-afternoon and minimum concentrations are observed at night.

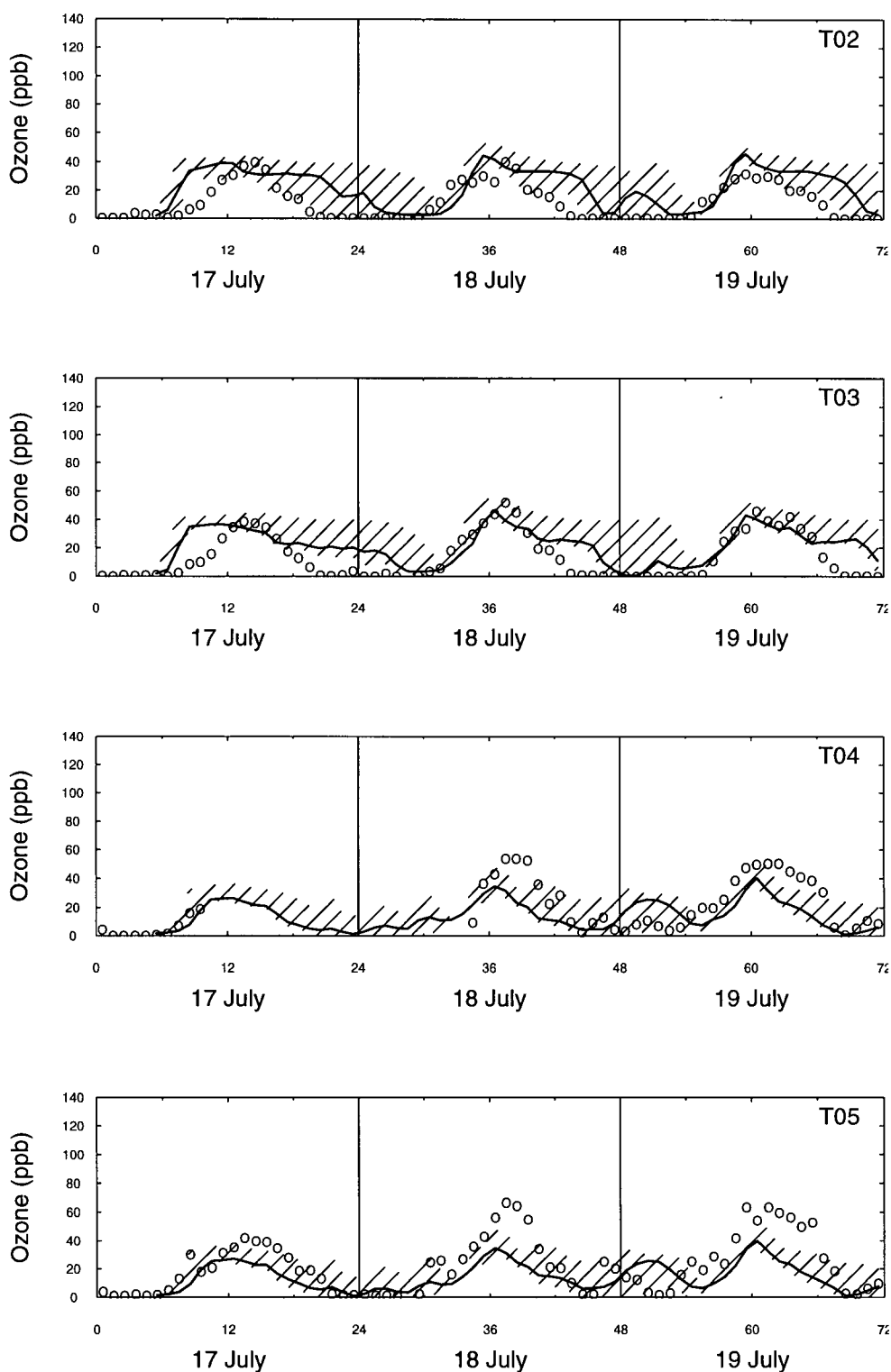


Figure 5.1: Predicted and observed O_3 concentrations at stations T02, T03, T04 and T05 in the LFV, 17-19 July 1985. Solid lines represent predicted concentrations and hatched lines show the range in neighbouring grid cells. Open circles indicate observations.

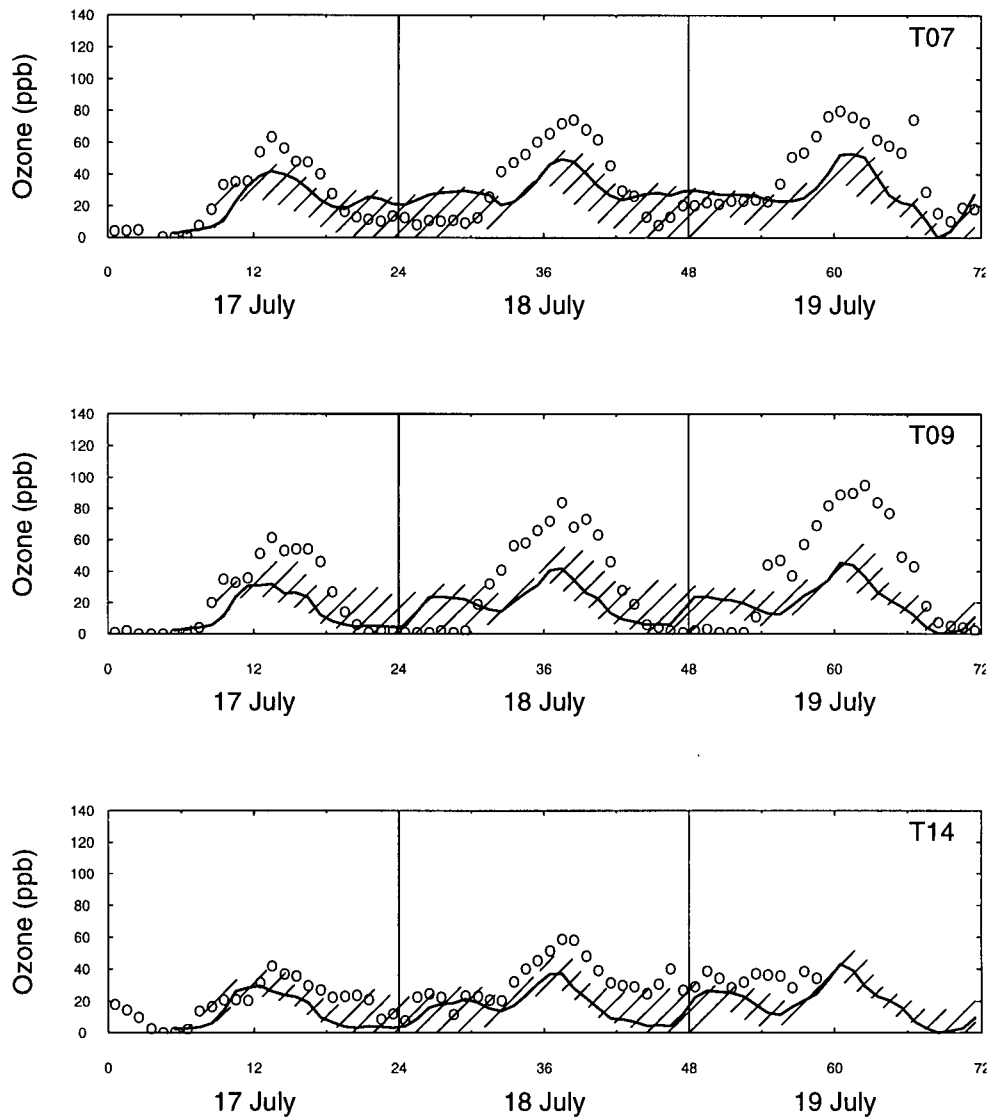


Figure 5.2: Predicted and observed O_3 concentrations at stations T07, T09 and T14 in the LFV, 17-19 July 1985. Solid lines represent predicted concentrations and hatched lines show the range in neighbouring grid cells. Open circles indicate observations.

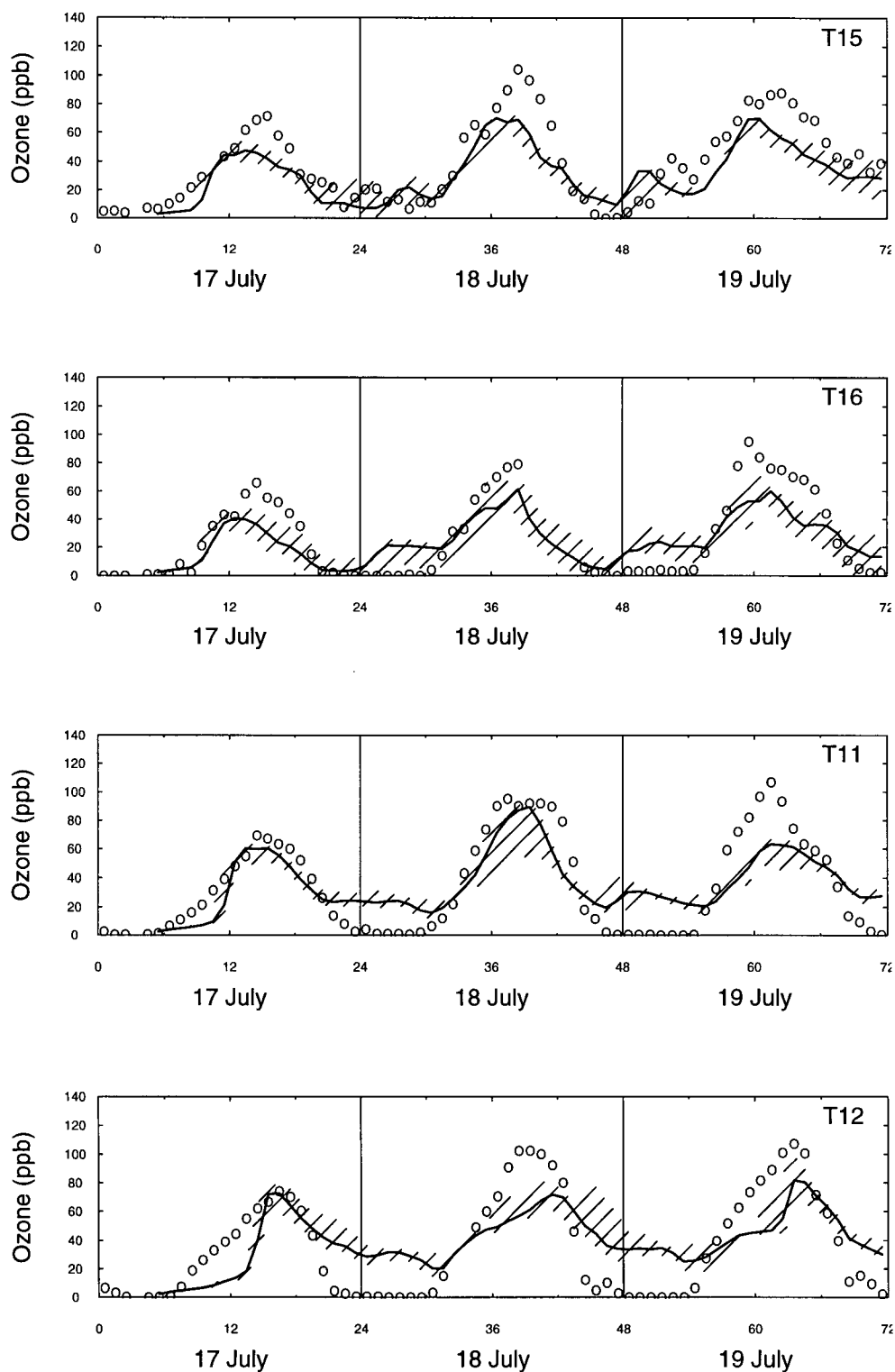


Figure 5.3: Predicted and observed O_3 concentrations at stations T15, T16, T11 and T12 in the LFV, 17-19 July 1985. Solid lines represent predicted concentrations and hatched lines show the range in neighbouring grid cells. Open circles indicate observations.

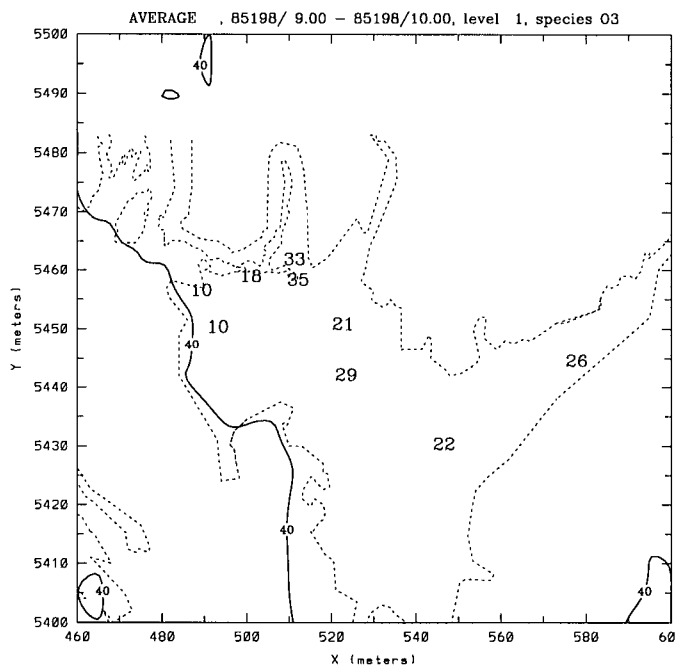
- The model tends to underpredict O_3 concentrations during the day, and overpredict at night when observed values approach zero. The latter feature is particularly noticeable at stations T11 and T12, which are located downwind of the main source region.
- With the exception of the first day of the simulation, the morning buildup of O_3 is represented quite well at most stations. However, the predicted morning buildup of O_3 levels at stations T07 and T09 is seen to lag the observations, even though there is good agreement in the timing of the daily maximum. The buildup of O_3 at rural sites T11 and T12 is also very poorly reproduced on 19 July.

Spatial patterns of predicted O_3 concentrations (surface layer) are depicted in Figures 5.4-5.6. For each day of the simulation, O_3 isopleths at 0900, 1200, 1500 and 1800 PST are presented. Contours are plotted at 20 ppb intervals, beginning at 40 ppb.

As shown in Figure 5.4, the morning of 17 July is characterized by relatively low O_3 concentrations throughout the entire modelling domain. By 1500 PST, concentrations in excess of 60 ppb are found over a wide band extending eastward along the Coast Mountains from Burrard Inlet, and a smaller area extending up-valley from Abbotsford to Chilliwack. As expected, O_3 levels are depressed over the major source region, most likely the result of NO scavenging. By 1800 PST, ozone patterns are displaced further up the valley.

The predicted patterns for 18 July shown in Figure 5.5 are characterized by higher concentrations over a much broader area than the previous day. At 0900 PST, spatial patterns are still very disorganized, but it is clear that levels are depressed over an area including Burrard Inlet and downtown Vancouver. At 1200 PST, O_3 levels in excess of 60 ppb are located over the Coast Mountains, north of Indian Arm and Pitt Lake, and over a wide band extending eastward from Boundary Bay in South Surrey towards

(a)



(b)

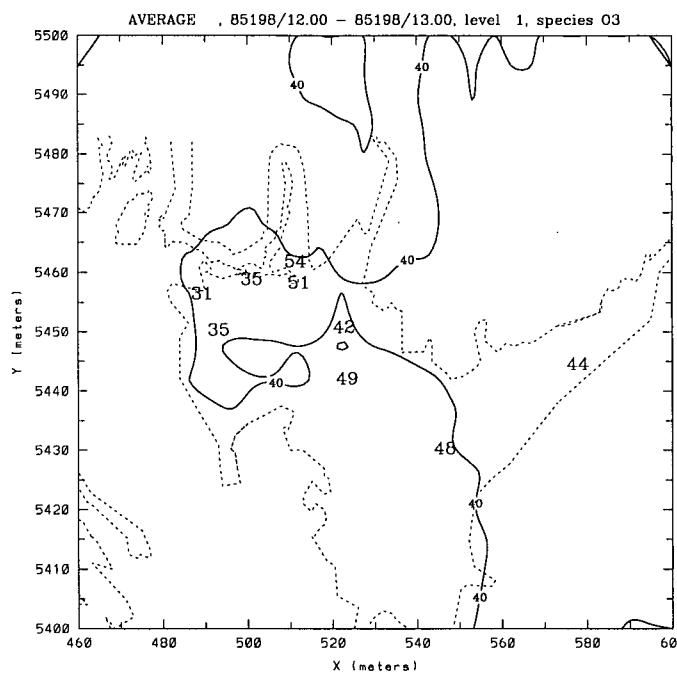
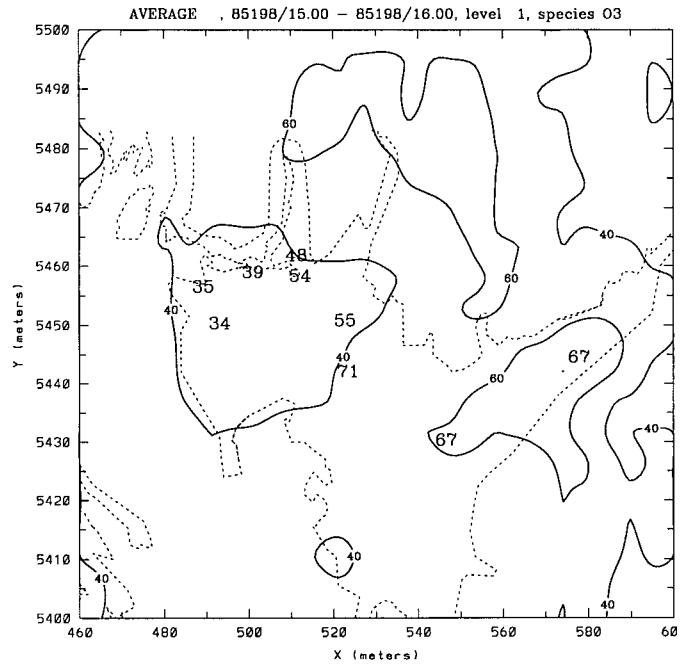


Figure 5.4: Contours of predicted O₃ at 20 ppb intervals on 17 July 1985 at (a) 0900 PST, (b) 1200 PST, (c) 1500 PST and (d) 1800 PST. Large numbers indicate observed concentrations. Missing values are indicated by “-99”.

(c)



(d)

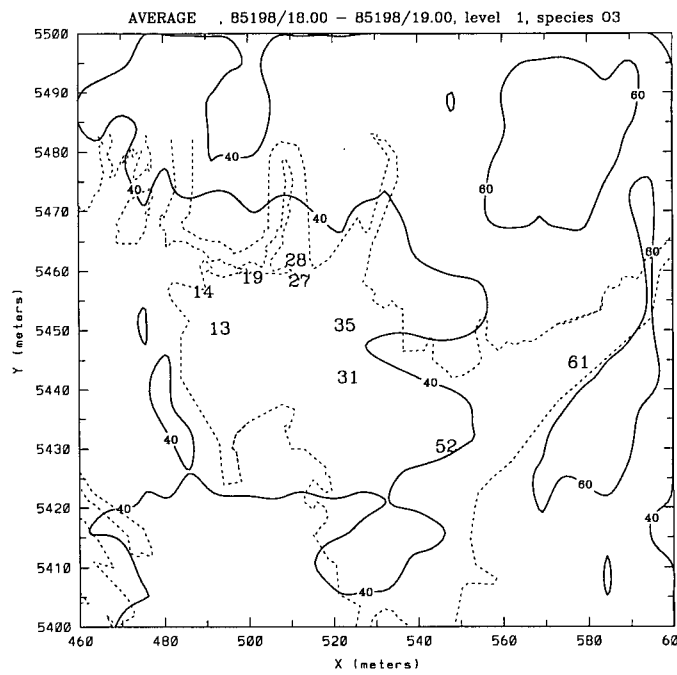
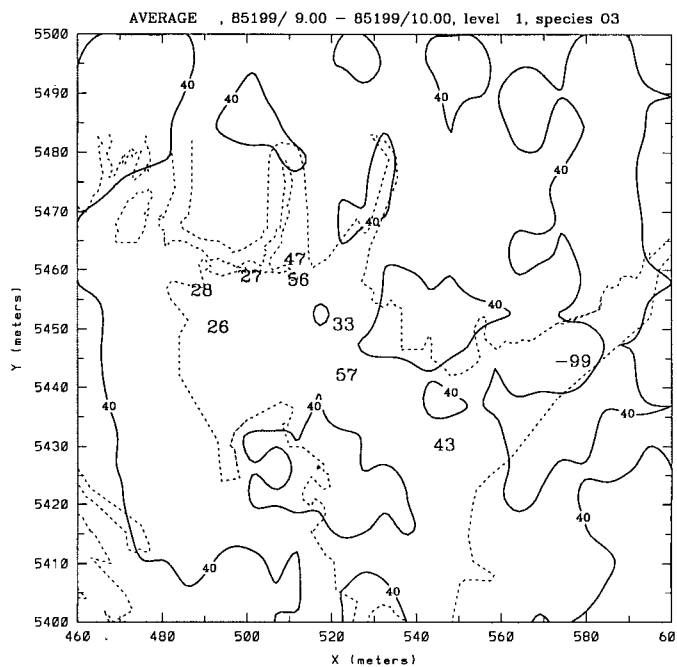


Figure 5.4 (Continued).

(a)



(b)

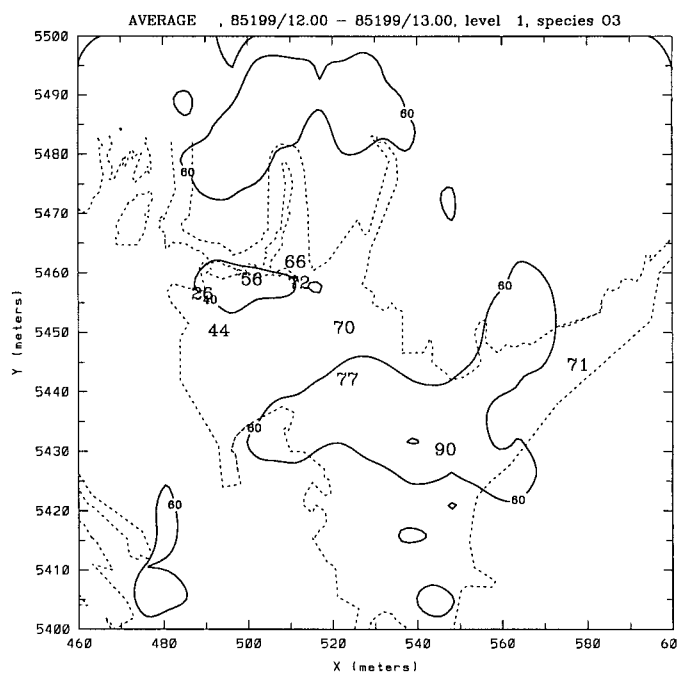
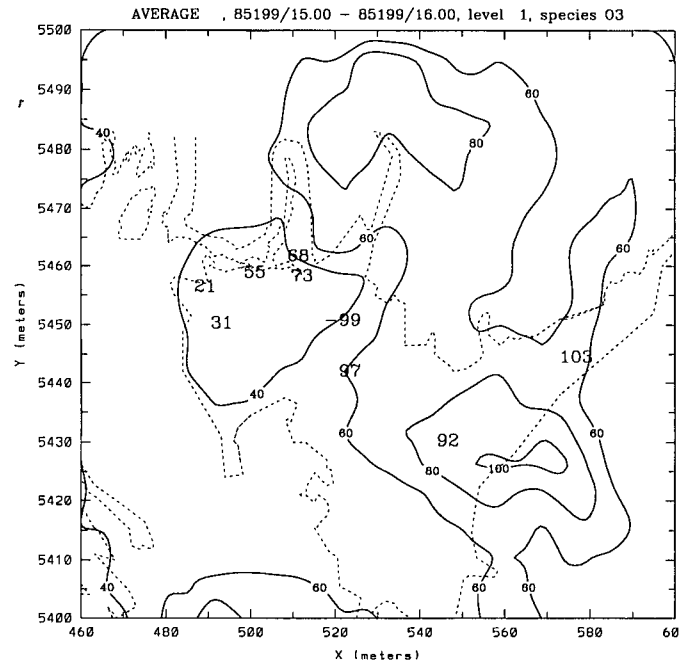


Figure 5.5: Contours of predicted O₃ at 20 ppb intervals on 18 July 1985 at (a) 0900 PST, (b) 1200 PST, (c) 1500 PST and (d) 1800 PST. Large numbers indicate observed concentrations. Missing values are indicated by “-99”.

(c)



(d)

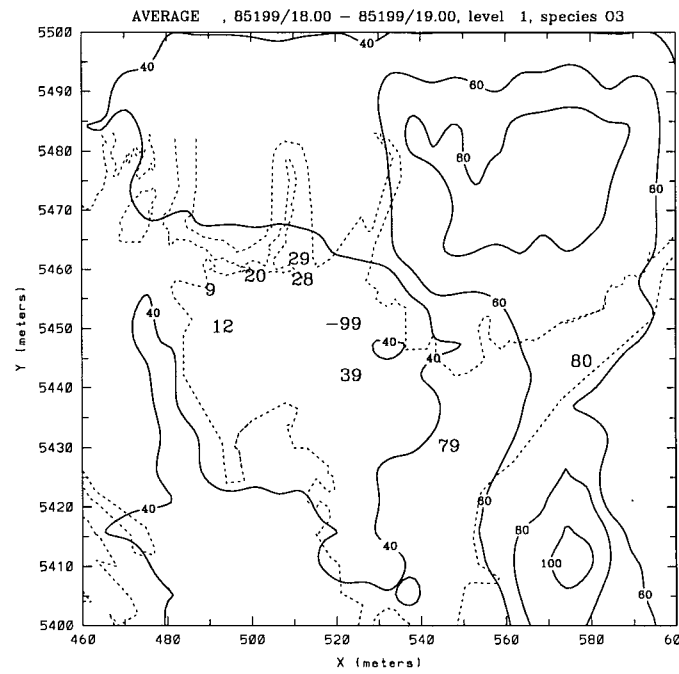
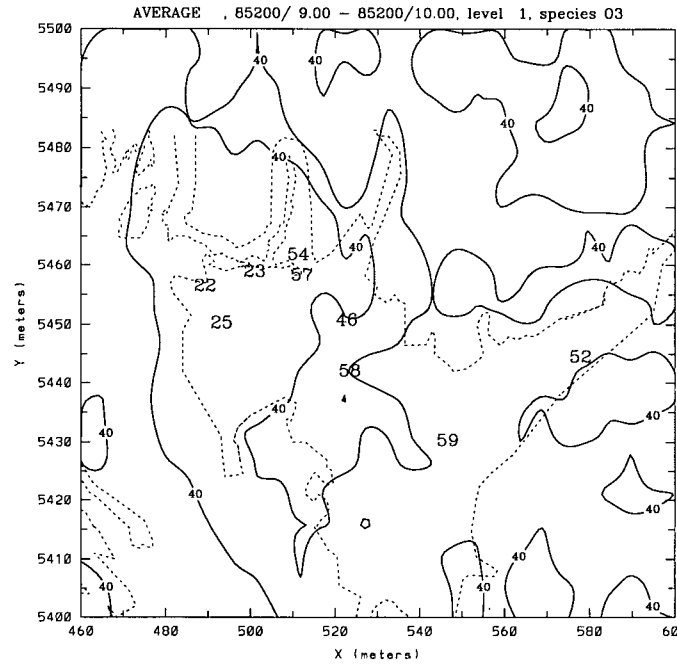


Figure 5.5 (Continued).

(a)



(b)

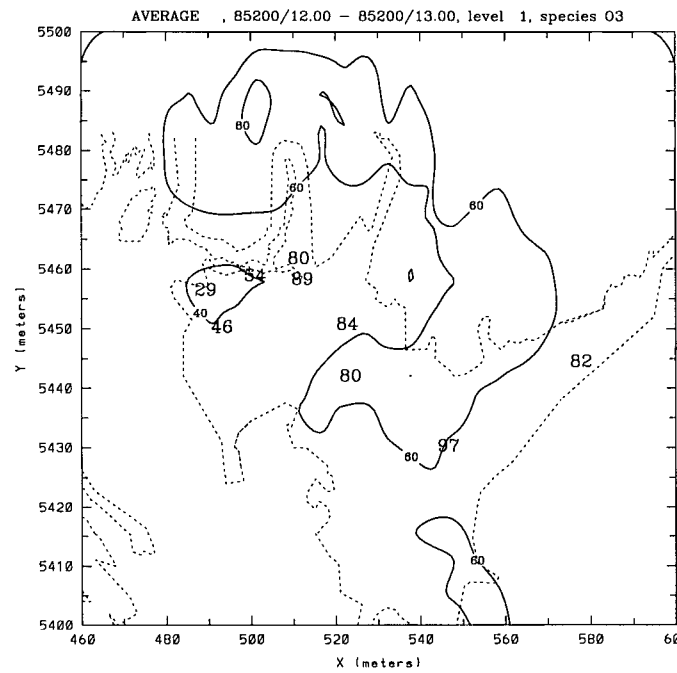
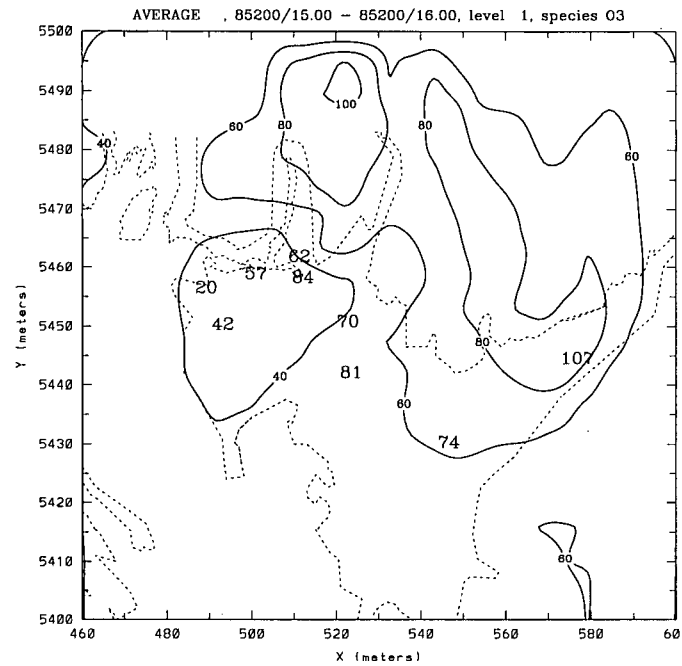


Figure 5.6: Contours of predicted O_3 at 20 ppb intervals on 19 July 1985 at (a) 0900 PST, (b) 1200 PST, (c) 1500 PST and (d) 1800 PST. Large numbers indicate observed concentrations. Missing values are indicated by “-99”.

(c)



(d)

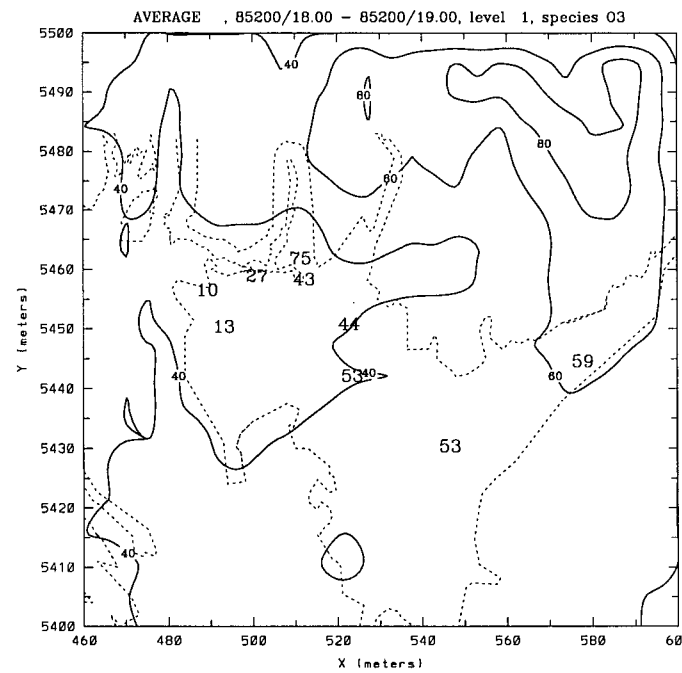


Figure 5.6 (Continued).

Chilliwack. An additional region of elevated O_3 is found over the Strait of Georgia, to the south of Saturna Island. In contrast, depressed concentrations less than 40 ppb are found over an area encompassing Burrard Inlet. At 1500 PST, a large band of elevated O_3 concentrations extends in an almost north-south fashion over the central valley. Maximum concentrations are found at the northern and southern ends of this band, with O_3 concentrations in excess of 80 ppb at the north end of Pitt Lake and more than 100 ppb to the southeast of Abbotsford. The very high concentrations observed at downwind sites T15 (97 ppb) and T12 (103 ppb) and the moderately high concentrations at T07 and T09 were not predicted by the model. The small region of elevated O_3 concentrations located off Saturna Island at 1200 PST has now moved in a southeasterly direction down the Strait of Georgia. The area of depressed concentrations observed over Burrard Inlet at 1200 PST has now grown to encompass most of Vancouver, North Burnaby and Port Moody. By 1800 PST, the large area of elevated O_3 concentrations stretching across the valley has been displaced to the southeast, suggesting transport over the Cascade Mountains. The area of depleted O_3 has grown further to include most of the GVRD and much of the Washington State side of the LFV.

Similar patterns are observed for 19 July, although maximum concentrations are somewhat higher. At 1200 PST, O_3 concentrations in excess of 80 ppb are found over the Coast Mountains. The model fails to capture the elevated concentrations observed at T07 and T09. In contrast to the previous day, elevated O_3 levels are not found off Saturna Island. At 1500 PST, the O_3 patterns are displaced further northward than found on the previous day. Peak concentrations in excess of 100 ppb are found to the north of Pitt Lake. High concentrations observed at stations T15 and T16 are not captured. By 1800 PST, the entire pattern is shifted eastward.

Maximum predicted and observed ground-level O_3 concentrations are presented in Table 5.1 on a daily basis for each station. The times of the respective maxima are also

Table 5.1: Observed and predicted maximum one-hour O₃ concentrations in ppb and corresponding hour (PST) at monitoring stations in the LFV, 17-19 July 1985.

Station	17 July 1985				18 July 1985				19 July 1985			
	Obs.	Hr	Pred.	Hr	Obs.	Hr	Pred.	Hr	Obs.	Hr	Pred.	Hr
1	29.6	15	33.2	13	42.2	13	39.4	13	33.0	14	40.8	12
2	39.5	15	39.3	12	39.9	14	44.3	12	31.7	12	45.7	12
3	38.4	14	36.6	12	51.9	14	46.4	13	45.6	13	43.3	12
4	19.1	10	26.6	13	53.6	15	34.7	13	50.3	14	40.5	13
5	41.7	14	26.9	13	66.6	14	34.6	13	63.4	12	39.7	13
6	-	-	-	-	-	-	-	-	42.0	14	43.4	13
7	63.7	14	41.7	14	74.2	15	49.5	14	79.9	13	53.2	14
9	61.0	14	32.0	14	84.0	14	41.9	14	95.0	15	45.3	13
11	69.2	15	60.5	16	95.4	14	89.7	16	106.7	14	63.1	14
12	73.9	17	72.6	17	102.5	16	71.9	18	107.2	16	81.7	16
14	42.1	14	29.8	13	58.7	14	37.1	14	39.0	2	43.4	13
15	71.3	16	47.6	14	104.4	15	70.1	13	87.8	15	69.9	13
16	66.0	15	40.6	13	79.0	15	61.3	15	95.0	12	59.9	14

presented. Maximum observed O₃ concentrations increased over the three-day period, registering 73.9 ppb (T12), 104.4 ppb (T15) and 107.2 ppb (T12) on the 17th, 18th, and 19th, respectively. Maximum predicted concentrations over the same period were 72.6 ppb (T12), 89.7 ppb (T11) and 81.7 ppb (T12), respectively. The time of the predicted maxima coincided with observations on the 17th and 19th, and lagged by one hour on the 18th. As indicated previously by the time series in Figures 5.1-5.3, there is an overwhelming tendency for the model to underpredict O₃ levels.

All predicted concentrations and all residuals calculated between the predicted and observed concentrations are compared against hourly observations in Figure 5.7. These plots indicate that there is a tendency for the model to overpredict low concentrations

(i.e. <20 ppb) and to underpredict concentrations in excess of 40 ppb.

Mean bias and error based on predicted and observed O₃ concentrations are presented for each station in Table 5.2. Paired observations and model predictions were only included where observations exceeded 20 ppb, and the number of pairs is also provided in Table 5.2. Although a slight tendency to overpredict O₃ concentrations is noted for the two stations located on the west side of Vancouver (T01 and T02) on each day of the simulation, data from the other stations indicate an overwhelming tendency to underpredict peak O₃ concentrations. This is evident even when relaxing spatial criteria to include the predicted concentrations in the nine nearest grid cells. Mean normalized bias ranged from 15.2% at T01 to -49.9% at T09 on the 17th, 14.8% at T01 to -57.7% at T09 on the 18th, and 38.8% at T01 to -61.8% at T09 on the 19th. Mean normalized gross error ranged from 14.4% at T03 to 49.9% at T09 on the 17th, 17.2% at T03 to 57.7% at T09 on the 18th, and 14.2% at T03 to 61.8% at T09 on the 19th.

From the time series shown in Figures 5.1-5.3 and these performance statistics, it is evident that model performance is worst for those sites located immediately on the downwind side of the urban core, which is the main source region. Model performance was particularly poor for stations T04, T05 and T09, which are each located toward the eastern end of Burrard Inlet and in close proximity to petroleum refineries, and station T14, which is an elevated site. Averaged over all paired data from all stations, normalized bias ranged from -28.5 to -31.3% and normalized gross error ranged from 35.6% to 36.9% over the three days of the simulation.

As a further measure of model performance, the accuracy of peak O₃ concentrations paired and unpaired in space and time for the three-day simulation are summarized in Table 5.3, together with mean bias and gross error. Peak unpaired accuracy increased over the three-day simulation from -1.8% to -23.8%. However, results generally agreed with the performance goal of ± 15 -20% recommended by Tesche et al. (1990). The

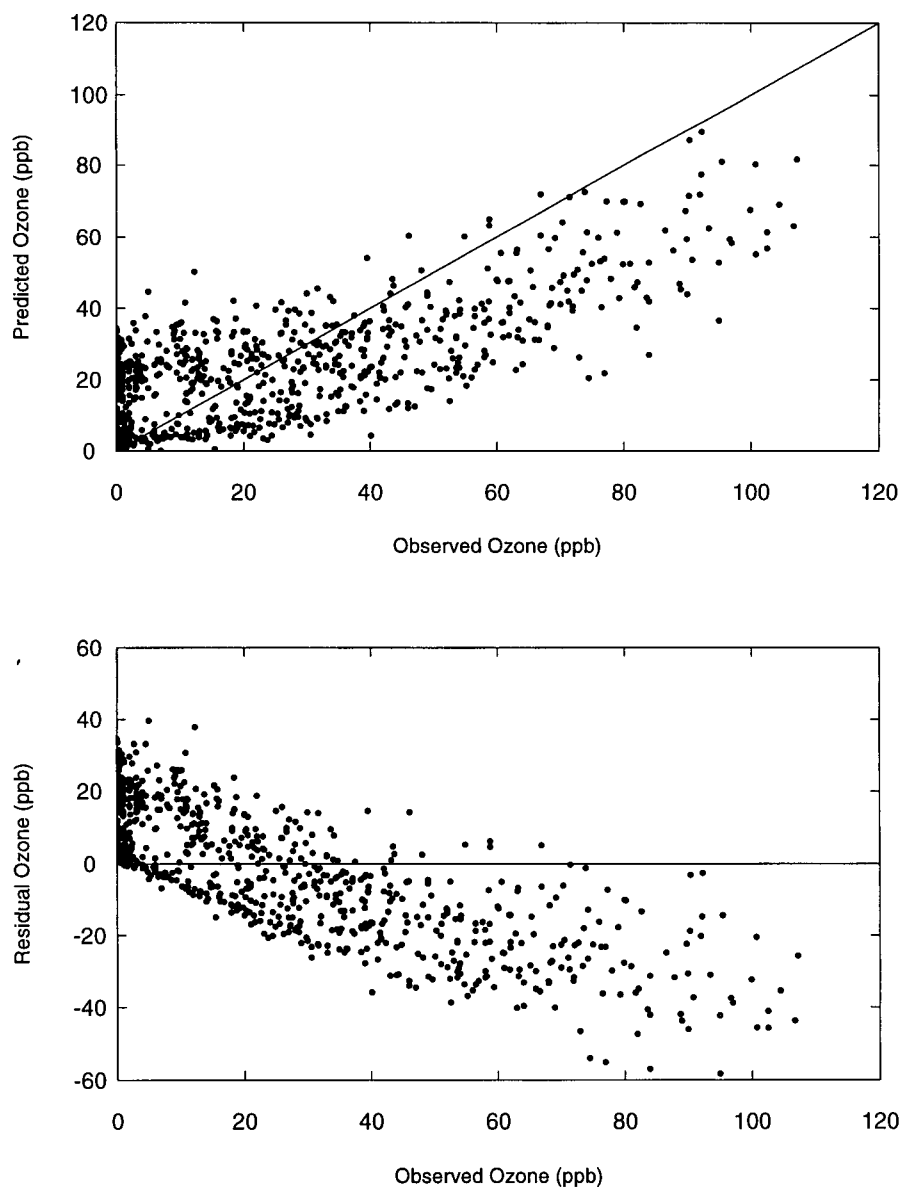


Figure 5.7: Comparison of predicted vs. observed O_3 concentrations (above) and comparison of residual (predicted-observed) vs. observed O_3 concentrations (below), all sites 17-19 July 1985.

Table 5.2: Model performance based on predicted and observed maximum one-hour O₃ concentrations at stations in the LFV, 17-19 July 1985.

Station	17 July 1985			18 July 1985			19 July 1985		
	Bias	Error	No.	Bias	Error	No.	Bias	Error	No.
1	0.152	0.153	4	0.148	0.174	5	0.388	0.388	4
2	0.122	0.263	6	0.096	0.402	8	0.263	0.263	6
3	-0.012	0.144	6	-0.122	0.172	7	-0.079	0.142	9
4	-	-	-	-0.468	0.467	8	-0.470	0.470	10
5	-0.353	0.405	9	-0.493	0.493	14	-0.551	0.551	12
6	-	-	-	-	-	-	-0.168	0.168	2
7	-0.336	0.336	10	-0.277	0.348	14	-0.231	0.387	20
9	-0.499	0.499	10	-0.577	0.577	12	-0.618	0.618	13
11	-0.225	0.250	12	-0.191	0.219	12	-0.250	0.288	12
12	-0.355	0.389	11	-0.223	0.285	10	-0.188	0.262	13
14	-0.388	0.484	13	-0.490	0.490	22	-0.384	0.385	11
15	-0.344	0.348	13	-0.297	0.312	14	-0.325	0.325	19
16	-0.383	0.383	10	-0.203	0.223	7	-0.256	0.311	12
Total	-0.291	0.356	104	-0.313	0.375	133	-0.285	0.369	143

timing of peak predictions agreed well with observations on 17 and 19 July, and lagged the observed maxima by one hour on 18 July. The mean normalized gross error, which averaged 37% over the three-day period, was just outside of the performance goal of 30-35%. The poorest performance was for mean normalized bias, which averaged 30% and compared poorly to the goal of 5-15%. This statistic reflects the fact that there was an overwhelming tendency for the model to underestimate O₃ concentrations.

Table 5.3: Model O₃ performance statistics for the LFV, 17-19 July 1985.

Performance measure	17 July 1985	18 July 1985	19 July 1985
Maximum observed O ₃ concentration (ppb)	73.9 (T12)	104.4 (T15)	107.2 (T12)
Maximum predicted O ₃ concentration (ppb)	72.6 (T12)	89.7 (T11)	81.7 (T12)
Peak accuracy			
paired in space and time	-1.8%	-32.6%	-23.8%
unpaired in space	-1.8%	-19.4%	-23.8%
unpaired in space and time	-1.8%	-14.1%	-23.8%
Time of observed O ₃ maximum	1600-1700 PST	1400-1500 PST	1500-1600 PST
Time of predicted O ₃ maximum	1600-1700 PST	1500-1600 PST	1500-1600 PST
Mean normalized bias	-29.1%	-31.3%	-28.5%
Mean normalized gross error	35.6%	37.5%	36.9%

5.3 Nitrogen Dioxide

Model performance is also evaluated in terms of the model's ability to reproduce NO_2 concentrations. Time series of modelled and observed NO_2 concentrations are compared in Figures 5.8-5.10. The following observations can be made from these time series:

- The model can reproduce diurnal patterns of NO_2 at those stations located near Burrard Inlet (T04,T05,T07 and T09) and in South Vancouver (T03).
- Reproduction of observed patterns is very poor at stations T02 and T14, where the timing of peak levels is out of phase.
- The model tends to underpredict peak NO_2 concentrations.

Poor model performance at station T02 reflects the inability of the model to simulate rather unusual local conditions in which observed NO_2 concentrations monotonically increased throughout the episode. The characteristic diurnal patterns were not evident. Monitor malfunction was ruled out by the local monitoring agency (GVRD, personal communication). Factors which may have contributed to this result include large and persistent NO_x emissions and/or depressed mixing heights in the vicinity of the station, which is located on the roof of a high school in a residential/light commercial area of Vancouver.

Spatial patterns of NO_2 concentrations predicted for 17-19 July 1985 are depicted in Figures 5.11-5.13. For each day, NO_2 isopleths at 0900 PST, 1200 PST, 1500 PST and 1800 PST are presented along with observed values. Contours are plotted at 10 ppb intervals, beginning at 10 ppb.

At 0900 PST on 17 July, the 10 ppb contour extends across the valley in a northwest-southeast fashion. Concentrations in excess of 30 ppb are found to the northeast of

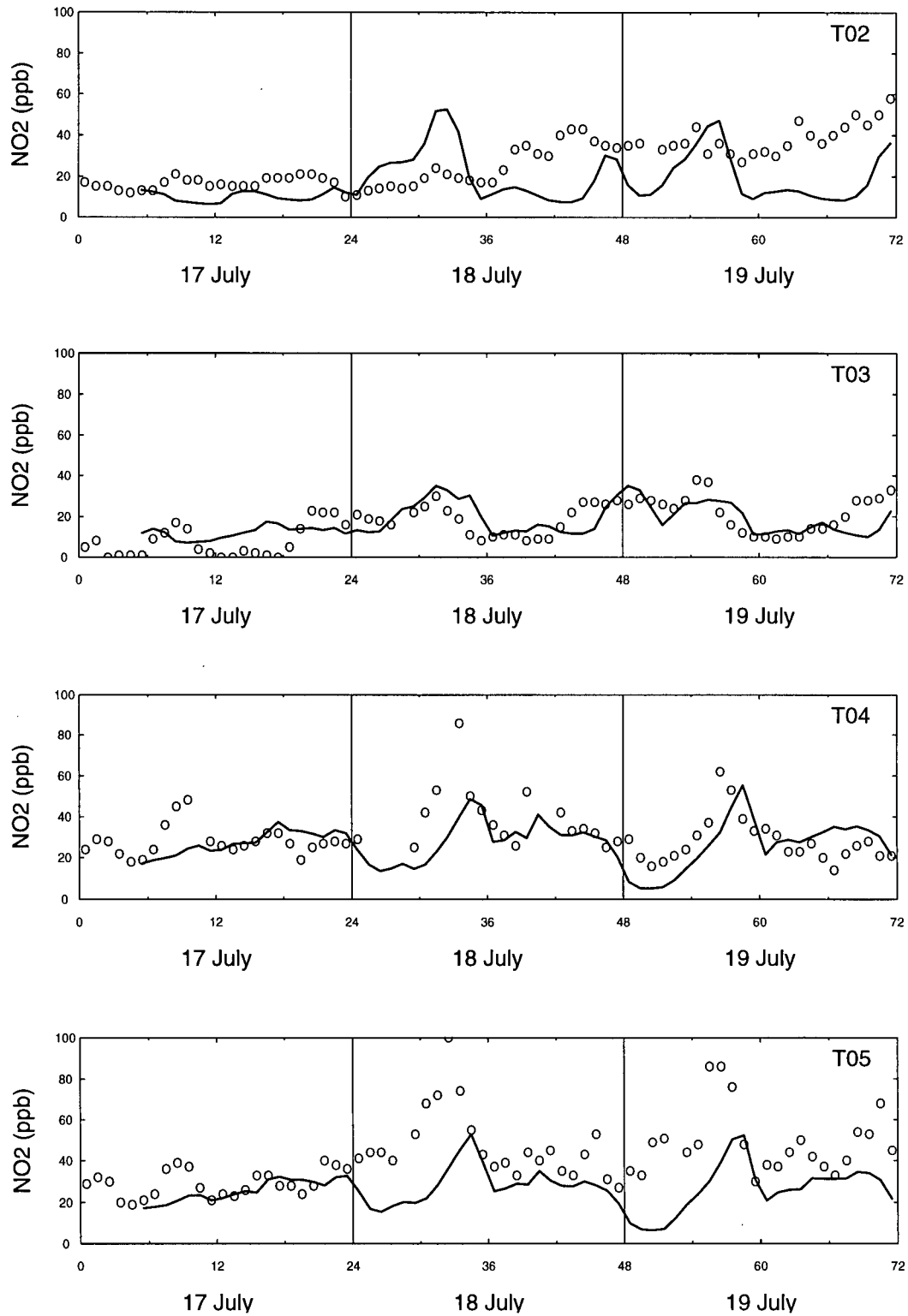


Figure 5.8: Predicted and observed NO₂ concentrations at stations T02, T03, T04 and T05 in the LFV, 17-19 July 1985. Solid lines show predicted values. Open circles indicate observed data.

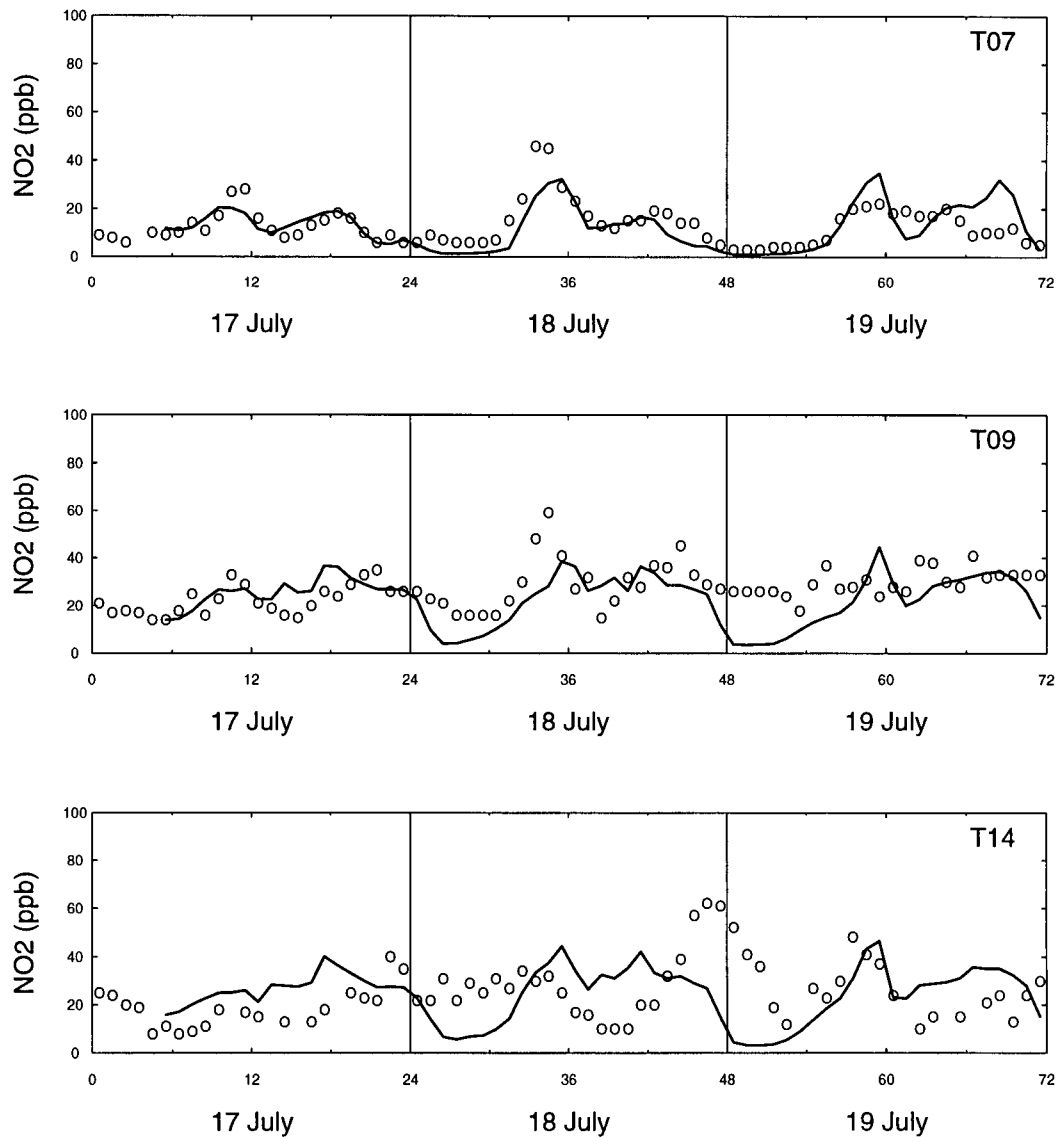


Figure 5.9: Predicted and observed NO₂ concentrations at stations T07, T09 and T14 in the LFV, 17-19 July 1985. Solid lines show predicted values. Open circles indicate observed data.

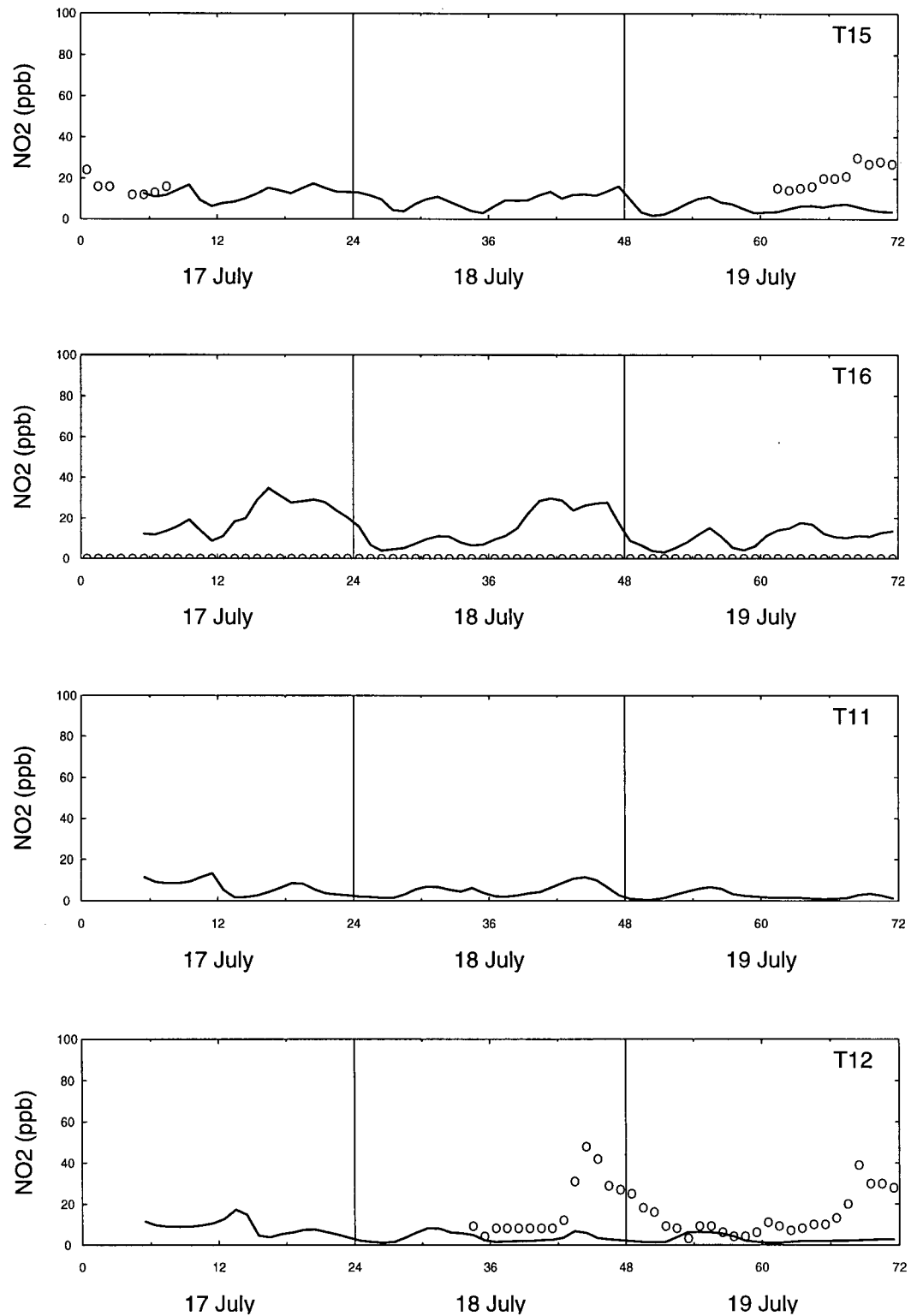
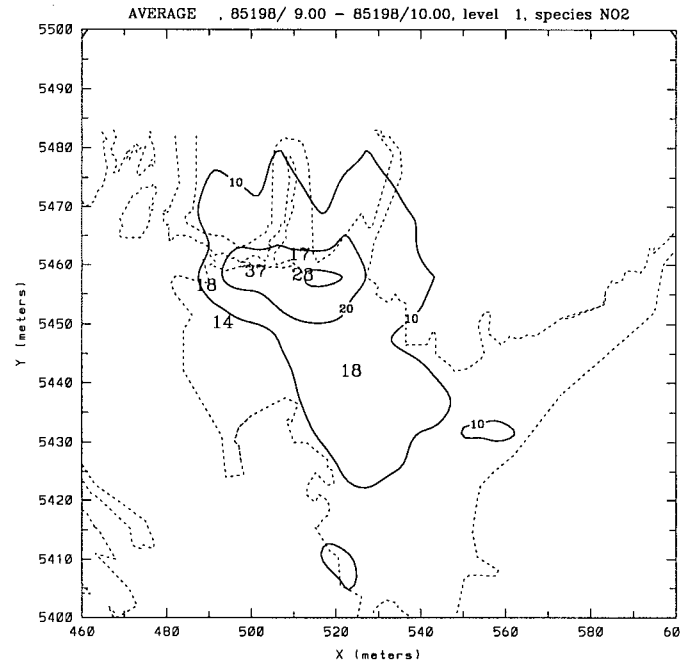


Figure 5.10: Predicted and observed NO₂ concentrations at stations T15, T16, T11 and T12 in the LFV, 17-19 July 1985. Solid lines show predicted values. Open circles indicate observed data.

(a)



(b)

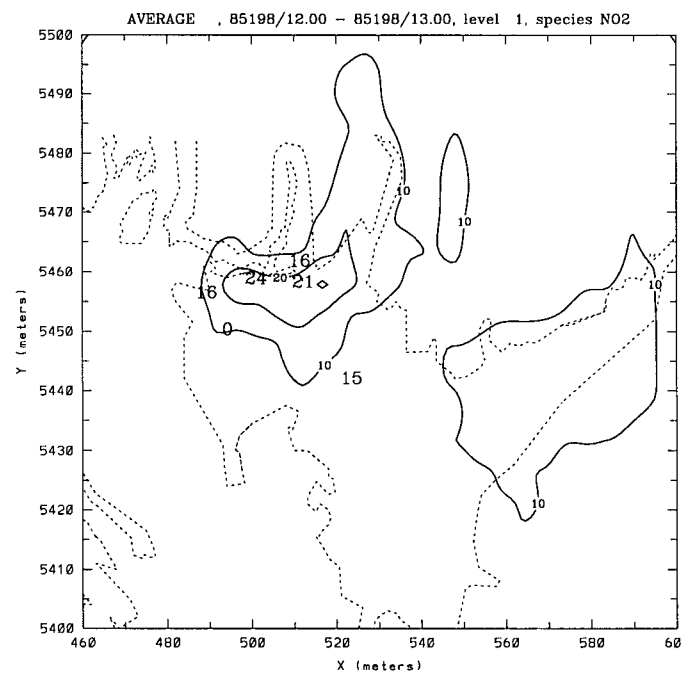
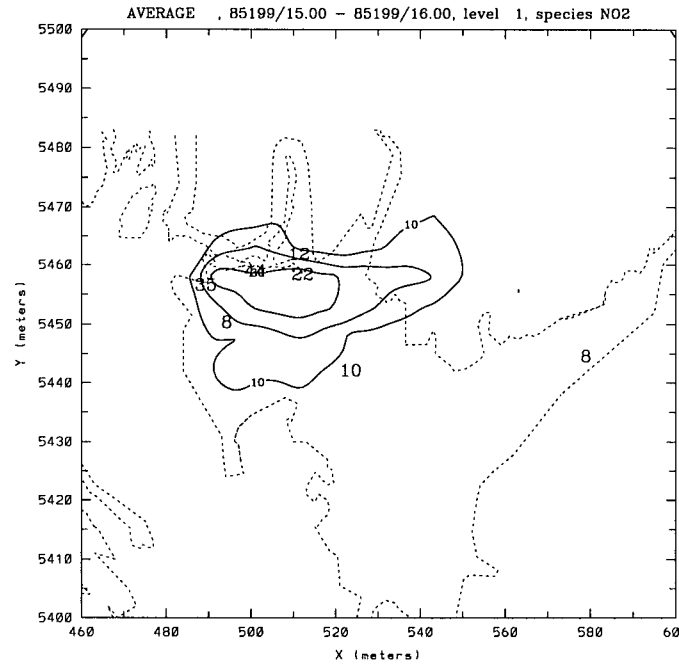


Figure 5.11: Contours of predicted NO₂ at 20 ppb intervals on 17 July 1985 at (a) 0900 PST, (b) 1200 PST, (c) 1500 PST and (d) 1800 PST. Large numbers indicate observed concentrations.

(c)



(d)

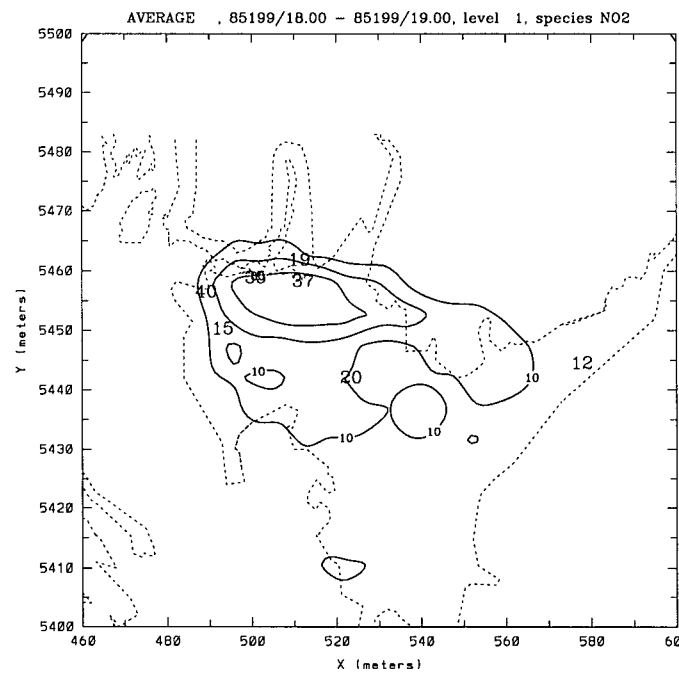
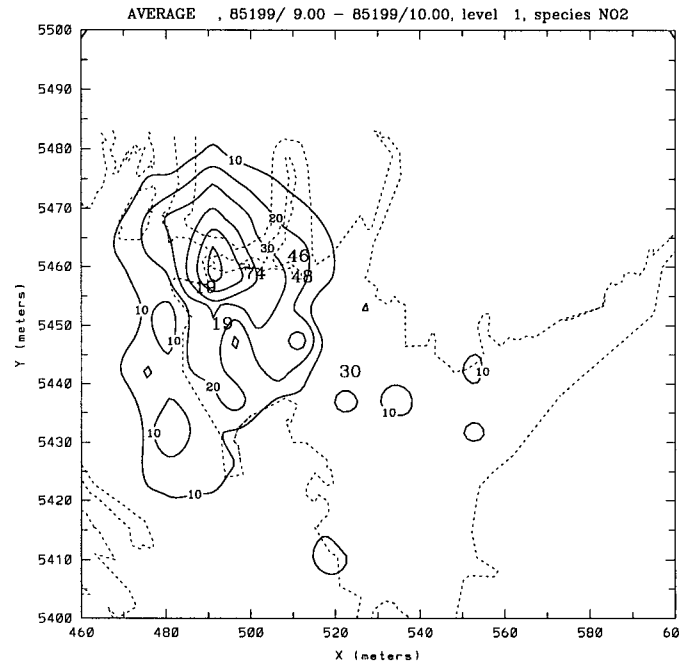


Figure 5.11 (Continued).

(a)



(b)

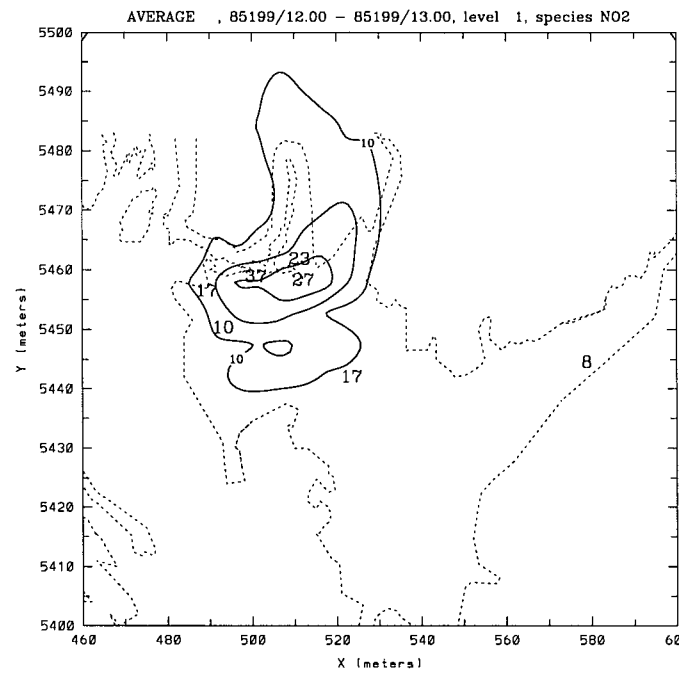
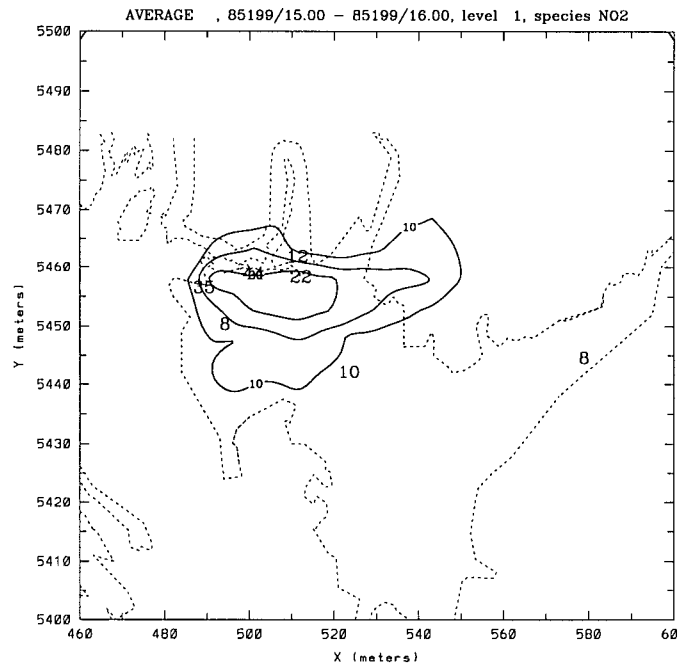


Figure 5.12: Contours of predicted NO_2 at 20 ppb intervals on 18 July 1985 at (a) 0900 PST, (b) 1200 PST, (c) 1500 PST and (d) 1800 PST. Large numbers indicate observed concentrations.

(c)



(d)

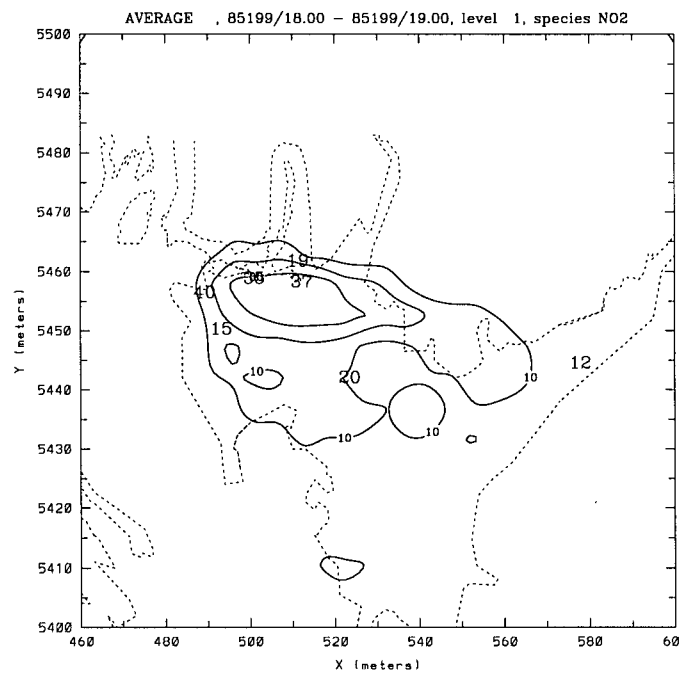
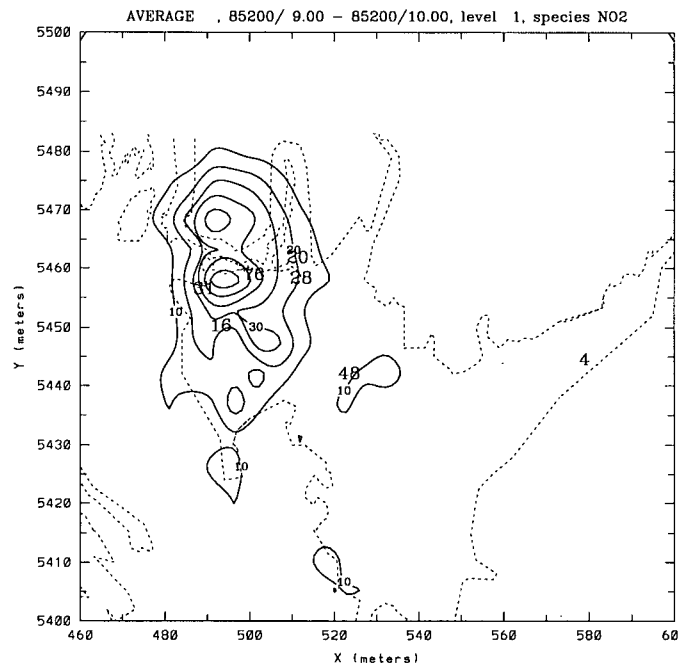


Figure 5.12 (Continued).

(a)



(b)

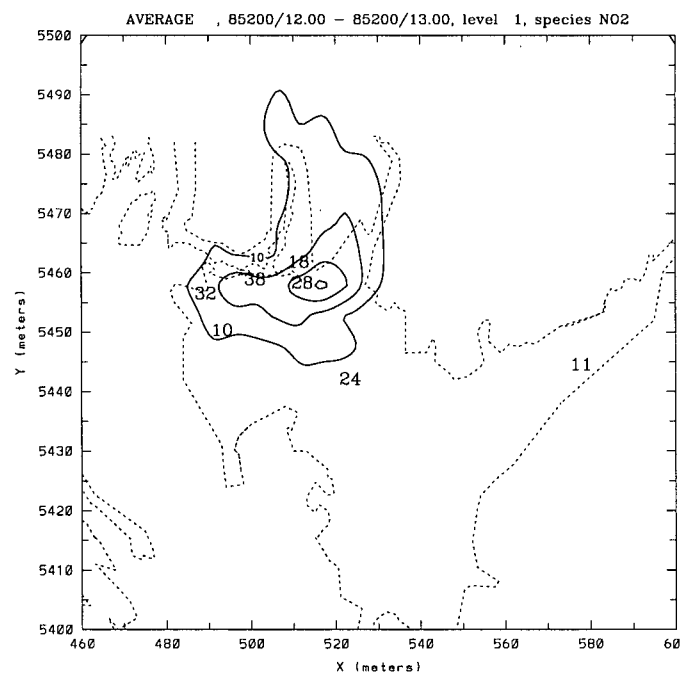
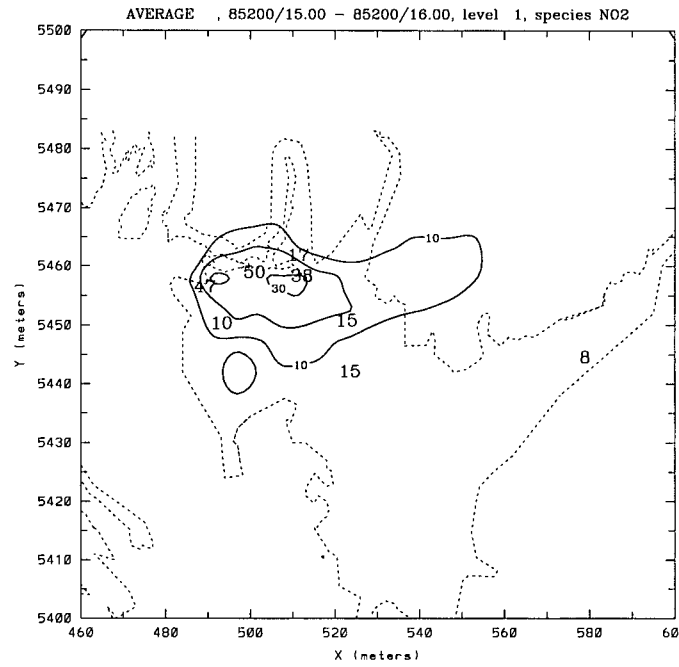


Figure 5.13: Contours of predicted NO_2 at 20 ppb intervals on 19 July 1985 at (a) 0900 PST, (b) 1200 PST. (c) 1500 PST and (d) 1800 PST. Large numbers indicate observed concentrations.

(c)



(d)

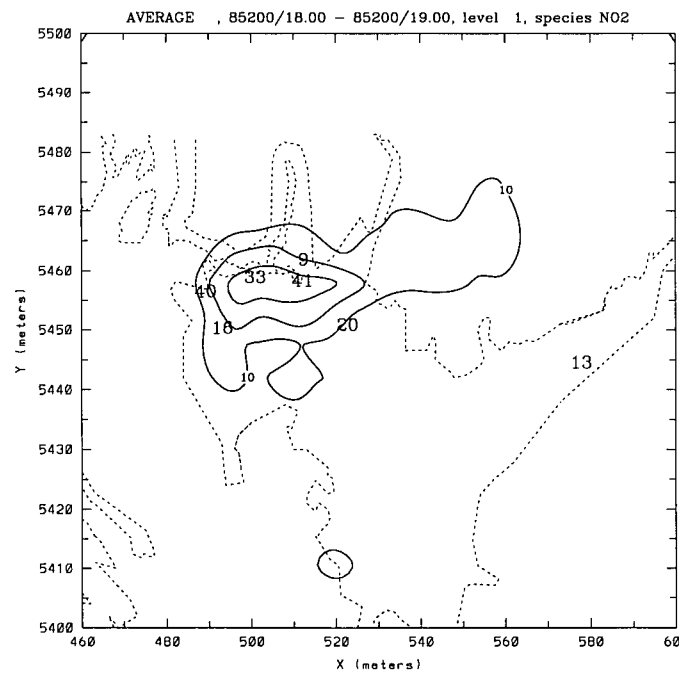


Figure 5.13 (Continued).

Burrard Inlet, toward the Pitt River valley. At 1200 PST, the L-shaped plume extends from the eastern end of Burrard Inlet to the Pitt River, and then spreads up the Pitt River valley to Pitt Lake. However, little change in the maximum concentrations are noted. By 1500 PST, the northern extension of the plume is no longer evident. NO_2 concentrations in excess of 40 ppb are predicted over the area between Burrard Inlet and the Pitt River.

Predicted NO_2 concentrations at 0900 PST on 18 and 19 July are much higher than predicted on 17 July. Strong concentration gradients are centred over Burrard Inlet and North Burnaby. However, comparisons with observed values at station T05 in Burnaby (100 ppb) indicate that NO_2 concentrations in this region were still greatly underpredicted during the morning hours. The afternoon hours are characterized by lower concentrations and weaker gradients, with predicted values in excess of 30 ppb found to the east of Burrard Inlet.

These observations are further reflected in Table 5.4, which lists the daily maximum predicted and observed NO_2 concentrations, and the respective times of these maxima, for each station. Maximum concentrations are greatly underpredicted at stations T04, T05 and T12 on 18 July, and at stations T05 and T12 on 19 July. The timing of observed maximum concentrations occurs during the late morning/early afternoon at most stations. However, at the downwind station T12 and the elevated station T14, the model predicts maxima to occur in the late evening.

Predicted concentrations and the associated residuals (predicted - observed) are compared against observations in Figure 5.14. It is clear from this figure that the model has a tendency to underpredict NO_2 concentrations above 30 ppb.

Similar model performance statistics as calculated for O_3 were also calculated for NO_2 , and the results are shown for individual stations in Table 5.5 and overall in Table 5.6. Paired predictions and observations were only included where observations exceeded 20

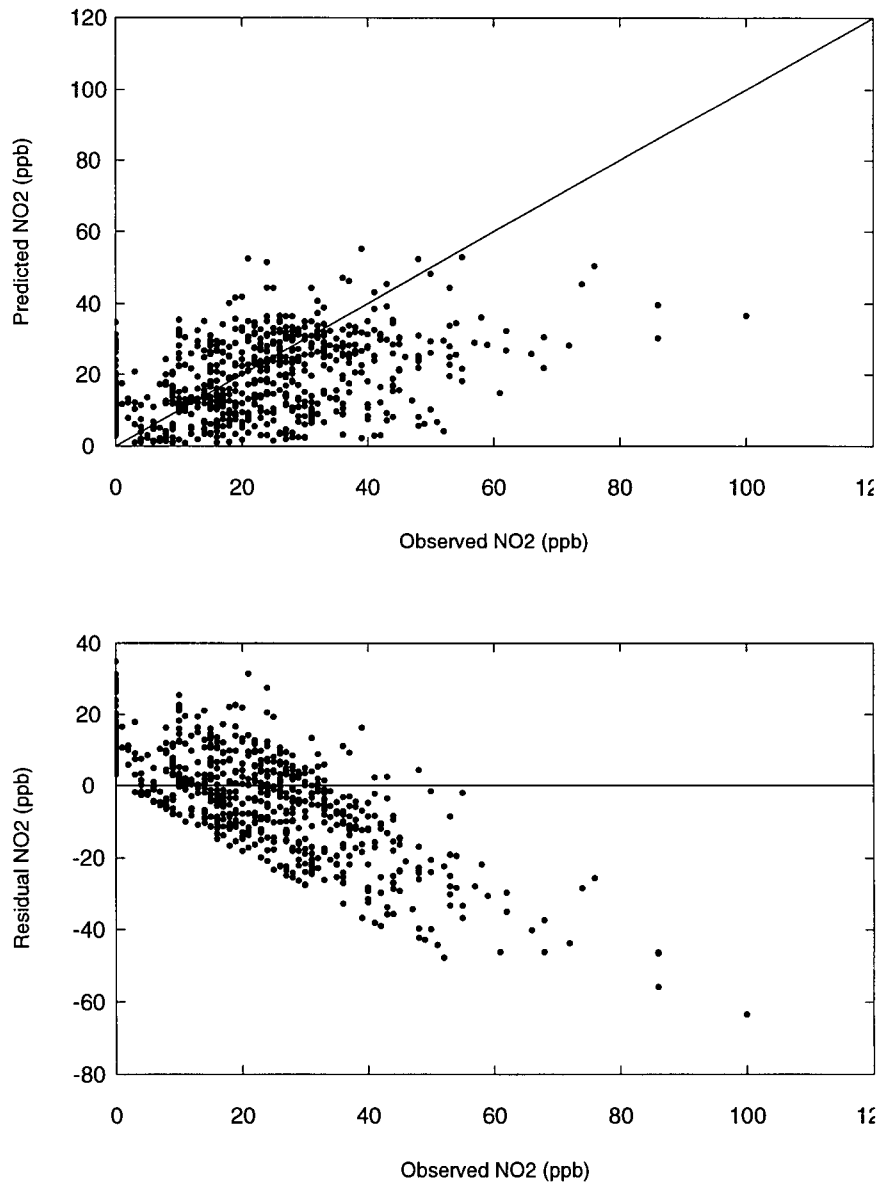


Figure 5.14: (a) Comparison of predicted vs. observed O_3 concentrations, and (b) comparison of residual (predicted-observed) vs. observed O_3 concentrations, all sites 17-19 July 1985.

Table 5.4: Observed (Obs.) and predicted (Pred.) maximum one-hour NO₂ concentrations in ppb at monitoring stations in the LFV, 17-19 July 1985, along with the respective time of day (Hr).

Station	17 July 1985				18 July 1985				19 July 1985			
	Obs.	Hr	Pred.	Hr	Obs.	Hr	Pred.	Hr	Obs.	Hr	Pred.	Hr
1	-	-	-	-	-	-	-	-	-	-	-	-
2	21.0	21	14.6	23	43.0	21	52.5	9	58.0	24	47.1	9
3	23.0	21	17.6	17	30.0	8	35.0	8	38.0	7	35.0	1
4	48.0	10	37.3	18	86.0	10	48.4	11	62.0	9	55.3	11
5	40.0	22	32.7	24	100.0	9	53.0	11	86.0	9	52.4	11
6	-	-	-	-	-	-	-	-	66.0	20	47.2	10
7	28.0	12	20.4	10	46.0	10	32.2	12	22.0	12	34.8	12
8	-	-	-	-	-	-	-	-	-	-	-	-
9	35.0	22	36.7	18	59.0	11	38.6	12	41.0	19	44.5	12
10	38.0	12	32.7	19	55.0	10	35.0	13	42.0	8	40.8	12
11	-	-	-	-	-	-	-	-	-	-	-	-
12	-	-	-	-	48.0	21	8.0	7	39.0	21	6.3	7
13	48.0	11	17.3	21	55.0	11	32.7	24	44.0	11	27.6	1
14	40.0	23	40.2	18	62.0	23	44.3	12	52.0	1	46.3	12
15	24.0	1	17.4	21	-	24	-	-	30.0	21	11.0	8
16	-	-	-	-	-	-	-	-	-	-	-	-

ppb. From Table 5.5, it is seen that the lowest mean bias and error is reported for stations T03 and T04. The highest mean bias and error values are reported for stations T02, T12, T13 and T15. However, poor data availability at stations like T15 prevent any further discussion of these results.

On each day of the episode, maximum observed NO₂ concentrations were recorded in North Burnaby, at monitoring stations in close proximity to existing oil refineries located along Burrard Inlet: 48.0 ppb (T04) on the 17th, 100.0 ppb (T05) on the 18th, and 86.0 ppb (T05) on the 19th. A station in North Delta, T13, also recorded a maximum NO₂

Table 5.5: Model performance based on observed and predicted maximum one-hour NO₂ concentrations at stations in the LFV, 17-19 July 1985.

Station	17 July 1985			18 July 1985			19 July 1985		
	Bias	Error	No.	Bias	Error	No.	Bias	Error	No.
2	-0.606	0.606	3	-0.274	0.682	13	-0.485	0.556	21
3	-0.373	0.373	3	-0.094	0.295	10	-0.156	0.292	11
4	-0.038	0.207	16	-0.194	0.248	17	-0.069	0.335	17
5	-0.114	0.183	19	-0.365	0.365	23	-0.418	0.430	21
6	-	-	-	-	-	-	-0.201	0.312	7
7	-0.307	0.307	2	-0.214	0.258	5	0.522	0.522	2
9	0.038	0.188	12	-0.209	0.326	19	-0.282	0.390	21
10	-0.048	0.185	11	-0.247	0.338	12	-0.210	0.341	17
12	-	-	-	-0.247	0.338	12	-0.931	0.931	3
13	-0.612	0.612	9	-0.429	0.480	10	-0.487	0.533	11
14	0.071	0.283	5	-0.334	0.463	17	-0.217	0.458	12
15	-	-	-	-	-	-	-0.758	0.758	3
Total	-0.144	0.269	80	-0.295	0.405	131	-0.307	0.433	146

concentration of 48.0 ppb on the 17th.

Maximum predicted concentrations on each of the three days were 40.2 ppb at T14, 53.0 ppb at T05 and 55.3 ppb at T04, respectively. Peak concentrations were underpredicted by 49.0%, 63.3% and 53.9% on the three days, when paired in space and time. Relaxing spatial and temporal requirements, peak concentrations were underestimated by 16.3%, 47.8% and 37.1%. This was well within the acceptable NO₂ criteria used by CARB (1990). The time of peak concentrations was a minimum of 7 hours late on the 17th and 2 hours late on the 18th, when compared to observations. Poor performance on the 17th may be attributed to model start-up effects. Peak modelled concentrations

Table 5.6: Model NO₂ performance statistics for the LFV, 17-19 July 1985.

Performance measure	17 July 1985	18 July 1985	19 July 1985
Maximum observed NO ₂ concentration (ppb)	48.0 (T04/T13)	100.0 (T05)	86.0 (T05)
Maximum predicted NO ₂ concentration (ppb)	40.2 (T14)	53.0 (T05)	55.3 (T04)
Peak accuracy paired in space and time	-49.0%	-63.3%	-53.9%
unpaired in space and time	-16.3%	-47.8%	-37.1%
Time of observed NO ₂ maximum	0900-1100 PST	0800-0900 PST	0800-1100 PST
Time of predicted NO ₂ maximum	1700-1800 PST	1000-1100 PST	0800-0900 PST
Mean normalized bias	-14.4%	-29.5%	-30.7%
Mean normalized gross error	26.9%	40.5%	43.3%

were within the period of maximum observed concentrations on the 19th. Mean normalized bias increased from -14.4% to -30.7% over the three-day simulation. This compares favourably with the performance goal of +/- 30%. Mean normalized gross error similarly increased, from 26.9% to 43.3%, but were well within the performance goal of 50%.

5.4 Discussion

Although the general features of the 17-19 July 1985 O₃ episode were reproduced, it is clear that the model tended to underpredict both O₃ and NO₂ concentrations. Due to the number of input requirements by the model, it is difficult to isolate just one factor which may have contributed to these findings. However, some of the more important factors are discussed in the following.

Firstly, the evaluation of model performance was based on comparisons between observations made at a single point and model results volume-averaged over a grid cell with dimensions of 5 km by 5 km in the horizontal and 100 m or greater in the vertical. Hence, some discrepancies are expected between observed and predicted values. Previous studies have indicated that predicted peak O₃ concentrations decrease with increasing grid size (Seigneur et al., 1981). Where sub-grid-scale effects are masked by grid cell averages, the discrepancy between predicted and observed concentrations will be larger. This may explain the poor characterization of NO₂ concentrations at station T02 in Vancouver, as shown in Figure 5.8.

A comparison of predicted wind fields and observations in Section 4.2.1 indicated that modelled wind fields had a greater southerly component than observed winds during the morning hours. This suggests that the influence of the Coast Mountains on local wind fields may have been overestimated. As a result, precursors emissions occurring in the Vancouver/Burnaby area during the morning rush hour would have been transported northwards, as reflected by the isopleths of predicted NO₂ concentrations at 0900 PST shown in Figures 5.11-5.13. This may partly explain the underpredicted O₃ concentrations at sites located further up the valley. However, this does not discount the finding that elevated O₃ concentrations may occur along the valley walls. In fact, lidar data collected by McKendry et al. (1997) during Pacific'93 (Steyn et al., 1997) support this

finding, showing that pollutants are vented along the valley walls during the daytime.

The mixed layer depth defines the vertical extent of mixing in the atmosphere. As such, an overestimate of z_i will yield an underestimate of predicted concentrations. It was shown in Figure 4.4) that values of z_i were slightly underpredicted at sites in Vancouver, Delta and Surrey. While it is possible that z_i values were overpredicted at sites further inland, maximum predicted values for Abbotsford on 18 and 19 July (660 and 750 m) compared well with measurements made during Pacific'93 (Hayden et al., 1997). However, it is possible that the influence of marine bodies such as Burrard Inlet was underestimated, resulting in overpredicted values of z_i near sites such as T07 and T09.

The evaluation of model performance has been limited to an assessment of surface level concentrations, due in large part to the lack of measurements aloft. Station T14 on Burnaby Mountain provides an opportunity to investigate how well the vertical profiles were resolved. While predicted O_3 concentrations agreed well with observations, NO_2 concentrations were poorly characterized, particularly on 18 July when the predicted maximum was approximately 12 hours out of phase with the observed maximum. A number of factors in addition to the vertical structure may have contributed to this finding, including a failure to accurately characterize wind trajectories and local emissions near this site.

The chemical mechanism represents a condensed version of the hundreds, if not thousands of reactions taking place in the atmosphere. Hence, it is accepted that the chemical mechanism introduces some degree of uncertainty in the predicted values. In a comparison of CBM-IV (Whitten et al., 1980; Gery et al., 1988, 1989) and the CAL (Carter et al., 1986; Lurmann et al., 1987) and Stockwell mechanisms (1990), Dodge (1989) found that the three mechanisms generally yielded similar results. Although this does not imply that the mechanisms were therefore correct, they do include the most up-to-date kinetic data and therefore, the "best science" of the time.

The emissions inventory is typically one of the largest sources of uncertainty in any modelling study due to the fact that it is impossible to characterize all sources contributing to NO_x and VOC emissions. Depending on whether conditions are NO_x- or VOC-sensitive, underestimated NO_x or VOC emissions may respectively result in under-predicted O₃ concentrations. It has been acknowledged that the 1985 inventory used in this simulation provided a rough first estimate (GVRD, 1988) and further refinements have since been made to this inventory (GVRD, 1994). As noted in Section 4.3, although overall changes were not large, changes within specific sectors were significant. They included a 23.5% reduction in NO_x emissions from point sources and a 34.1% increase in VOC emissions from area sources. Mobile emission estimates used in the simulation were based on Mobile3c and Mobile4.1c estimates. The Cassiar Tunnel study conducted during Pacific'93 (Gertler et al., 1997) showed that Mobile4.1c underpredicted observed NO_x and VOC concentrations by 29 and 23%, respectively. However, it was noted that the observed data were obtained under a best case scenario in which vehicles operated under hot-stabilized conditions and at constant speeds. Hence, higher emissions would be expected from vehicles operating under more normal conditions (i.e. variable speed and acceleration).

As a means of explaining how errors in VOC or NO_x emissions may have effected predictions, sensitivity indicators were considered. Sensitivity indicators are used to determine whether regions are VOC- or NO_x-sensitive (Sillman, 1994; Milford et al., 1994; Chameides et al., 1992; Kleinman, 1986; Kleinman, 1991). They provide a means of estimating airshed characteristics without the use of photochemical air quality models. Sensitivity indicators can similarly be applied to the analyses of modelling results as tools for model performance evaluation.

The following sensitivity indicators were used: NO_y (Milford et al., 1989; Rao et al., 1993; Sillman et al., 1993; Milford et al., 1994), HCHO-to-NO_y ratio (Sillman, 1995),

and O_3 -to- NO_x ratio (Sillman, 1995). VOC-sensitive conditions were indicated by the following values: NO_y concentration >20 ppb; O_3 -to- NO_x ratio <7 ; and HCHO-to- NO_y ratio <0.28 . The indicators were calculated for daytime conditions only, when photochemical activity is occurring. NO_y estimates are for the period from 0700-1800 PST, while the other indicators are for the period from 1200-1800 PST. Only those values from 18-19 July 1985 are shown, thereby excluding values which may have been influenced by model start-up effects on 17 July.

Sensitivity indicators calculated for stations T02, T03 and T05 are shown in Figure 5.15. Each of these stations is located slightly upwind of or in close proximity to the main source region, and so VOC-limited conditions would be expected. None of the three stations had consistent results for all three indicators, but both NO_y concentrations and the HCHO-to- NO_y ratio indicated that conditions near station T05 were VOC-limited. As shown in Figure 5.1, O_3 concentrations are underpredicted at this site. Hence, the indicator results suggest that VOC emissions or at least the reactivity of VOC emissions may have been underestimated near T05.

Sensitivity indicators for stations T07, T09 and T14 are depicted in Figure 5.16. While the O_3 -to- NO_x ratio indicated NO_x -limited conditions, both NO_y and the HCHO-to- NO_y ratio indicated VOC-limited conditions at all three sites. This finding is also supported by the fact that NO_2 concentrations were underestimated at these sites, suggesting insufficient radicals to drive NO_2 formation, as depicted in Equations 1.7-1.9. Uncertainties with respect to the vertical profile of pollutants at station T14, an elevated site, also likely contributed to the poor performance at this site.

Finally, indicators for stations T15, T11 and T12 are presented in Figure 5.17. All three indicators show NO_x -limited conditions for most hours of the afternoon. This is as expected for an aged air mass at such downwind sites. Underpredicted peak O_3 concentrations (Figure 5.3) at the three sites suggests that NO_x emissions, either locally

or downwind, were underestimated. The fact that the model could not reproduce the very low O₃ concentrations observed at night also suggests that local NO_x emissions were underestimated.

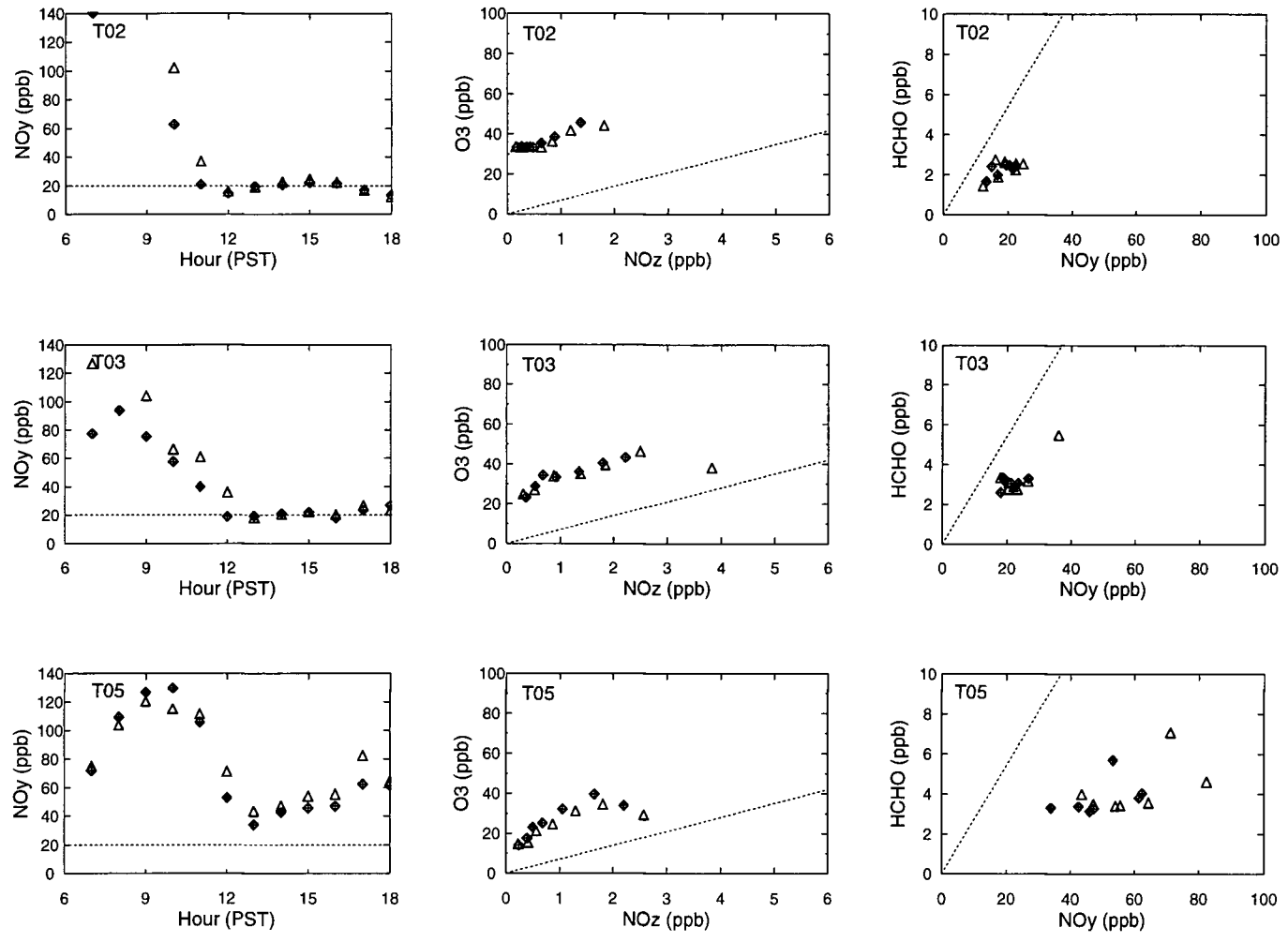


Figure 5.15: Sensitivity indicators based on predictions at stations T02, T03 and T05. Triangles show values for 18 July, diamonds for 19 July.

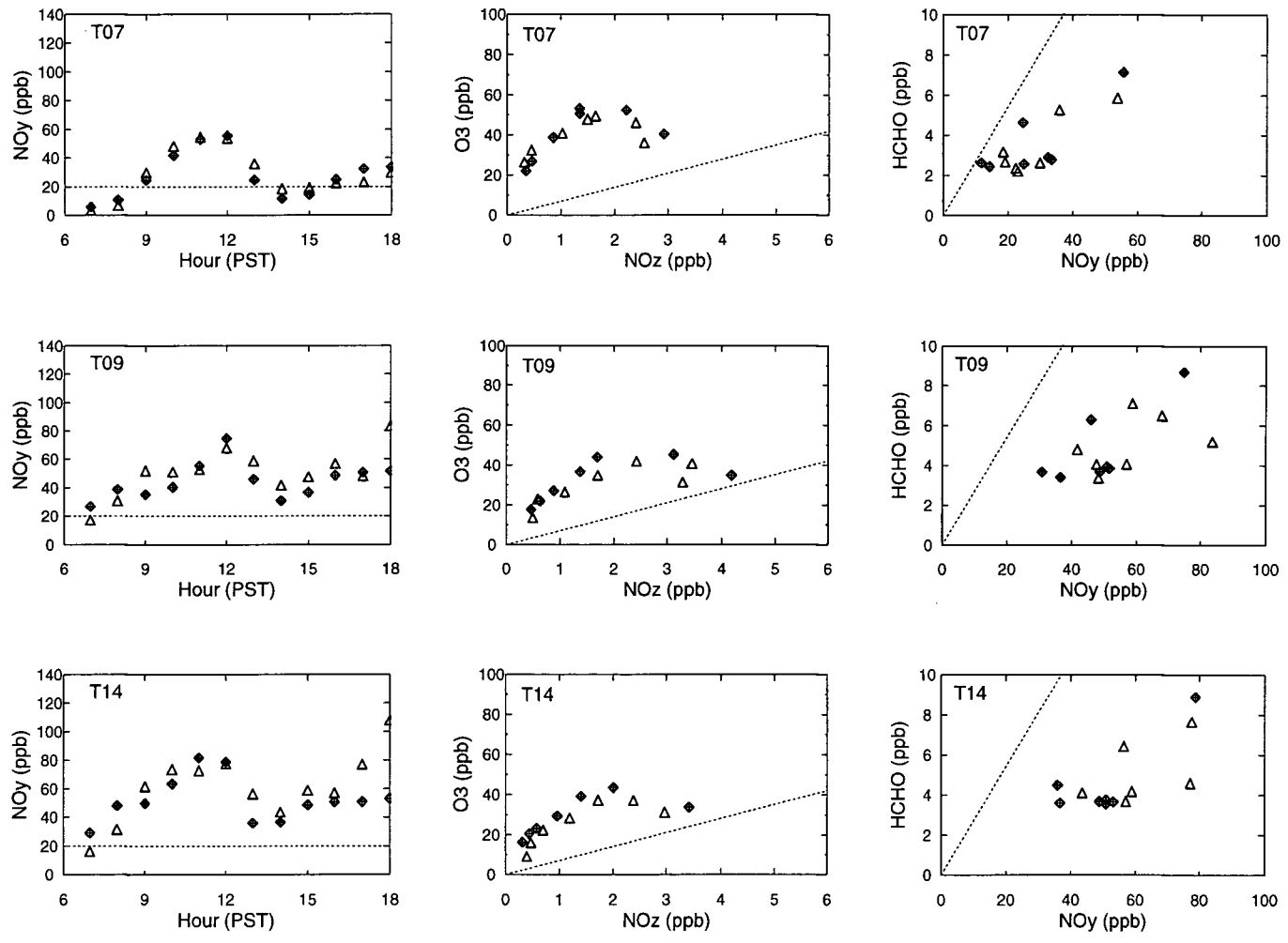


Figure 5.16: Sensitivity indicators based on predictions at stations T07, T09 and T14. Triangles show values for 18 July, diamonds for 19 July.

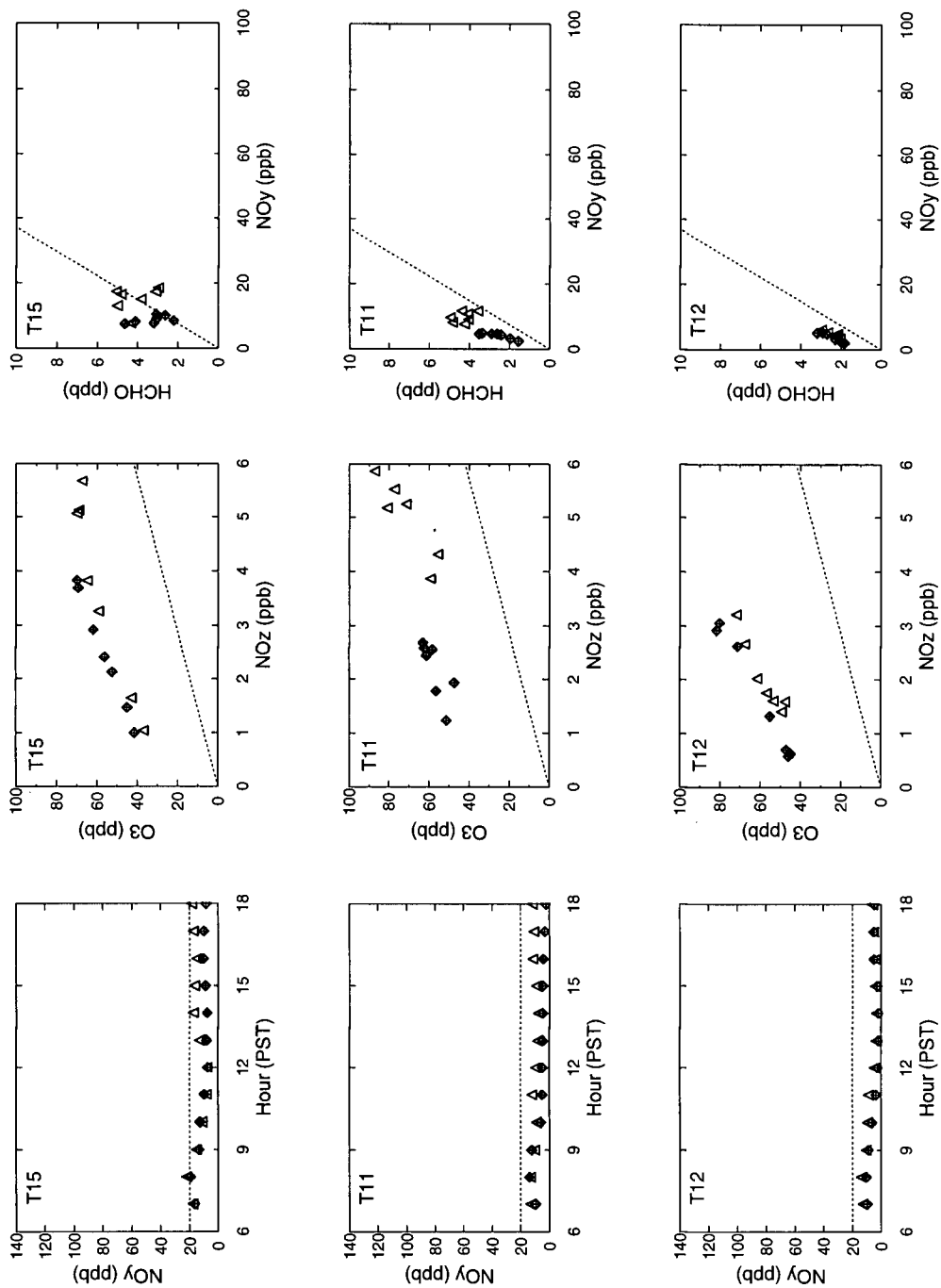


Figure 5.17: Sensitivity indicators based on predictions at stations T15, T11 and T12. Triangles show values for 18 July, diamonds for 19 July.

Chapter 6

Summary

The UAM-IV was applied to the LFV for an historical O₃ episode occurring between 17-19 July 1985. Model performance was evaluated in terms of its ability to reproduce O₃ and NO₂ concentrations observed during this episode. Major findings included the following:

- Diurnal characteristics of ambient O₃ and NO₂ concentrations were generally reproduced in the model simulation.
- Unpaired peak accuracy, mean normalized bias and mean gross error averaged -13%, -30% and 37%, respectively, for O₃. Model performance was worst for those sites located immediately on the downwind side of the main source region.
- Corresponding statistics for NO₂ were -34%, -25% and 37%, respectively.
- The model typically underpredicted peak O₃ and NO₂ concentrations.
- Some degree of underprediction was expected since comparisons were made between observations taken at a single point and model results volume-averaged over a grid cell of dimensions 5 km x 5 km in the horizontal and 100 m or greater in the vertical.
- The model also overpredicted nocturnal O₃ concentrations at those stations in which observed concentrations approached zero.
- Spatial patterns showed depressed O₃ concentrations over much of Vancouver and Burnaby, reflecting the titrating effect of NO emissions in the urban areas.

- These patterns also indicated that higher O_3 concentrations occurred along the valley walls as opposed to the valley floor where most of the population resides. In particular, areas of elevated O_3 concentrations were predicted to occur at the head of the Pitt River valley and to the southeast of Abbotsford in Washington State. Observations made during Pacific'93 by McKendry et al. (1997) support the findings over the Pitt River valley.
- Spatial patterns of NO_2 revealed high concentrations and strong gradients to the north of station T05 in North Burnaby.
- These findings and a comparison of predicted and observed winds suggests that the influence of the Coast Mountains on local winds during the morning hours, as manifested by a southerly wind component, was overestimated. As a result, O_3 concentrations may have been overpredicted along the valley walls and underpredicted at inland sites along the valley floor, such as at sites in Surrey, Abbotsford and Chilliwack.
- A further source of large uncertainty in the modelling study was the emissions inventory.
- Sensitivity indicators (NO_y , HCHO-to- NO_y ratio and O_3 -to- NO_z ratio) calculated using predicted concentrations indicated that sites in Burnaby and Port Moody were VOC-limited. Underpredicted O_3 concentrations at these sites may be partially attributed to either underestimated VOC emissions or underestimated reactivity of the VOC mixture in the main source region.
- Indicators also showed that downwind sites in Surrey, Abbotsford and Chilliwack were NO_x -limited. This helps to explain why the model overpredicted nocturnal O_3 concentrations, particularly in Abbotsford and Chilliwack.

List of References

- B.H. Levelton (1989) Vancouver Oxidants Study: Control technology options and costs for volatile organic compound emissions from gasoline marketing. Prepared for Waste Management Branch, Ministry of Environment, Lands and Parks, and Conservation and Protection, Environment Canada, May.
- B.H. Levelton (1993) 1990 U.S. Lower Fraser Valley Emissions Inventory. Prepared for Atmospheric Environment Service, Environment Canada, Vancouver, BC, March.
- B.H. Levelton and Western Research (1993) 1990 Air Emissions Inventory for the Lower Fraser Valley: Area Sources. Prepared for Greater Vancouver Regional District, Burnaby, BC, June.
- Banta R.M., Shepson P.B., Bottenheim J.W., Anlauf K.G., Wiege H.A., Gallant A., Biesenthal T., Olivier L.D., Zhu C-J, McKendry I. and D.G. Steyn (1997) Nocturnal cleansing flows in tributary valley. *Atmospheric Environment* 31(14) 2147-2161.
- Bates D. and S. Vedal (1994) *Air Pollution Health Effects in the Lower Mainland and Lower Fraser Valley*. A report prepared for the B.C. Ministry of Environment, Lands and Parks, November 5.
- Boris J.P. and D.L. Book (1973) Flux-corrected transport: I. SHASTA, a fluid transport algorithm that works. *J. Comput. Phys.* 11, 38-69.
- Brauer M. and J.R. Brook (1997) Ozone personal exposures and health effects for selected groups residing in the Fraser Valley. *Atmospheric Environment* 31(14), 2113-2121.

- Briggs G.A. (1975) Plume rise predictions. In: *Lectures on Air Pollution and Environmental Impact Analyses*, American Meteorological Society, Boston, Massachusetts.
- Builtjes P.J.H., van den Hout K.D. and S.D. Reynolds (1982) Evaluation of the performance of a photochemical dispersion model in practical applications. 13th International Technical Meeting of Air Pollution Modeling and Its Application, Ile des Embiez, France, 14-17 September.
- Cai X.-M. and D.G. Steyn (1995) Mesoscale meteorological modelling study of the Lower Fraser Valley, B.C., Canada from July 17 to 20, 1985. Report prepared for Science Division, Environmental Conservation Branch, Environment Canada Pacific and Yukon Region, Vancouver, BC.
- Cardelino C.A. and W.L. Chameides (1990) Natural hydrocarbons, urbanization and urban ozone. *J. Geophys. Res.* 95(9), 13971-13979.
- Cardelino C.A. and W.L. Chameides (1995) An observation-based model for analyzing ozone precursor relationships in the urban atmosphere. *J. Air & Waste Man. Assoc.* 45, 161-180.
- Carter W.P.L. (1990) A detailed mechanism for the gas-phase atmospheric reactions of organic compounds. *Atmospheric Environment* 24A, 481-518.
- Carter W.P.L., Lurmann F.W., Atkinson R. and A.C. Lloyd (1986) Development and testing of a surrogate species chemical reaction mechanism, Report EPA/600/3-86/031, U.S. Environmental Protection Agency, Research Triangle Park, N.C.
- Causley M. (1990) User's Guide for the Urban Airshed Model. Volume IV: User's Guide for the Emissions Processing System. EPA-450/4-90-077d, U.S. Environmental Protection Agency, Research Triangle Park, NC.

- CCME (1990) Management Plan for Nitrogen Oxides (NO_x) and Volatile Organic Compounds (VOCs). Phase I. Canadian Council of Ministers of the Environment, November.
- Chameides W.L., Fehsenfeld F., Rodgers M.O., Cardleino C., Martinez J., Parrish D., Lonneman W., Lawson D.R., Rasmussen R.A., Zimmerman P., Greenberg J., Middleton P. and T. Wang (1992) Ozone precursor relationships in the ambient atmosphere. *J. Geophys. Res.* 97(D5) 6037-6055.
- Chang J.S., Brost R.A., Isaksen I.S.A., Madronich S., Middleton P., Stockwell W.R. and C.J. Walcek. (1987) A three-dimensional Eulerian acid deposition model: Physical concepts and formulation, *J. Geophys. Res.* 92, 14,681-14,700.
- Coligado M. (1988) Air parcel trajectories during ozone episodes in the Lower Fraser Valley. In conference proceedings of: Chemicals in the Environment, 25th Annual Meeting of the Pacific Northwest International Section, Air & Waste Management Association, Whistler, BC, November 9-11.
- CSC (1982) Final Report, Vancouver Oxidant Study, Air Quality Analysis. Prepared for Environmental Protection Service, Environment Canada, Vancouver, BC.
- CSC (1985) Vancouver Oxidants Study. Air Quality Analysis Update 1982-84, Prepared for Environmental Protection Service, Environment Canada, Toronto, ON, 86 pp.
- Dennis R.L. and M.W. Downton (1984) Evaluation of urban photochemical models for regulatory use. *Atmospheric Environment* 18, 2055-2069.
- Dodge M.C. (1989) A comparison of three photochemical oxidant mechanisms. *J. Geophys. Res.* 94, 5121-5136.

- Dodge M.C. (1990) Formaldehyde production in photochemical smog as predicted by three state-of-the-science chemical oxidant mechanisms. *J. Geophys. Res.* 95, 3635-3648.
- Emslie J.H. (1968) Wind flow in Burrard Inlet, Vancouver, BC. A Summary of six years of data. Circular TEC-686, Meteorological Branch, Dept. of Transport, Canada, Toronto, ON, 14pp.
- Franzmann A. (1992) Personal communication.
- Gertler A.W., Wittorff D.N., McLaren R., Belzer W. and T. Dann (1997) Characterization of vehicle emissions in Vancouver BC during the 1993 Lower Fraser Valley Oxidants Study. *Atmospheric Environment* 31(14), 2107-2112.
- Gery M.W., Whitten G.Z. and J.P. Killus (1988) Development and Testing of the CBM-IV for Urban and Regional Modeling. EPA/600/3-88/012, U.S. Environmental Protection Agency, Research Triangle Park, N.C., 1988.
- Gery M.W., Whitten G.Z., Killus J.P. and M.C. Dodge (1989) A photochemical kinetics mechanism for urban and regional computer modeling. *J. Geophys. Res.*
- Greenberg J.P., Zimmerman P.R. and P. Haagenson (1990) Tropospheric hydrocarbon and CO profiles over the U.S. West Coast and Alaska. *J. Geophys. Res.* 95(9), 14,015-14,026.
- GVRD (1988) Lower Mainland Emission Inventory. A. Summary, Volume I: Lower Mainland Emissions. Greater Vancouver Regional District Pollution Control, May 1988.

- GVRD (1994) GVRD Air Quality Management Plan Technical Report. GVRD Emissions Inventory, Greater Vancouver Regional District, Air Quality and Source Control Dept., Burnaby, BC, February.
- Haagen-Smit A.J. (1952) Chemistry and physiology of Los Angeles smog, *Ind. Eng. Chem.* 44, 1342-1346.
- Haney J.L. (1997) Memorandum to B.C. Hydro.
- Haney J.L., Douglas S.G., Gardner L.A. and C.S. Burton (1990) Urban Airshed Model for Seven Parish Baton Rouge Area Study, Air & Waste Management Association's International Specialty Conference on Tropospheric Ozone and the Environment, Los Angeles, California.
- Hay J. and T.R. Oke (1985) *Climate of Vancouver*. B.C. Geophysical Series, Number 23. Tantalus Research Ltd.
- Hayden K.L., Anlauf K.G., Hoff R.M., Strapp J.W., Bottenheim J.W., Wiebe H.A., Foude F.A. and J.B Martin (1997) The vertical chemical and meteorological structure of the boundary layer in the Lower Fraser Valley during Pacific'93. *Atmospheric Environment* 31(14), 2089-2105.
- Hedley M. and D.L. Singleton (1997) Evaluation of an air quality simulation of the Lower Fraser Valley – I. Meteorology. *Atmospheric Environment* 31, 1605-1615.
- Hedley M., Jiang W., McLaren R. and D.L. Singleton (1996) Modelling of a future year emissions control strategy for the Lower Fraser Valley: Impact of a retrofit dedicated propane fuelled light duty vehicle fleet. PET-1379-96S, Prepared for Alternative Energy Division, Energy Technology Branch, CANMET, Natural Resources Canada, Ottawa, ON.

- Hedley M., McLaren R., Jiang W. and D.L. Singleton (1997) Evaluation of an air quality simulation of the Lower Fraser Valley – II. Photochemistry. *Atmospheric Environment* 11, 1617-1630.
- Jeffries H.E. and S. Tonnesen (1994) A comparison of two photochemical reaction mechanisms using mass balance and process analysis. *Atmospheric Environment* 28, 2991-3003.
- Kelly R.F. (1981) User's Manual for Mixing Height Computer Program. EPA-450/4-81-022, U.S. Environmental Protection Agency.
- Killus J.P., Myer J.P., Durran D.R., Anderson G.E., Jerskey T.N., Reynolds S.D. and J. Ames (1984) Continued research in mesoscale air pollution simulation modeling, Volume V: Refinements in numerical analysis, transport, chemistry and pollutant removal. EPA-600/3-84-095A, U.S. Environmental Protection Agency, Research Triangle Park, NC.
- Kleinman L.I. (1986) Photochemical formation of peroxides in the boundary layer. *J. Geophys. Res.* 91(D10), 10889-10904.
- Kleinman L.I. (1991) Seasonal dependence of boundary layer peroxide concentration: The low and high NO_x regimes. . *J. Geophys. Res.* 96(D11), 20721-20733.
- Lamb R.G. (1983) A regional scale (1000 km) model of photochemical air pollution, I. Theoretical formulation. EPA/600/3-83/035, U.S. Environmental Protection Agency, Research Triangle Park, NC.
- Lefohn A.S., Jackson W., Shadwick D.S. and H.P. Knudsen (1997) Effect of surface ozone exposures on vegetation grown in the southern Appalachian Mountains: Identification of possible areas of concern. *Atmospheric Environment* 31(11), 1695-1708.

- Lin X., Trainer M. and S.C. Liu (1988) On the nonlinearity of the tropospheric ozone production. *J. Geophys. Res.* 93(D12) 15879-15888.
- Lolk N.K., Guo Z., Douglas S. and J.L. Haney (1995) Draft Demonstration Application of UAM-V for the Lower Fraser Valley, SYSAPP-95/075d, Systems Applications International, Prepared for Atmospheric Environment Service, Environment Canada, Vancouver, BC, November.
- Lurmann F.W., Carter W.P.L. and L.A. Coyner (1987) A surrogate species chemical reaction mechanism for urban-scale air quality simulation models, EPA./600/3-87/014, U.S. Environmental Protection Agency, Research Triangle Park, N.C.
- Mass C. (1982) The topographically forced diurnal circulations of western Washington State and their influence on precipitation. *Mon. Wea. Rev.* 110, 170-183.
- McKendry I.G. (1994) Synoptic circulation and summertime ground-level ozone concentrations at Vancouver, British Columbia. *J. Appl. Meteor.* 33,627-641.
- McLaren R. (1993) Personal communication.
- McNider R.T. and R.A. Pielke (1981) Diurnal boundary-layer development over sloping terrain. *J. Atmos. Sci.* 38, 2198-2212.
- McRae G.J., Goodin W. and J.H. Seinfeld (1982) Numerical solution of the atmospheric diffusion equation for chemically reacting flows. *J. Comput. Phys.* 95, 1-42.
- McRae G.J. and J.H. Seinfeld (1983) Development of a second-generation mathematical model for urban air pollution—II. Evaluation of model performance. *Atmospheric Environment* 17, 501-522.

- McKendry I., Steyn D.G., Lundgren J., Hoff R.M., Strapp. W., Anlauf K., Froude F., Martin J.B., Banta R.M. and L.D. Olivier (1997) Elevated ozone layers and vertical down-mixing over the Lower Fraser Valley, BC. *Atmospheric Environment* 31(14), 2135-2146.
- Miao Y. (1993) Mesometeorological modelling and trajectory studies during an air pollution episode in the Lower Fraser Valley, British Columbia, Canada. Masters Thesis, Dept. of Geography, University of British Columbia, Vancouver, BC.
- Milford J.B., Russell A.G. and G.J. McRae (1989) A new approach to photochemical pollution control: Implications of spatial patterns in pollutant responses to reductions in nitrogen oxides and reactive organic gas emissions, *Environ. Sci. Technol.* 23, 1290-1301.
- Milford J.B., Gao D., Sillman S., Blossey P. and A.G. Russell (1994) Total reactive nitrogen (NO_y) as an indicator of the sensitivity of ozone to reductions in hydrocarbon and NO_x emissions. *J. Geophys. Res.* 99, 3533-3542.
- Morris R.E. and T.C. Myers (1990) User's guide for the Urban Airshed Model - Volume I: User's guide for UAM (CBIV). EPA-450/4-90-007a. U.S. Environmental Protection Agency, Research Triangle Park, NC.
- Morris R.E., Myers T.C., Causley M.C., Gardner L.A. and E.L. Carr (1990a) Urban Airshed Model study of five cities - Low-cost application of the model to Atlanta and evaluation of the effects of biogenic emissions on emission control strategies. EPA-450/4-90-006C, U.S. Environmental Protection Agency, Research Triangle Park, NC.

- Morris R.E., Myers T.C. and E.L. Carr (1990b) Urban Airshed Model study of five cities – Evaluation of the base case model performance for the cities of St. Louis and Philadelphia using rich and sparse meteorological inputs. EPA-450/4-90-006C, U.s. Environmental Protection Agency, Research Triangle Park, NC
- Nichols R.A. and B. Hardcastle (1983) Canadian service station fuel transfer emissions. Prepared for Petroleum Association for Conservation of the Canadian Environment, Ottawa, Ontario, 211 pp.
- NRC (1991) *Rethinking the Ozone Problem in Urban and Regional Air Pollution*. National Research Council, National Academy Press, Washington, D.C., 489 pp.
- Oke T.R. (1978) *Boundary Layer Climates*. Methuen, London, England, 372 pp.
- Peters L.K., Berkowitz C.M., Carmichael G.R., Easter R.C., Fairweather G., Ghan S.J., Hales J.M., Leung L.R., Pennell W.R., Potra F.A., Saylor R.D. and T.T. Tsang (1995) The current state and future direction of Eulerian models in simulating the tropospheric chemistry and transport of trace species: A review. *Atmos. Environ.* 29(2), 189-222.
- Pielke R.A. (1974) A three-dimensional numerical model of the sea breeze over south Florida. *Mon. Wea. Rev.* 102, 115.
- Pierson W.R., Gertler A.W., Robinson N.F. and R.L. Bradow (1990) Comparison of the SCAQS tunnel study with other on-road emission data. *J. Air & Waste Man. Ass.* 40, 1495-1504.
- Pryor S. (1994) Personal communication.
- Rao S.T. and G. Sistla (1993) Efficiency of nitrogen oxides and hydrocarbons emissions control in ozone attainment strategies as predicted by the urban airshed mode.

- Intl. J. Water Air Soil Pollut.* 67, 95-116.
- Rao S.T (1987) Application of the Urban Airshed Model to the New York metropolitan area. EPA-450/4-87-011, U.S. Environmental Protection Agency, Research Triangle Park, NC.
- Reynolds S.D., Seinfeld J.H. and P.M. Roth (1973) Mathematical modeling of photochemical air pollution – I. Formulation of the model. *Atmospheric Environment* 7, 1033-1061.
- Reynolds S.D., Liu M.K., Hecht T.A., Roth P.M. and J.H. Seinfeld (1974) Mathematical modeling of photochemical air pollution—III. Evaluation of the model. *Atmospheric Environment* 8, 563-596.
- Robinson N.F., Pierson W.R., Gertler A.W. and J.C. Sagebiel (1996) Comparison of MOBILE4.1 and MOBILE5. Predictions with measurements of vehicle emission factors in Fort McHenry and Tuscarora Mountain Tunnels, *Atmospheric Environment* 30(12), 2257-2267.
- Rogak S.N., Caton R.B. and A. von Stuermer (1993) GVRD and Lower Fraser Valley Ambient Air Quality Review. Prepared for Greater Vancouver Regional District by Concord Environmental Corporation, June 30, 1993.
- Rowe M.D., Novak K.M. and P.D. Moskowitz (1983) Health effects of oxidants. *Environment International* 9, 515-528.
- Runeckles V.C. and B.I. Chevone (1992) Crop response to ozone. In: *Surface Level Ozone Exposures and Their Effects on Vegetation*. A.S. Lefohn, Ed., Lewis Publishers, Chelsea, Michigan, p. 189-270.

- SAI (1995) Demonstration application of UAM-V for the Lower Fraser Valley. Report prepared by Systems Applications International for Atmospheric Environment Service, Environment Canada, Vancouver, BC.
- SCAQMD (1990) *Air Quality Management Plan 1991 Revision. Technical Report V-B. Ozone Modelling - Performance Evaluation.* South Coast Air Quality Management District, December 1990.
- Scheffe R.D. and Morris R.E. (1993) A review of the development and application of the Urban Airshed Model. *Atmospheric Environment* 27B(1), 23-39.
- Seinfeld J.H. (1988) Ozone air quality models. A critical review. *J. Air Pollut. Control Assoc.* 38(5), 616-644.
- Sheih B.F., Wesley N.L. and Walcek C.J. (1986) The dry deposition module for regional acid deposition models. Draft report to the U.S. Department of Energy and the U.S. Environmental Protection Agency, contract no. DW89930060-01, Argonne National Laboratories.
- Sillman S. (1995) The use of NO_y, H₂O₂ and HNO₃ as indicators for ozone-NO_x-hydrocarbon sensitivity in urban locations. *J. Geophys. Res.*
- Sillman S., Logan J.A. and S.C. Wofsy (1990) A regional scale model for ozone in the United States with subgrid representation of urban and power plant plumes. *J. Geophys. Res.* 95(D5), 5731-5748.
- Sillman S., Samson P.J. and J.M. Masters (1993) Ozone production in urban plumes transported over the water: Photochemical model and case studies in the north-eastern and midwestern U.S., *J. Geophys. Res.* 98, 12687-12699.

- Smolarkiewicz P.K. (1983) A simple positive definite advection scheme with small implicit diffusion. *Mon. Weath. Rev.* 111, 479-486.
- Steyn D.G. and X. Cai (1994) A multi-day meteorological modelling study of the Lower Fraser Valley, BC, Canada, under a stagnant synoptic situation. Atmospheric Science Programme, Dept. of Geography, University of British Columbia, Vancouver, BC.
- Steyn D.G. and Faulkner (1986) The climatology of sea breezes in the Lower Fraser Valley. *B.C. Clim. Bull.* 20(3), 21-39.
- Steyn D.G. and I.G. McKendry (1988) Quantitative and qualitative evaluation of a three-dimensional mesoscale numerical model simulation of a sea breeze in complex terrain. *Mon. Wea. Rev.* 116, 1914-1926.
- Steyn D.G. and C.H. Wallis (1986) Spatial and Temporal Variability of the Daytime Mixed Layer Depth Over Greater Vancouver. Report prepared for Waste Management Branch, B.C. Ministry of Environment, Lands and Parks, Victoria, BC.
- Steyn D.G., Roberge A. and C. Jackson (1990) Anatomy of an Extended Air Pollution Episode in British Columbia's Lower Fraser Valley. Report prepared for Waste Management Branch, B.C. Ministry of Environment, Lands and Parks, Victoria, BC.
- Steyn D.G., Bottenheim J.W. and R.B. Thomson (1997) Overview of tropospheric ozone in the Lower Fraser Valley, and the Pacific'93 field study. *Atmospheric Environment* 31(14), 2025-2035.
- Stockwell W.R., Middleton P., Chang J.S. and X. Tang (1990) The RADM2 chemical mechanism for regional air quality modeling. *J. Geophys. Res.* 95D, 16343-16367.

- Taylor E. (1991) Forecasting ground-level ozone in Vancouver and the Lower Fraser Valley of British Columbia, Report PAES-91-3, Scientific Services Division, Atmospheric Environment Service, Pacific Region, Vancouver, BC, 8pp.
- Tesche T.W. (1988) Accuracy of ozone air quality models. *J. Envir. Engng* 114, 739-752.
- Tesche T.W. and D.E. McNally (1991) Photochemical Modeling of Two 1984 SCC-CAMP Ozone Episodes. *J. Applied Meteorol.* 30(5), 745-763.
- Treshow M. and F.K. Anderson (1989) *Plant stress from air pollution*. J. Wiley & Sons, New York, NY, 283 pp.
- Tripoli G.J. and W.R. Cotton (1982) The Colorado State University three-dimensional cloud/mesoscale model – 1982. Part I: General theoretical framework and sensitivity experiments. *J. Rech. Atmos.* 16, 185-220.
- Wakamatsu S., Uno I. and M. Suzuki (1990) A field study of photochemical smog formation under stagnant meteorological conditions. *Atmospheric Environment* 24A(5), 1037-1050.
- Whitten G.Z., Hogo H. and J.P. Killus (1980) The Carbon-Bond Mechanism: A condensed kinetic mechanism for photochemical smog. *Atmospheric Environment* 14(6) 690-700.
- Wright E.F. (1988) The effect of ozone on horticultural crops important to the Lower Fraser Valley of British Columbia. Master's Thesis. University of British Columbia, Vancouver, Canada.
- Yamartino R.J., Scire J.S., Carmichael G.R. and Y.S. Chang (1992) The CALGRID mesoscale photochemical grid model – I. Model formulation. *Atmospheric Environment* 8, 1493-1512.

- Yanenko N.N. (1971) The method of fractional steps: The solution of problems of mathematic physics in several variables. English translation edited by M. Holt, Springer-Verlag, Berlin, 160 pp.